Processing high resolution digital elevation models for the Kula Badlands in Turkey

Sensitivity analysis for Landscape Evolution Models

Aleksei Gerasimov
900115-257-080

WAGENINGEN
UNIVERSITY & RESEARCH

August 2019
Chairgroup Soil geography and Landscape
Thesis Soil Geography and Earth Surface Dynamics

Processing high resolution digital elevation models for the Kula Badlands in Turkey
Sensitivity analysis for Landscape Evolution Models

Aleksei Gerasimov, August 2019
Registration number: 900115-257-080
SGL-80436
MSc-thesis Soil Geography and Earth Surface Dynamics, Wageningen University

Supervisor(s):
S. Aksay MSc.
Dr. J.M. Schoorl
Examiner(s)
Dr. J.M. Schoorl

Chairgroup Soil Geography and Landscape
Phone: +31 317 482024
office.sgl@wur.nl

Postal address:
PO. Box 47
NL-6700 AA, Wageningen
The Netherlands

Visiting address:
Gaia (building number 101)
Droevendaalsesteeg 3
NL-6708 PB, Wageningen
The Netherlands

Abstract

The accuracy and resolution of digital elevation models (DEMs) play an important role in numerically modeling the evolution of a landscape. One of the most important factors affecting the rate of erosion and sedimentation in modelling landscape change, in addition to water flow, is gradient or relief. The choice of the area of study namely the Kula badlands, Western Turkey, is determined by the presence of intensive Quaternary erosion processes and the development of rough terrains and steep gullies.

A high resolution Digital Elevation Model (DEM) was produced on the basis of high precision aerial photographs, following flight missions using Unmanned Aerial Vehicles (UAVs) in the field work area in the Kula region,. Four types of DEM resolutions: 2.5; 5; 10; 20 m were chosen to test the sensitivity response of each DEM to the erosion simulation. A DEM error in space was simulated based on the measured heights of the ground control points and randomly chosen points in the field. According to these spatial error results, 1000 DEMs were obtained of the DEM simulation by Monte Carlo method. These simulated DEMs were tested for Landscape Evolution Modelling (LEM) using LAPSUS. The simulation results in LAPSUS were used to determine the effect of the DEM error on erosion, deposition, and to determine the most optimal DEM resolution. The erosion modelling and deposition in LAPSUS was based on four different resolution scenarios with two different erosion rates (4.25 and 42.50 tons/ha/year, respectively) and different precipitation and evaporation sequences. The simulation was carried out for a period of 10 years.

In this thesis the problems of building a continuous DEM for the entire study area are discussed. In additon, the problem of the effect of elimination of vegetation from the DEM was noted. Also, sufficiency of the number of DEM simulations to determine the LEM sensitivity and sufficiency of the number of height measurements for DEM error interpolation have been discussed. The ratio of the deterministic and the simulated DEMs with the real terrain was described. Also, impact of the scenarios with transport limited conditions and detachment limited conditions on the erosion distribution and deposition depending on the DEM resolution has been described and discussed.

As a result, it was found that there is sedimentation in the gullies in the scenarios with increased erosion at a resolution of 2.5 and 5 m. For all scenarios the situation when the net erosion decreases with increasing DEM resolution for 10 years is typical. It was also found that the DEM error introduces a significant change in the erosion and deposition spatial distribution in the study area. According to the results of the study it was found that the resolution of 10 m is most accurate for erosion modeling in the study area of Kula badlands.

Table of contents

List of tables

List of figures

Introduction

The effect of the resolution and accuracy of the DEM on the modeling of erosion and soil movement was discussed previously in the articles of Schoorl et al. (2000), Claessens et al. (2006), Zhang et al. (2008). Moreover, the work of Vaze et al. (2010) reflects the impact of the resolution of the DEM from 1 m to 25 m on topographic indices. Also in the paper Lu et al. (2017) the effect of accuracy and resolution of the DEM on erosion modeling was described, the work is curious because a DEM with very high resolution from 1 to 30 cm was used, but it is worth noting that studies were conducted for a small area of about 400 m^2. Despite this, the impact of the DEM resolution and accuracy on deposition and erosion modelling using LEMs remains a relevant issue and requires additional research for high resolution DEMs covering large areas.

As study area Kula badlands was picked, the formation and development of the Kula badlands (Western Turkey) is a typical example where the landscape development is not fully understood. It is possible to reconstruct the landscape evolution by studying the main driving factors that form the landscape of the Kula badlands. There are several drivers, such as tectonic extention, baseline change, volcanism, climate change, human intervention and poor land management. It should be noted that for the Kula badlands, overland flow and gully erosion and deposition processes are most important for landscape formation (Westaway et al. 2004, Maddy et al. 2008, van Gorp 2014, van Gorp et al. 2015, Maddy et al. 2015)

The study area can serve as an example for the erosion development in Mediterranean settings. Erosion in the territory of the Kula badlands effect economic activity in the region. In the article by Heineke et al. (2017) it is noted that upland erosion is the main source of material for silting up the water reservoirs in the region, which leads to a reduction in potential water resources for agricultural activities.

Currently, LEM methods are widely used to determine the processes of erosion and sedimentation. As indicated by van Gorp et al. (2015), the main advantage of using LEMs for this purpose is the ability to analyze landscape evolution at spatial and temporal scales without elaborated of costly field or laboratory experiments. To use LEMs, DEMs with sufficiently high resolution of less than 30 m are required (Schoorl et al. 2000, Claessens et al. 2006)

Currently, aerial photography using UAVs is a common technique to produce high-resolution DEMs. The use of UAVs has many advantages, such as the ability to quickly deliver images with high temporal and spatial resolution, rapid response in a number of critical situations, where immediate access to three-dimensional geographic information is extremely important, possibility of real-time rapid collection and transmission of information (Remondino et al. 2011, Uysal et al. 2015, Sammartano and Spano 2016).

In addition, Temme et al. (2009) note in their article that high-resolution DEMs describe the landscape better than low-resolution DEMs. On the other hand, high-resolution DEMs may still have greater uncertainty than low-resolution DEMs. Moreover, as also stated in Cantreul et al. (2018), DEMs with such high resolution have lower correlations for landscape analysis and modeling, while the smallest DEM pixel size is not the best solution for modeling.

To determine the impact of inaccuracies of the DEM built on the basis of aerial photographs, it is proposed to use a Monte Carlo method for DEM simulation, as in the work by Temme et al. (2009). The inaccuracy of the DEM was determined by fixed ground control points and randomly sampled points.

Despite the fact that the topic of the effect of the resolution and accuracy of the DEM on erosion and deposition was discussed in the work of Schoorl et al. (2000), Claessens et al. (2006), Lu et al. (2017) this problem remains relevant. The following aim and objectives were set the presented master's thesis.

Aim of the research is assessing the impact of the DEM error and resolution on changes in the LEM erosion and deposition simulations in the study area.

Objectives of the research:

- Building a deterministic DEM and a set of simulated DEMs taking into account the DEM error.

- To conduct the LEM sensitivity analysis, based on the different resolution DEM sets.
- Selecting the optimal DEM resolution whose criterion is the accuracy of erosion modeling.

Hypothesis

It is assumed that the DEM error and resolution significantly affect numerical erosion and sedimentation modelling in the study area.

1. Study area

The Kula Badlands, located in Western Turkey, was chosen as the study area because the area is characterized by Quaternary high erosion rates. The study area is located in the upper reaches of the Geren river catchment a tributary of the Gediz River in Turkey (see Figure 1). Therefore, the rate of erosion in the region according to the work of Heineke et al. (2017) range from 35 to 1043 ton/ha/year. The study area used for the UAV flying is about 22 km^2. The small subcatchment for which the simulation of erosion was carried out was only 1.2 km^2 (see Figure 1). The rationale for selecting this small subcatchment for modelling is explained in the methodology section. The heights of the area on which the research was carried out vary from 400 to 800 m. The relief of the Kula Badlands is characterized by the presence of numerous ravines with a depth of 10 to 20 meters and small streams. The badlands are covered with sparse vegetation in small areas, on the steep slopes of ravines and more densely on the slopes facing north than on the slopes facing south.

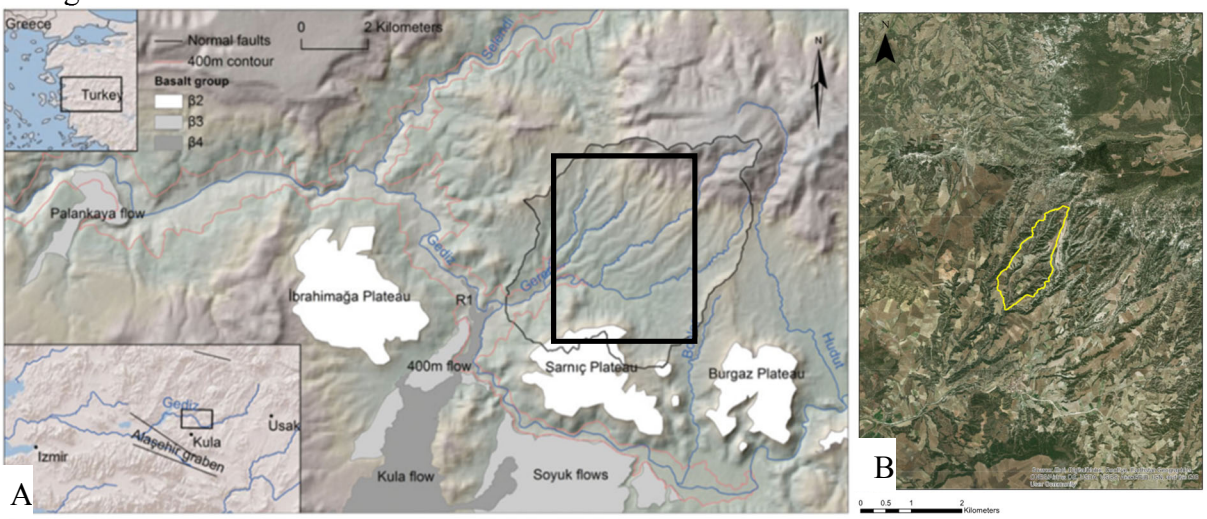

Figure 1 with A - Overview maps of the study area (van Gorp et al., 2016), B - Area of interest

The Kula Badlands area is characterized by a Mediterranean climate with hot and dry summers and mild winters. The largest amount of precipitation falls as rain in winter, summer is dry, with a characteristic high evaporation potential. The mean annual temperature is about 16° C, the annual rainfall is about 700 mm, with most of the precipitation falling from November to March and the annual evaporation is 209 mm/year (Heineke, 2017, Kale, 2017).

Also worth noting is the composition and origin of the main rock formations and units in the area. According to Van Gorp et al., 2014, the Gediz and Geren tributary were severely dammed due to early and Late Pleistocene lava dams, although the river's trunk was only slightly disturbed. The complex stratigraphy of the study area is described in Ersoy et al., (2010) and van Gorp et al., (2015).

Stratigraphy of the area is represented by the Quaternary sediments and lavas that lie upon heavily eroded Miocene basin infills. Below Quaternary sediments, the pre-dominantly fluvial facies of the Ahmetler Formation, together with the overlying continental carbonate deposits of the Ulubey Formation, can be found. The aforemntioned are located on top of predominantly metamorphic Basement rocks (typically schist, gneiss, marble and quartzite), and furthermore comprises basal alluvial fan and high energy fluvial facies, These sediments are accompanied, towards the centre of the study area, by thick volcaniclastic detritus, dated to the Mid-Miocene, emanating from a basin-central stratovolcano (Maddy et al. 2012). Intensive erosion processes are probably the main factor influencing the development of the Kula badlands. The Ulubey limestone cliff is the northern boundary of the Geren catchment. The southernmost boundary of the Geren watershed is the Early Pleistocene lava plateau with unconsolidated Ahmetler Miocene sands, silt and gravel below. The area is usually characterized by deep ravine and gully systems cutting down

into the Ahmetler formation deposits. These deposits consist of coarse river gravel of carbonate origin, fine sands and silts, which indicates a change in the regime of river flows. Fluvial fill sequences and channels are also found at different levels (van Gorp et al., 2015). Thus Kula badlands can serve as a good example of the development of erosion in the Mediterranean setting. Following the above simplified stratigraphic information, the study area has a rather complex geological structure with easily erodible sediments.

2. Methodology

2.1. Methodology of field work

In order to produce a digital elevation model (DEM) of the study area, field work was carried out from 7 to 22 September 2018.

As part of the field work, aerial photography was carried out using three UAVs, two Falcon Pro 5 Flying Wings (see Figure 2) and one DJI Inspire 2 Quadrocopter (see Figure 3). The Falcon Pro 5 was equipped with a Sony A6000 cameras with a resolution of 24.3 MP and a 12mm Samyang lens, DJI Inspire 2 was equipped with a camera with a resolution of 20.8 MP. The aerial photography was conducted with 80% over- and sidelap between aerial photographs for each flight, which exceeds the 60% minimum required percentage of overlapping between adjacent photographs and is in the range of 80-90% photograph overlapping, which is in accordance with recommendations from Ruzgiene et al. (2004). A total of 5904 aerial photographs were obtained as a result of all the UAV flights.

Figure 2 Two Falcon Pro 5 UAVs

Figure 3 DJI Inspire 2 quadrocopter (the photograph is taken from [https://store.dji.com)](https://store.dji.com)

In order to geotag aerial photographs (for non-geotagged aerial photographs) and assess the accuracy of aerial photography conducted, the coordinates and height of ground control points (GCPs) were measured (see Figure 4). In some studies, typical terrain points (with measured coordinates and height) that can be easily found in the image are used as GCPs, such as intersections, houses (Leitão et al. 2016). Since it is difficult to find a sufficient number of typical terrain points in the study area, artificial GCPs, as in the study described by Uysal et al. 2015, were placed strategically. The GCPs were located at the intersection of the UAV flight plan. In addition, GCPs were located based on availability due to rough terrain in the study area.

Figure 4 Measuring the GCP coordinates and height with a Rover.

GCPs were placed before the flight, so they can be seen on the aerial photograph (see Figure 5). Further, using a two-phase GNSS receiver, the GCP coordinates and height were determined (see Appendix Table A.1). To increase the precision of the GCP position measurement, the kinematic method was applied (Sickle 2015). Measuring the coordinates and height at one selected point takes 5 to 15 minutes. Requirements for the use of kinematic GPS-photography were described in Sickle (2015). The base GNSS receiver is fixed on one point on the roof of the Geopark office building in Kula. The rover (mobile GNSS receiver) moved from one GCP to another, recording the coordinate data for 5-15 minutes in each GCP location. The collected data provide vectors between the rover and the base receiver. A total of 46 GCP coordinates and heights were measured.

To independently verify the accuracy of the DEM, the coordinates and height of random points (RP) in the study area were measured (see Appendix Table A.2). The cross-validation method is used to determine the DEM error (Sunila and Virrantaus, 2011). During the field work, 70 RPs were measured. The method of measuring the coordinates and height of random points was carried out using the same two-phase GNSS receiver rover as described before, the adjustment of the coordinates and height of the GCP and RPs was made using the data from the base point.

According to Höhle (2009), the spatial location of the RPs should be chosen randomly. In addition, the RPs should be located along the break lines, on steep slopes, in places of sudden slope change, near buildings, etc., as there the possible DEM errors might be larger. It should be noted that the RP location can be called random only conditionally, since the work in the field was limited by time and the point's reachability. As described above, the study area is characterized by quite steep slopes, and all RPs were located in the open areas not covered with vegetation (GNSS signal becomes weak if there is an obstacle between the receiver and satellites).

To determine the accurate position of the terrain depicted in the aerial photographs, GNSS receivers were installed on the UAVs as well, a standard GNSS receiver was installed on the quadcopter by the manufacturer. The UAV position and orientation for each photo are needed for building a sparse point cloud, point cloud later were used or DEM producing (Agisoft PhotoScan User Manual: Professional Edition, Version 1.4., 2018).

As a result of the field work, a set of data necessary and sufficient for the DEM construction and the DEM accuracy evaluation was obtained.

Figure 5 Aerial photograph with a GCP

2.2. Field data post-processing

This chapter describes the methodology for "raw" field data processing. The data obtained in the field are not suitable for direct use in the study, they must be formatted. Data processing involves obtaining the coordinates and heights of GCPs and randomly located points, as well as spatial tagging of aerial photographs.

Initially, the files with coordinates and point heights are downloaded directly from the GNSS receiver (rover and base station) in the .sbp and .nav formats. The algorithm for obtaining the coordinates and the height of the GCPs and random points is given below:

1) .sbp coordinate files of all points (including the base point that remained stationary on the roof of the building) are converted to .obs files using the sbptoRinex.exe program.

2) Next the RTKpost.exe program was used for converting GCP and RP .obs and .nav files in relation to the base station data files (.obs) in the GCPs and RPs .pos file. In Figure 6 shows some settings which were picked in RTKpost.exe, static position mode was picked because kinematic method was used for GNSS method and Geodetic height was picked because GNSS implemented on the quadrocopter also used the Geodetic parameter. The recording time of the GCP or RP files must match the recording time of the file on the base point. Thus, the coordinates

of the point are synchronized relative to the coordinates of the base station, which are more accurate, since it did not change its position for a relatively long time (10 days).

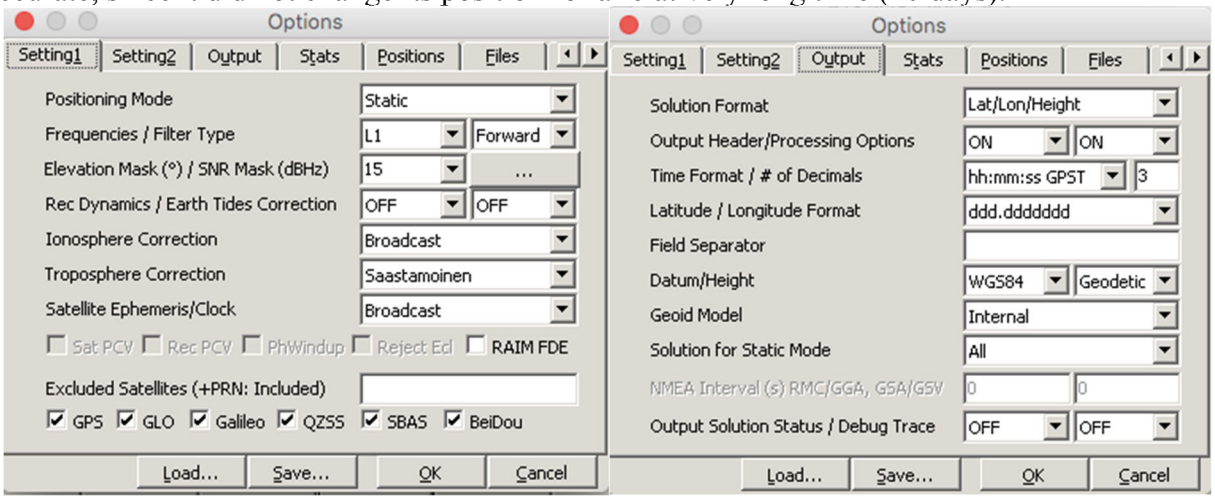

Figure 6 RTKpost.exe options windows

3) from the received GCP and RP .pos files the coordinates and heights are extracted and put into the .xls file.

The scheme of the above algorithm for obtaining the GCP and RP coordinates is shown in Figure 7.

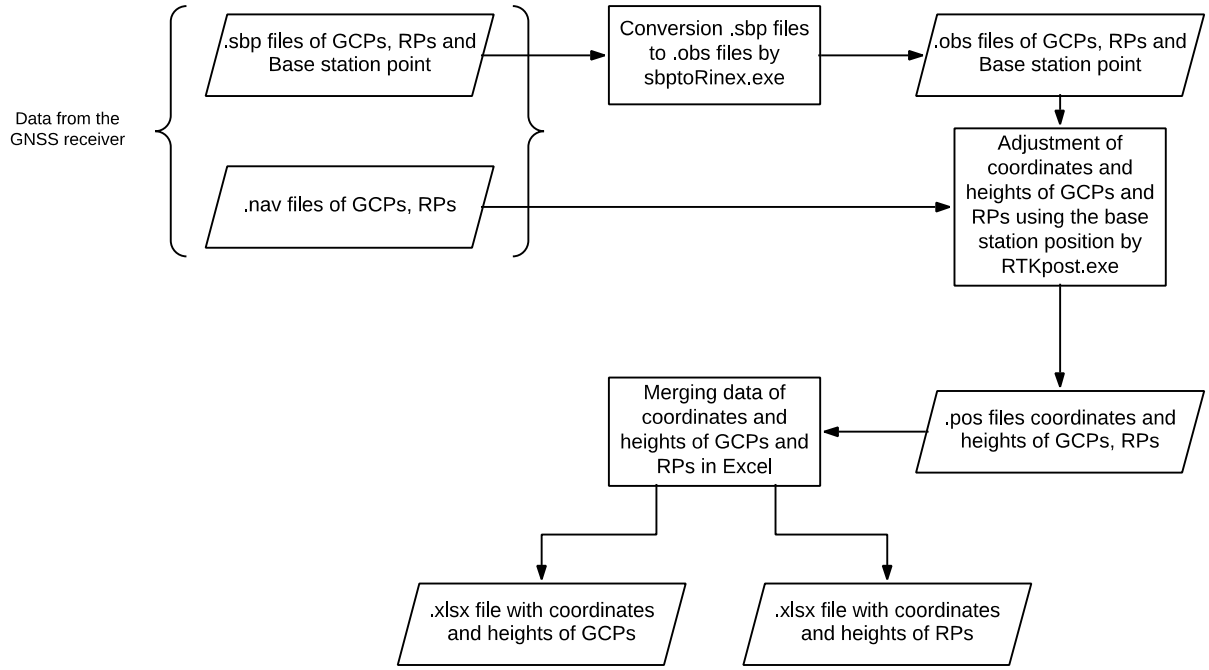

Figure 7 Flowchart of the algorithm for obtaining GCPs and random points coordinates

Initially, the files with the camera position and aerial photographs are downloaded from the UAV in .jpg and .jpeg formats, respectively. The algorithm of geotagging the aerial photographs is given below:

1) The files containing the coordinates and position of the camera in the .log format and the files of the photographs themselves in the .jpeg format are processed by MissionPlanner.

2) As a result, aerial photographs tagged to the coordinates of the UAV position at the time of photoshooting were obtained.

The algorithm described above for geotagging aerial photographs is presented in Figure 8.

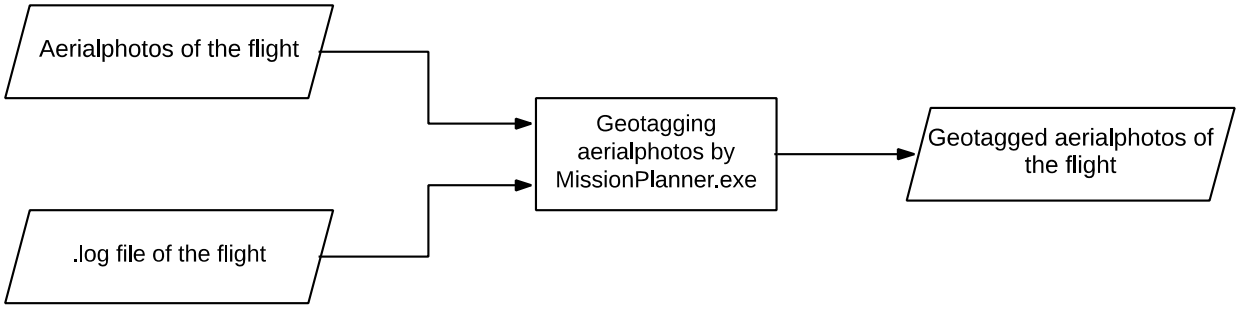

Figure 8 Flowchart of the algorithm of geotagging aerial photographs algorithm

2.3. DEM building methodology

This chapter describes the process and algorithm that was used to build the DEM of the study area. For creating the DEM, raw data was processed in the AgiSoft Photoscan program.

In a study conducted by Sona et al. (2014), 4 software programs for processing aerial photographs were compared. The DEMs from Erdas-LPS, EyeDEA (University of Parma), Agisoft Photoscan and Pix4UAV PhotoModeler Scanner were compared using the same data input. It was concluded that the Agisoft Photoscan program showed the best result, because the standard error was the lowest compared to other programs (Sona et al. 2014).

The following is an algorithm for creating a DEM using AgiSoft Photoscan (see Figure 9):

1) Importing the geotagged aerial photographs in the AgiSoft Photoscan program. AgiSoft Photoscan also allows to import non-geotagged aerial photographs. We had to use non-geotagged aerial photographs obtained on the last field day.

2) All uploaded photographs were checked visually by the operator to remove photographs with errors (for example, black photographs or test photographs taken to check the trigger). After visual selection function of the program, the ”photograph quality check” feature was used. In the AgiSoft Photoscan user manual, it is stated that the indicator of photograph quality is desirable not to exceed 0.5 (a standard unit in the AgiSoft PhotoScan program). Unfortunately, in our case, about 30% of aerial photographs were with the quality from 0.5 to 1.0. It was decided to leave all the photographs after checking their quality by the program, as we did not want to lose information, since in many places of the study area this would lead to a too small overlap of aerial photographs and the inability to create a DEM.

3) AgiSoft Photoscan program independently determines the position of the cameras, combining the same points in the photographs. The program uses the Alignment function with the "high quality" parameter. For geotagged and non-geotagged aerial photographs, the procedure is carried out in different directories of the program. The result is a point cloud (coordinates and heights without tagging to the coordinate system).

4) Then the common points on geotagged and non-geotagged aerial photographs are determined. To do this, the Alignment of chunks command is used.

5) Using the Merging of the chunks command, a single directory was created with a combined point cloud for geotagged and non-geotagged aerial photographs.

6) The converted data with the height and coordinates of the GCPs was uploaded into the AgiSoft Photoscan program.

7) Since the GCPs and aerial photographs are geotagged, the downloaded GCPs are automatically displayed in the photographs. The GCP markers were combined with the markers on the photographs (yellow marker bands that we placed in the study area, see Figure 5). As a result, the GCPs were located in the right place at aerial photographs, and thus retained their initial coordinates. The correct location of the GCP markers reduces the error in the height and

coordinates of the DEM at the GCP locations (Agisoft PhotoScan User Manual: Professional Edition, Version 1.4., 2018).

8) Launching of the Optimize Camera Alignment function tagged the position of the camera aerial photographs relative to the GCP coordinates, so we produced a geotagged point cloud.

9) Launching the Build Dense Point Cloud function with the mean quality of the processing (to reduce the computer operation time). After a couple of days of progress, the dense point cloud was produced.

10) To eliminate vegetation from the point cloud, an algorithm built into the AgiSoft PhotoScan program was used. It should be noted that the filtering program cannot correctly distinguish the ground points and vegetation. Moreover, the filter gives only an approximate height of vegetation. As described in Yilmaz et al. (2018), working digital cameras installed on UAVs cannot determine the height of vegetation that causes changes between DSM and DEM. However, Yilmaz et al. (2018) argue that it is possible to generate a high resolution DEM using point clouds. The selection of parameters for the selection of areas with vegetation was made, the quality of the selection of areas with vegetation was determined visually, and the division of points into "ground points" and "other" was made. All "other" points were removed from the dense point cloud. The remaining "ground points" were used further. Thus, an additional inaccuracy was introduced in the DEM due to the elimination of vegetation in the absence of information on vegetation height.

11) By running the DEM Build function based on a dense point cloud, only "ground points" were taken into account. The result was a 0.25 m resolution deterministic DEM without vegetation.

12) The last step is to export the DEM. It should be noted that the DEM must be translated into UTM projection to use the metric system and it is also necessary to select the required resolution not lower than that obtained in the previous step. The 0.25 m raw DEM was exported to the ArcGIS program in the .tif raster format.

The described method allows to obtain a DEM with high resolution (up to 0.25 m). But it should be noted that there are points in the method that need to be improved such as vegetation removal.

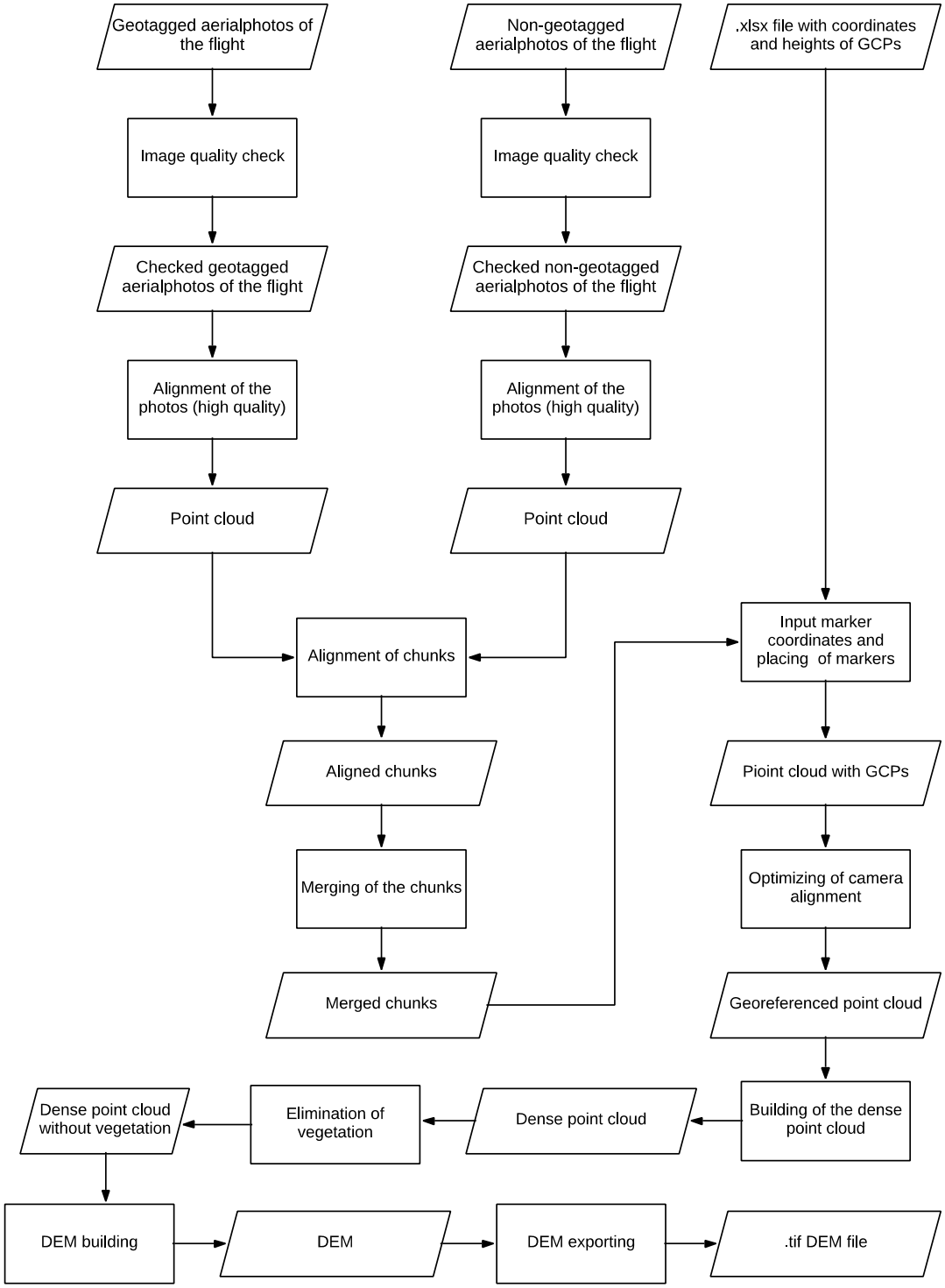

Figure 9 Flowchart of the algorithm of building high resolution DEMs in the AgiSoft Photoscan program

2.4. Selecting the DEM area for modelling and DEM resolution

To model erosion processes adequatly, a complete draining catchment area must be selected. For this purpose, the possibility of using several different catchments was analyzed on the basis of the constructed DEM.

The north-eastern part of the study area (i.e. Selendi catchment) is not included for further analysis for a couple of reasons. It is quite a difficult terrain to map as it is part of the scarp area

of the large limestone plateau. Besides, the unexpected windy weather conditions was another struggle on that particular mapping day. So this part of the DEM was produced including over- and side-lapping issues resulting in major errors in height. Due to these rather expected errors and issues, the later work is conducted without including this area. This led to the fact that in some GCPs in this area the error in height exceeded 100 m.

In particular, the very northeastern part of the area had significant overlap issues, which led to irreversible errors in the DEM building (see Figure 10).

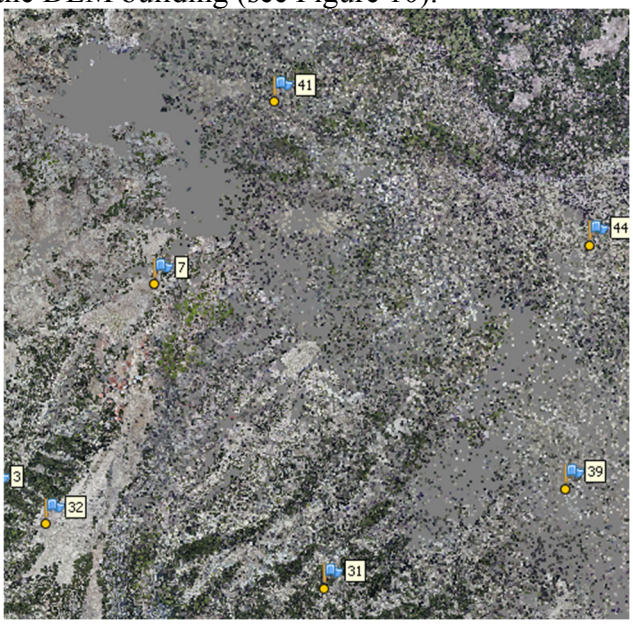

Figure 10 Point cloud, north-eastern part of the study area, grey colour shows the gaps in the point cloud.

Small overlap of aerial photographs was caused by the fact that the area has a steep slope of the earth's surface, which reduces the photographed area, also it maybe cause that the source of the elevation which were used for the flight planning was not accurate enough for scarp area. Moreover, the hard wind conditions or trigger mechanism of the photocamera could also causes these missing areas in our DEM. Such problems can be solved only by running the flight missions again at higher flight marks, which in turn will reduce the quality and resolution of aerial photographs.

In the south-eastern part of the study area there are also visible gaps having a rectangular shape (see Figure 11). This error is caused by the lack of overlap between the aerial photographs. Even a relatively small increase in the surface height can lead to loss of aerial photographs overlap.

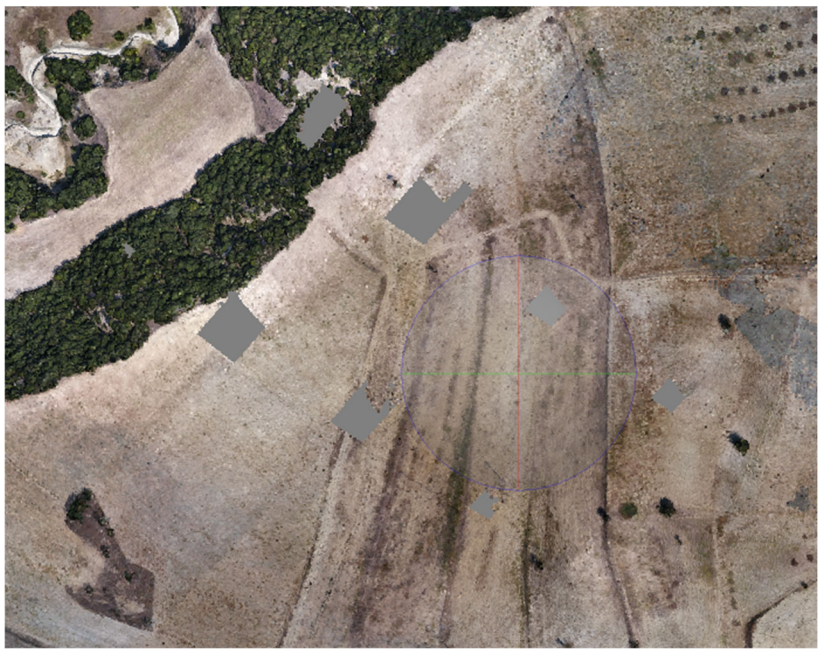

Figure 11 Point cloud, South-Eastern part of the study area, grey colour shows the gaps in the point cloud.

When choosing an area for modeling, the distribution of GCPs and RPs was also taken into account. The areas, where GCPs and RPs were missing, were discarded.

Consequently, a catchment area, where there is a complete overlap of aerial photographs and suitable for further procedure was selected. The selected catchment is isolated from other catchment areas with overlapping or height issues photographs. The area of the selected complete catchment is 1.2 km^2.

The raw DEM produced in AgiSoft Photoscan had a resolution of 0.25 m. After testing the DEM with different resolutions in the LAPSUS program to assess the possibility of calculations with such a high resolution, it was concluded that the erosion modeling is possible at least at the resolution of 2.5 m. The erosion modeling at the resolution of 2.5 m for a period of 1000 years took 17 minutes. At a higher resolution, the program did not work. For this reason, DEMs with 4 different resolutions were produced, in which further work was carried out; 2.5, 5, 10 and 20 m. The new resolutions were processed by the aggregation method in ArcGIS, cells of the raw DEM with resolution of 0.25 m were merged into a new cell. The new cell values were assigned the mean valueof all merged cells (sample size N will depend on the resolution and ranged between 100 to 6400 raw values) .

Since one of the objectives of this MSc work is to assess the resolution impact on the erosion changes, DEMs with 4 different resolutions were chosen. The possible effects of the change in DEM resolution on the modelled erosion and sedimentation was described in Schoorl et al. (2000).

2.5. DEM simulations

To assess the accuracy of the DEM built, two types of DEM errors were simulated, conventionally so-called the first and second type of errors. The first type of error is a GCP error. GCPs give an error of the DEM georeferencing relative to the actual position of points in space and show how well the DEM is tagged vertically. In our study, we proceed from the assumption that the height of the GCPs and RPs is measured more accurately than the height of the raw DEM in the same coordinates.

The second type of error is the error obtained on the basis of the difference in the DEM height and the height of RPs (random points). This type of error helps us to independently assess how different the DEM is from the measurements made by the GNSS receiver.

Understanding the DEM accuracy allows us to further use the inaccuracy of the DEM building to assess the degree of influence on the erosion change, depending on both the DEM tagging error (the first type) and the DEM independent error (the second type).

To estimate the spread of erosion values, it was decided to use the Monte Carlo method to obtain a spatial simulation of the first and second type errors. Temme et al. (2009) argue that the Monte Carlo method is the most commonly used for error propagation because it is versatile and flexible. Raaflaub and Collins (2006) state that one of the drawbacks of the Monte Carlo method is the computational necessity, since a large number of simulations are needed to obtain statistically reliable results. Raaflaub and Collins (2006) also noted that it is not known how many error simulations are satisfactory. Various authors argue that the number of simulations can vary from 100 to 5000 (Raaflaub and Collins 2006, Pohjola et al. 2009, Temme et al. 2009). Since one of the objectives is to determine the optimal DEM resolution for further calculation of sedimentation and erosion in LAPSUS, the sets of DEMs with different resolutions were compiled on the basis of first type and second type of errors. It was decided to conduct 125 simulations for each resolution and for each type of error separately.

To simulate spatially the first type and second type of errors for each DEM with different resolutions, a code was generated in the R Studio program. In the code, the kriging method was used to simulate the error. For each type of error and each resolution, different semivariograms were selected, since the error for GCPs and RPs differed in different resolutions due to the aggregation effect. The semivariograms parameters and semivariograms themselves can be seen in Table 1 and Figure 12 and Figure 13 respectively. In the semivariogram model, the nugget equals zero. Note that Temme et al. (2009) state, in assessing the DEM accuracy, the nugget must be zero so that the error at the measurement point does not change in all simulations. In our work, the "Spherical" model was chosen for the semivariogram, since only such a model allowed to produce error simulations and the model satisfactorily fell on the distribution of pairs on the semivariogram. Moreover, because semivariograms must be fitted as good as possible, it cause difference in range and in sill of the semivariograms for the different DEM resolutions. There is no direct dependence of range and sill from DEM resolution, but it is obvious that DEM resolution is crucial for parameters of the semivariogram.

Table 1 Semivariogram parameters for simulating type first and second types of DEM errors.

N	Resolution (m)	Nugget	Sill	Range
First type of error				
1	20	0	4	600
2	10	0	8	200
3	5	0	1,5	1050
4	2.5	0	7	150
Second type of error				
5	20	0	2	1000
6	10	0	7	150
7	5	0	2	1200
8	2.5	0	7,5	150

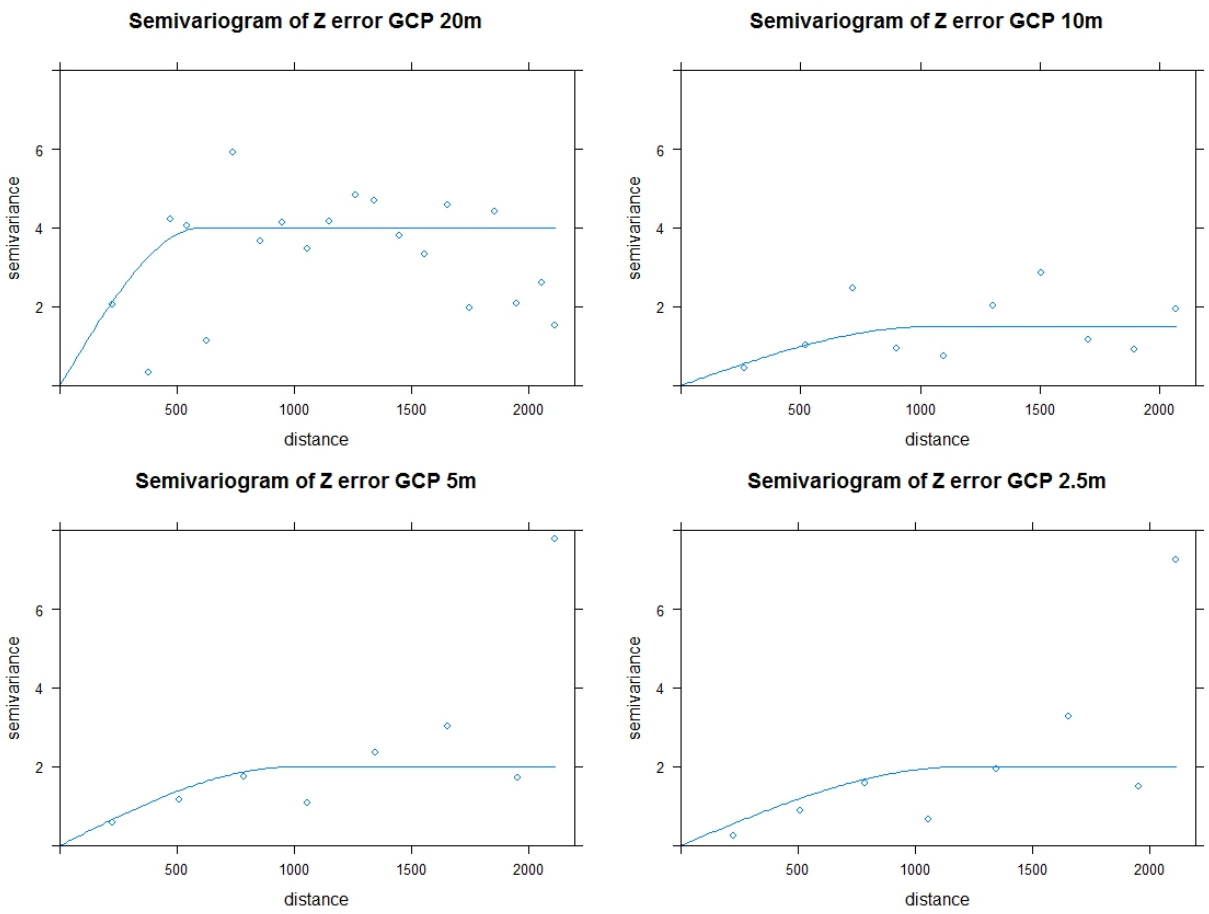

Figure 12 Semivariograms for first type of error simulation.

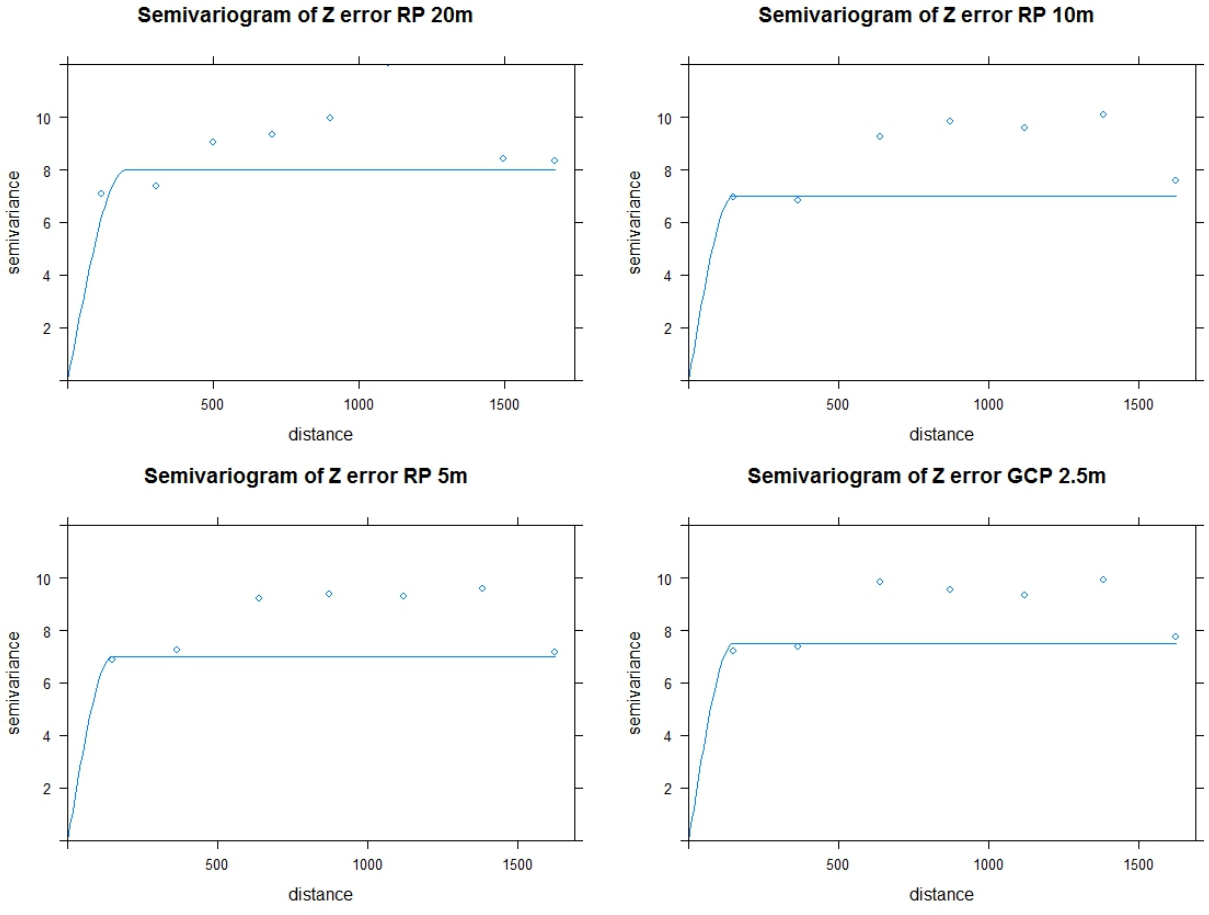

Figure 13 Semivariograms for second type of error simulation.

Based on the above parameters, 1000 DEM error simulations were created. Further, the error was calculated with the DEM built using AgiSoft with the appropriate resolution. After that, sinks were filled and flats were removed using the Wang and Lui (2006) method.

2.6. Erosion modeling in LAPSUS

The last step in our study is to model erosion and deposition change using LAPSUS. The modeling was performed for 1000 simulated DEMs and 4 original (deterministic) DEMs with 4 different DEM resolutions (2.5, 5, 10 and 20 m) with two types of DEM error. So 8 DEMs sets were picked.

The LAPSUS (LandscApe ProcesS modelling at mUlti-dimensions and Scales) modeling algorithms are described in detail in the work by Schoorl et al. (2000; 2002). The LAPSUS computational model is based on early works by Kirkby (1971, 1978, 1986) and Foster and Meyer (1972, 1975). According to Schoorl et al. (2000), the basic idea behind the LAPSUS model is that the potential energy of the water flowing over the landscape surface is the driving force behind the transport of solid sediments.

4 scenarios were selected for simulation:

1) L-scenario in which the annual erosion is 4.25 tons/ha according to the work of Heineke, et al. (2017). Precipitation of 0.7 m and evaporation of 0.21 m remained constant for all 10 years of modeling. This scenario is close to the real situation, but excludes the effects of precipitation and evaporation fluctuations over 10 years of simulation.

2) H-scenario in which the erosion is 42.5 tons/ha (10 times more than in the usual scenario). Precipitation of 0.7 m and evaporation of 0.21 m also remained constant for all 10 years of modeling. This scenario is an extremum at which the soil of the studied area is modeled as easily eroded. In this study it is assumed that the figures for erosion are higher than those stated in the article by Heineke et al. (2017).

3) LCL-a scenario in which the annual erosion is 4.25 ton/ha. Precipitation and evaporation vary over a period of 10 years. Precipitation and evaporation data for the scenario are taken from Climate4impact Infrastructure for the European Network of Earth System Modelling (2018) as presented in Table 2. I have chosen the MPI-ESM-LR climate model (Max Planck Institute Earth system Model running on low resolution grid). MPI-ESM-LR model takes into account the circulation of the atmosphere, the influence of the Earth's surface, the influence of the ocean, the ice cover of the seas and ocean, the circulation of carbon and biochemistry of the ocean. In the climate model, the 8.5 PSI climate warming scenario was chosen as the most pessimistic. This scenario is the closest to reality.

4) HCL is a scenario where the annual erosion is 42.5 ton/ha. Precipitation and evaporation vary over a period of 10 years, data on precipitation and evaporation for the scenario are presented in Table 2.

Table 2 Precipitation and evaporation over 10-year period.

№	Simulation year	Precipitation (m/year)	Evaporation (m/year)
1	2018	1.129	0.241
2	2019	1.318	0.26
3	2020	0.99	0.142
4	2021	1.165	0.289
5	2022	1.355	0.152
6	2023	0.757	0.264
7	2024	1.01	0.181
8	2025	1.504	0.341
9	2026	0.963	0.171
10	2027	1.046	0.245

The simulation time for scenarios in LAPSUS was set to 10 years. The selected period of time is not accidental, it was assumed that in the course of this time, the landscape should be quite flattened and the DEM error added to the deterministic DEM will be eroded.

Each of the 1000 simulated error DEMs had their own scenarios modeled. As a result, 4016 simulations of 10 years of erosion development were implemented.

Among the factors influencing the water erosion modeling in LAPSUS, the following driving parameters were taken into account: terrain, precipitation, evaporation and erodibility value in the scenario's calibration. The spatial distribution of the soil and its depth were not taken into account. Also, the spatial distribution of precipitation and evaporation, and economic use of land were not taken into account.

In LAPSUS, both the annual change in erosion and sedimentation in the whole of the selected area and the annual change in erosion and sedimentation in space were simulated. The results were saved with a time step of 1 year.

RMSE (Root-mean-square error) of erosion and sediment maps were constructed to assess the impact of the DEM's first and second type of errors on erosion and deposition. RMSE of erosion and sedimentation was calculated for total cumulative erosion and deposition for 10 years of simulation, as the actual value the simulated erosion or deposition based on the deterministic DEM were taken (see Formula 1). For each pixel of all simulations of all scenarios, the RMSE of erosion and deposition was calculated. As such the RMSE shows the impact of DEM error on erosion and deposition. In the work by Wechsler and Kroll (2006), it is indicated that in the absence of accurate information on the spatial structure, RMSE is the only statistic. The aim of this approach is to quantify the uncertainty caused by random errors in the DEM and the resulting parameters (i.e. erosion and deposition). This methodology uses RMSE as a mechanism to quantify the uncertainty of DEM using Monte Carlo simulations.

$$RMSE = \sqrt{\frac{\sum_{i=0}^{n}(\hat{y}-y_i)^2}{n}} \quad (1),$$

where, n – number of DEMs simulations, $\hat{y}$ – cumulative erosion and sedimentation for 10 years based on the deterministic DEM, y_i – cumulative erosion and sedimentation for 10 years based on the simuleted DEM.

3. Results

3.1. Results of the field work and DTM building

As a result of the September 2018 field work campaign, 5904 aerial photographs were taken and processed. The Aerial photographs cover about 22 km^2 of the northern part of the Geren catchment. The coordinates and heights of 44 GCPs and 71 RPs were obtained.

Based on the results of the field work, a deterministic DEM with a resolution of 0.25 m was built (see Figure 14). The DEM was cleared of vegetation. The height of the resulting DEM varies from 359 to 947 m.

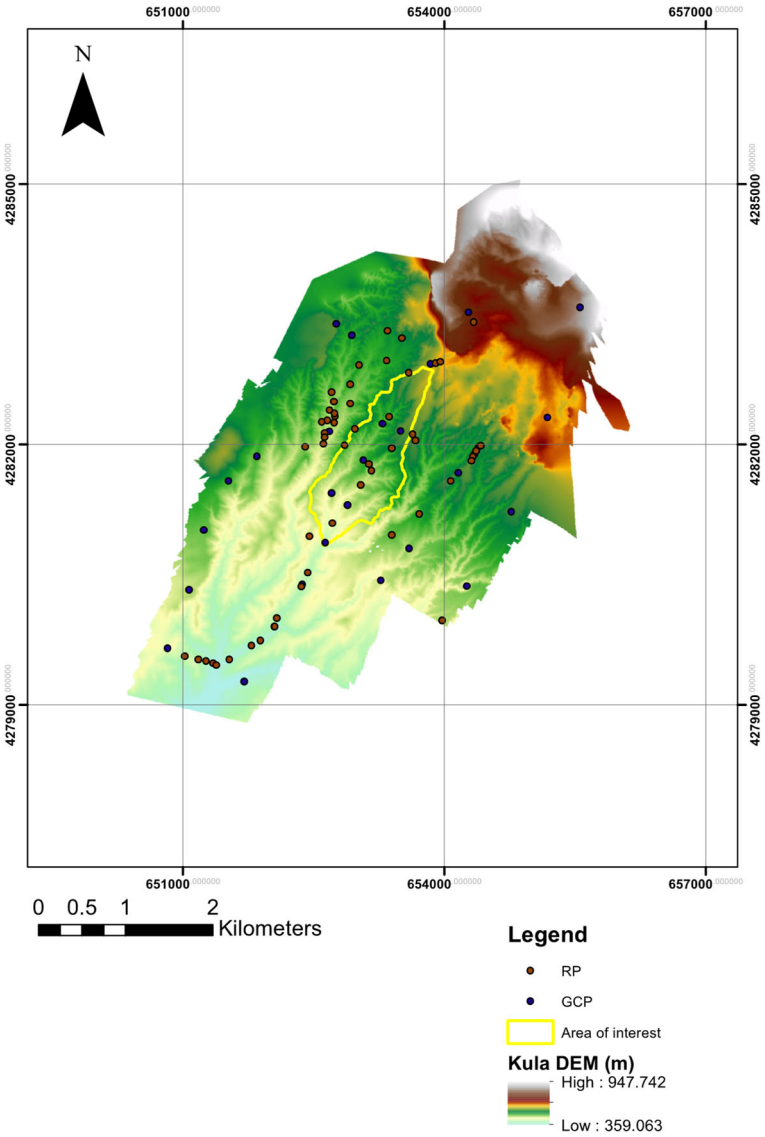

Figure 14 Deterministic DEM without vegetation

DEMs with a resolution of 2.5, 5, 10, 20 m were created. To compare how different the DEM errors are depending on the resolution, the mean error and standard deviation and the RMSE were calculated, the data are given in Table 3. The table shows that the mean error for GCPs varies from -0.064 m to 0.241 m and the coarser the resolution, the smaller the mean errors, but it is worth noting that the standard deviation is maximum at a resolution of 20 m and is 1.921 m. A similar situation is typical for RP, the mean error varies from 0.490 m to 0.909 m, and the mean error decreases with coarser resolution. The standard error deviation for the RPs is also maximum at a resolution of 20 m and is 3.022 m. According to paper Temme et al. (2009) RMSE for GCPs

and RPs were calculated. For GCPs lowest RMSE is for 10 m DEM resolution - 1178.310 m, For RPs lowest RMSE is for 5 and 10 m DEM resolution – 2757.221 and 2757.642 m respectively.

Table 3 Mean error, RMSE and standard deviation of the 4 different resolution DEMs for the GCPs and RPs

Parameter	DEM resolution			
	2.5 m	5 m	10 m	20 m
Mean error for GCP (m)	0.241	0.236	0.149	-0.064
Standard deviation of error for GCP (m)	1.456	1.521	1.306	1.921
RMSE for GCP (m)	1.475	1.539	1.314	1,922
Mean error for RP (m)	0.909	0.870	0.710	0.490
Standard deviation of error for RP (m)	2.926	2.865	2.910	3.022
RMSE for RP (m)	3.038	2.969	2.969	3.034

Error was calculated as the determinstic DEM elevation minus the GCP or RP elevation, so negative signify the DEM underestimation, and positive error signify the DEM overestimation (Holmes et al., 2000).

As a result of the analysis of the resulting DEM quality of the study area, a small but complete sub-catchment was selected. For the sub DEM of the area of interest there are no DEM gaps and it is not prone to erosion from watersheds in the neighborhood. The area of interest is shown in Figure 15. The height of the sub-catchmnet DEM of the area of interest ranges from 413 to 586 m.

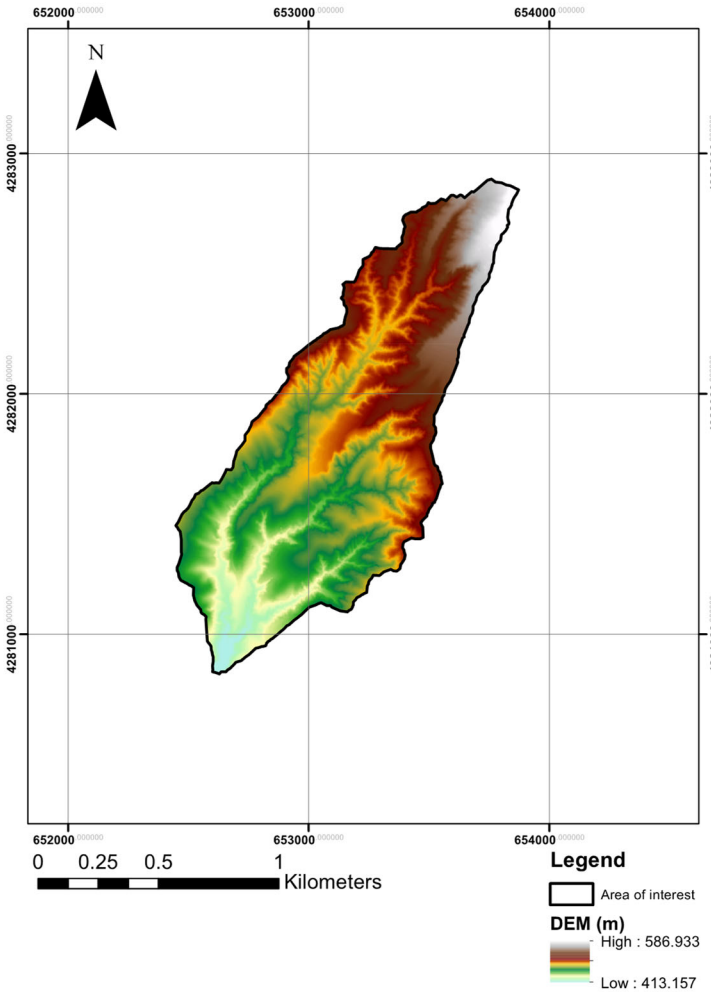

Figure 15 DEM of the sub-catchment used for the Error DEM and LEM simulations

3.2. Results of DEM simulations

As a result of the stimulation of the first and second types of DEM errors in space, 1000 DEM simulations were obtained, 500 simulations for each type of error and 125 simulations for each resolution, respectively.

Each simulation of a DEM error, as described in the methodology section, was added to the deterministic DEM with the appropriate resolution. Thus, 1000 simulated error DEMs were obtained. DEM errors are usually spatially autocorrelated — when the true elevation at some location is overestimated in the DEM, then the elevation at a neighboring location will also be overestimated (Temme et al. 2009). Figure 16 shows an example of an error DEM simulation, indicated with 3 maps, with 1) the deterministic DEM with a resolution of 2.5 m, 2) a spatial simulation of the first type DEM error for the resolution of 2.5 m, and 3) the sum of the deterministic DEM and the first type DEM error. It should also be noted that in the third map there are no sinks. The difference between deterministic and simulated DEM is poorly seen on maps of this scale.

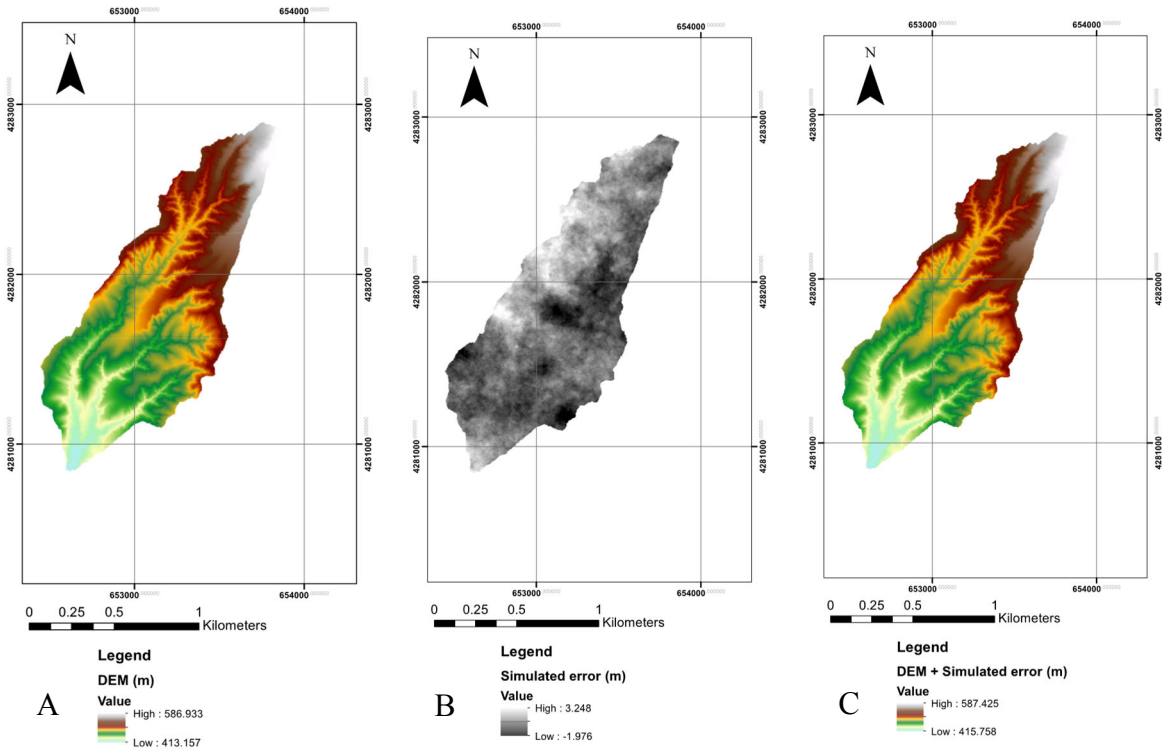

Figure 16 with A - Deterministic DEM (resolution 2.5 m), B - Simulated error of the first type for resolution of 2.5 m and C - Sum of the first type error and deterministic DEM with resolution of 2.5 m.

Kriging maps of the first and second type DEM errors with kriging parameters specified in the methodology chapter were used for the simulation. New error DEMs for 125 simulations for both types of errors were built. The kriging maps for different resolutions and error types are shown in Figure 17 and 18. Mean DEM error maps were constructed to determine the sufficiency of the number of DEM error simulations performed. Data on the mean error for DEM error kriging maps and mean simulated error maps are given in the Appendix (Tables A. 3 and 4 of Annex A). As can be seen from the tables, the mean value of the error between the kriging maps and mean simulated values differs by no more than 0.15 m, the standard deviation also differs slightly, no more than 0.15 m. The smallest differences are observed for simulations of first type of error for the resolution of 20 m. It can be argued that the 125 simulations of first and second types of DEM errors for all 4 types of DEM resolution in this study were sufficient to assess the impact of DEM errors on the erosion and sedimentation (Temme et al. 2009).

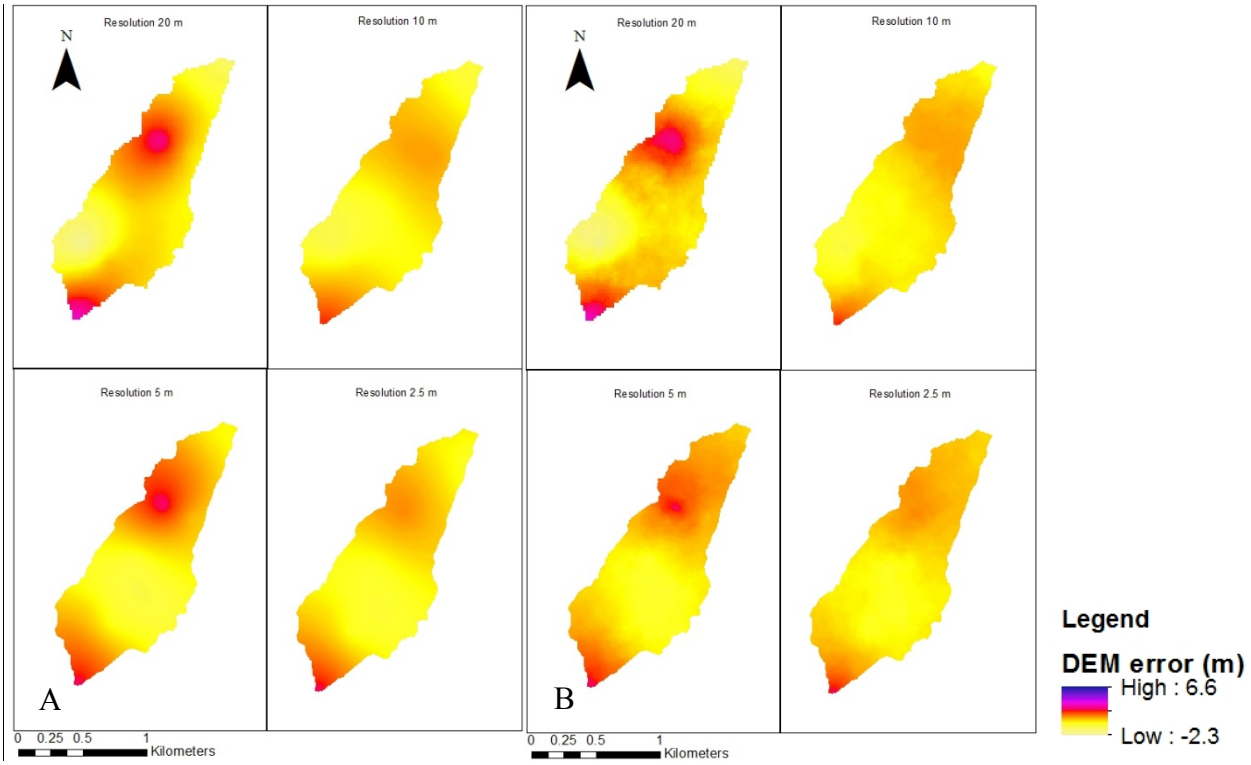

Figure 17 with A - Kriging maps of first type of DEM error for the 4 resolutions, B - Maps of the mean simulated error for 125 simulations of first type of DEM error for the 4 resolutions

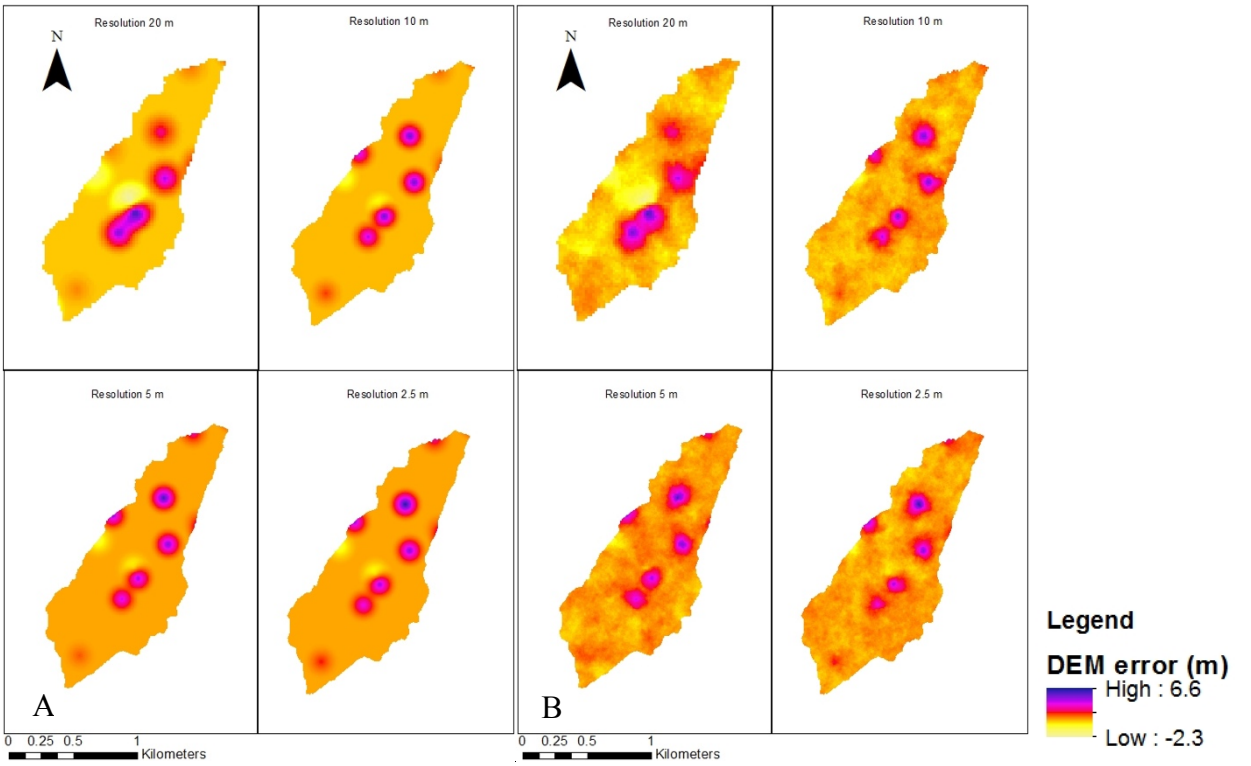

Figure 18 with A - Kriging maps of second type of DEM error for the 4 resolutions, B - Maps of the mean simulated error for 125 simulations of second type of DEM error for the 4 resolutions

3.3. Results of LAPSUS modelling

The processing of the results of LAPSUS modelling was carried out in R Studio. This chapter will summarize the simulation results in LAPSUS for the 4 scenarios described above for each of the 1000 simulated DEMs. These data, in the author's opinion, call for the greatest interest and are the basis for discussion and conclusions.

3.3.1. On cumulative net erosion for simulated DEMs

Data on mean annual cumulative net erosion obtained from deterministic DEMs and on the basis of simulated error DEMs are given in the Appendix (Table A. 8, A.9 of Annex A). Based on the data, cumulative net erosion graphs were made (see figures A. 1 - A. 8).

The graphs of Figure 19 and A. 1 clearly shows how the cumulative erosion varies over 10 years, depending on the resolution for different types of DEM errors. For the L-scenario and LCL scenario, the highest erosion is observed for the 20 m resolution DEM and the second type of error, and the lowest erosion is observed for the 2.5 m resolution DEM and also the second type of error. Whereas for the H-scenario and HCL-scenario, the highest erosion is observed for the DEM also with a resolution of 20 m but with the first type of error, and the lowest erosion - for the DEM with the lowest resolution of 2.5 m and also the first type of error.

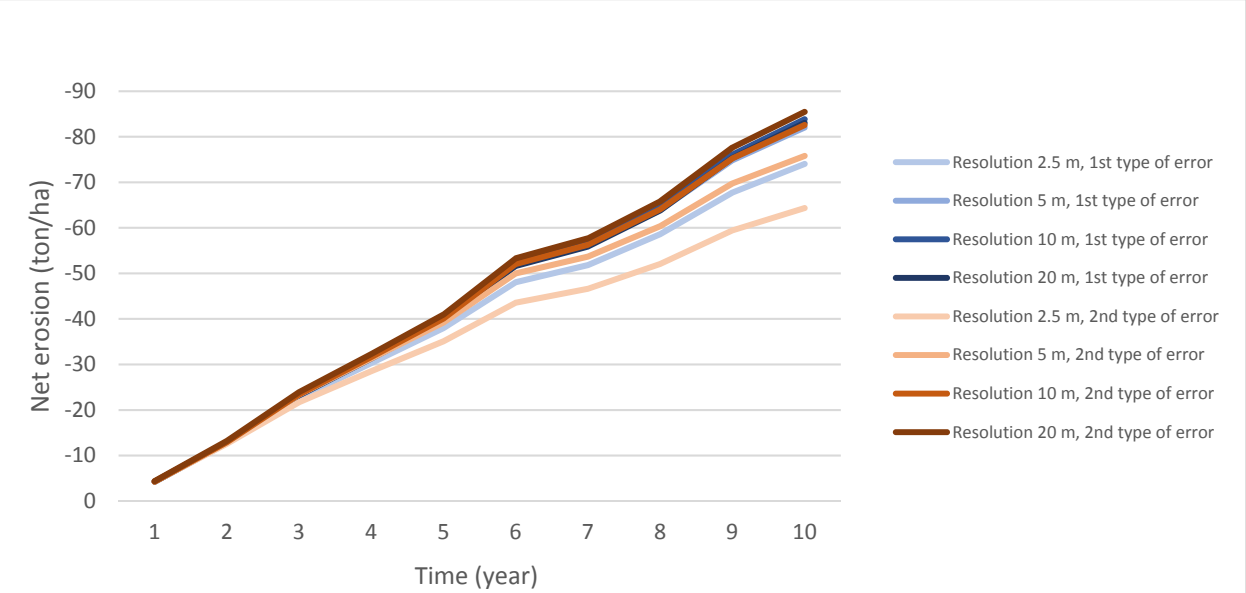

Figure 19 Mean cumulative net erosion based on simulated DEMs for LCL-scenario

In any scenario, the maximum erosion is observed for resolution of 20 m, whereas the minimum erosion is always at a resolution of 2.5 m. When predicting erosion, it should be taken into account that the erosion rates will be less when using the coarsest resolution.

From Table 4 it can be seen that the difference of the cumulative net erosion over the 10 years between scenarios with a resolution of 20 and 2.5 m. Lowest difference can be seen for L scenario with first type of DEM error - 1.112 m, biggest difference can be seen for HCL scenario based on deterministic DEM - 395.625 m.

Net erosion based on deterministic DEMs gives the greatest discrepancy for H-scenario and HCL-scenario compared to simulated scenarios. Whereas for the L-scenario and LCL-scenario, the net erosion spread based on deterministic DEM is closer to the net erosion spread based on DEM with first type of error.

Table 4 Variations of cumulative net erosion over 10 years depending on the simulation scenario.

Scenario	Difference of the cumulative net erosion over the 10 years between scenarios with a resolution of 20 and 2.5 m		
	Simulated error DEMs		Deterministic DEM (ton/ha)
	With first type of error (ton/ha)	With second type of error (ton/ha)	
L	1.112	5.876	1.338
H	213.754	206.534	239.472
LCL	9.008	21.124	9.803
HCL	349.739	316.826	395.625

The DEM error affects the net erosion spread depending on the resolution of the DEM only at low erosion in the study area. If erosion is higher, less important the DEM accuracy becomes.

I would also like to focus on the point that the trend of cumulative net erosion is different for each scenario. Thus, in LCL and HCL scenarios, the influence of precipitation is clearly expressed. While in the scenarios L and H, the trend of cumulative erosion is reversed. This is most evident in figure A. 2 and A. 6, where the trend change is clearly observed, the finer the DEM resolution is, the earlier the trend of cumulative erosion decreases. Moreover, figures A. 1 and 5 show that the trend change is insignificant for all resolution sets.

3.3.2. On the sediment delivery ratio in the area

The data on the sediment delivery ratio (SDR) were then analysed. It should be noted that the SDR indicator shows the ratio of the eroded materials that are transported out of the catchment to the total of all erosion in the catchment. SDR is the sediment delivery ratio, which is the fraction of erosion that is transported out of the catchment (Lesschen et al. 2009).

Therefore, with a decline in SDR, we expect to observe an increase in sedimentation in the area of interest. The graphs were drawn only for H and HCL scenarios (see Figure 20 and Figure 21), since for low erosion scenarios (L and LCL) the SDR fluctuated closer to 1.00 for each year (see table A. 8), it means that L and LCL scenarios are detachment limited. In Figure 17 the SDR graph is complicated by changes in precipitation, therefore, there are fluctuations in the SDR since the 6th year of modeling in LAPSUS.

Thus, it is possible to tell definitely that for scenarios H and HCL for DEMs with the resolution of 2,5 and 5 m, sediment deposition from the 2nd and 4th years of modeling is observed respectively.

The minimum SDR of about 0.45 for scenario H at the resolution of 2.5 m is achieved on the 5th year of simulation in LAPSUS, further the SDR increases and stabilizes at the level of about 0.65. The minimum SDR of about 0.75 for scenario H at 5 m resolution is achieved in the 8th year of simulation in LAPSUS and stabilizes at 0.75. For the HCL scenario, the SDR depends on fluctuations in precipitation. The finer the resolution is, the earlier the SDR starts to increase.

It is also worth noting that the finer the resolution is in these scenarios, the larger the deposition of material becomes in the study area.

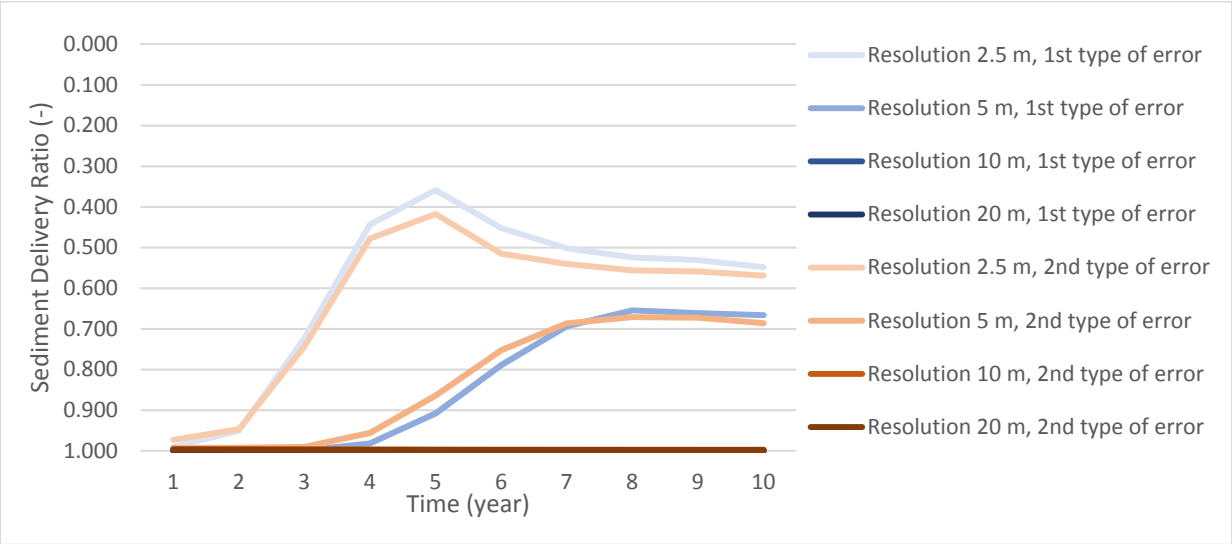

Figure 20 Sediment Delivery Ratio based on simulated DEMs for H-scenario

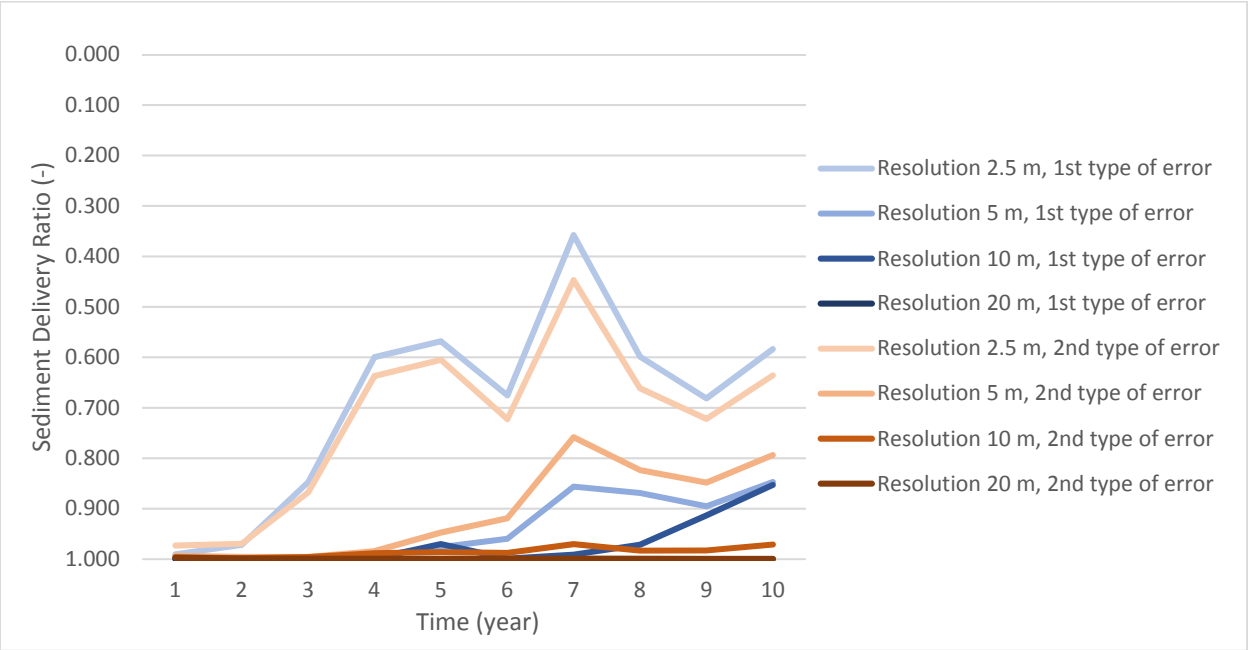

Figure 21 Sediment Delivery Ratio based on simulated DEMs for HCL-scenario

3.3.3. Changes in sediment deposition over time

Sediment deposition and standard deviation of material deposition are representative indicators of how the LAPSUS model responds to different scenarios. In the Appendix (Figures A. 9 - A. 40) all deposition charts are shown with standard deviation for all scenarios, for each type of DEM error for each type of resolution. The charts also show the deposition for the deterministic DEMs. On the charts, you can see the effect of adding a DEM error on material deposition.

The results from the L-scenarios show that the error of the second type affects the mean deposition much more than the error of the first type (see Appemdix Figures A. 9 - A. 16). In all scenarios the deposition based on the deterministic DEM is less than the deposition based on the simulated error DEMs. It is also worth noting that at the DEM resolution of 2.5 and 5 m, deposition decreases over time, while at the DEM resolution of 10 and 20 m, deposition has a positive trend. This ratio is typical for both simulated error DEMs and deterministic DEM. The same trends are typical for LCL-scenarios (see Appendix Figures A. 25 - A. 32. One exception to note is shown in Figure 22, at a resolution of 2.5 m and the first type of DEM error from 6th to 10th year, the simulated sediment deposition starts to behave differently, namely, the standard deviation is much higher than in previous years.

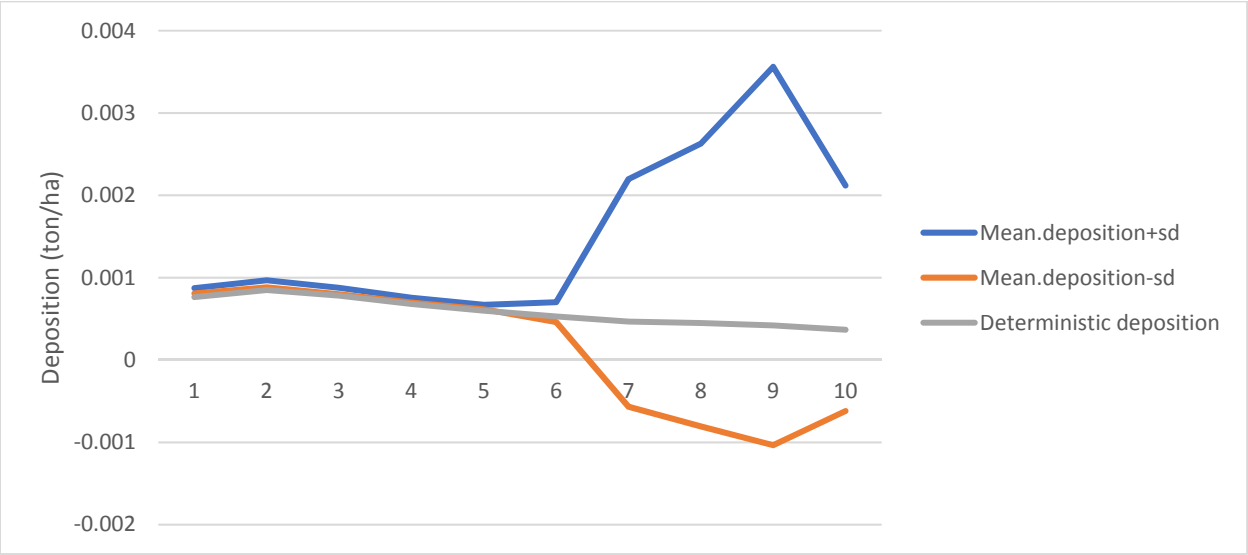

Figure 22 Deposition and standard deviation for DEM with resolution of 2.5 m, 1st type of error for LCL-scenario

The charts for the H-scenarios (see Appendix Figures A.17 ... A.24) also show that the error of the second type affects the deposition much more than the error of the first type. In all scenarios, the deposition based on the deterministic DEM is less than the mean deposition of the simulated error DEMs. It is also worth noting that at the DEM resolution of 2.5 m and 5 m, the deposition of material increases over time during the simulation period from 1st to 7th year of modeling. From the 7th year, simulated deposition of material begins to decrease. With the DEM resolution of 10 and 20 m, the deposition of material has a negative trend, this dependence is typical for both the simulated error DEMs and the deterministic DEM. The same trends are typical for the HCL scenario (see Appendix Figures A.33 - A.40).

The standard deviation of sediment deposition for the 10th year of modelling in LAPSUS was also evaluated for each simulation scenario and for each resolution. For L and LCL scenarios, the total deposition for each year is close to zero. While the H and HCL scenarios are characterized by quite noticeable amounts of re-sedimentation. Figure 23 and Figure 24 show the mean deposition from 125 simulations and the standard deviation of this deposition. Again there are high deposition rates for 2.5 and 5m resolutions for the H scenario. Moreover, at the DEM resolution of 2.5 m, the material deposition is by 6-7 tons/ha more than at the resolution of 5 m. Furthermore, it is worth noting that the standard deviation at the resolution of 10 meters significantly exceeds the standard deviation for a resolution of 5 m. The situation is the same for the first and second types DEM errors. Curiously, for the HCL scenario, rather a high deposition is characteristic for the resolution of 2.5, 5 and 10 m. There also is a trend for reducing sediments as the DEM resolution decreases (Schoorl et al., 2000). The standard deviation of material deposition over the 125 simulations is still the biggest for the resolution of 5 m. The situation is the same for the first and second types of errors.

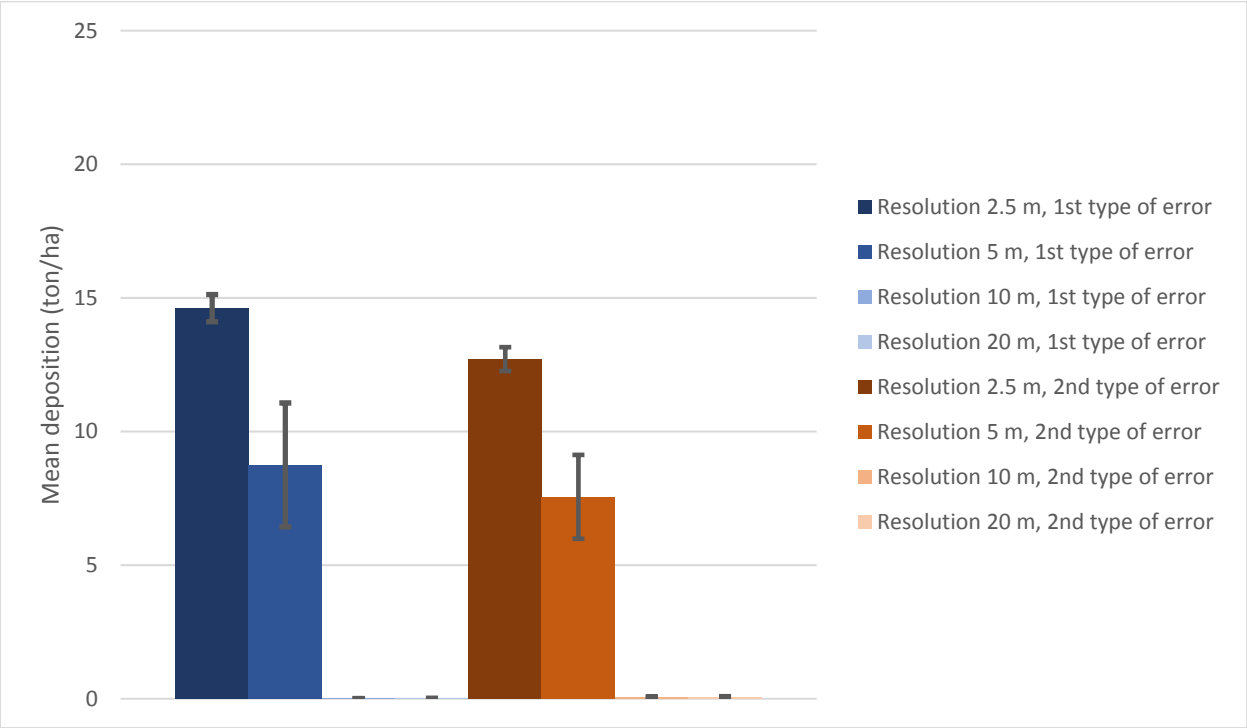

Figure 23 Mean deposition and SD based on simulated error DEMs for 10th year for H-scenario

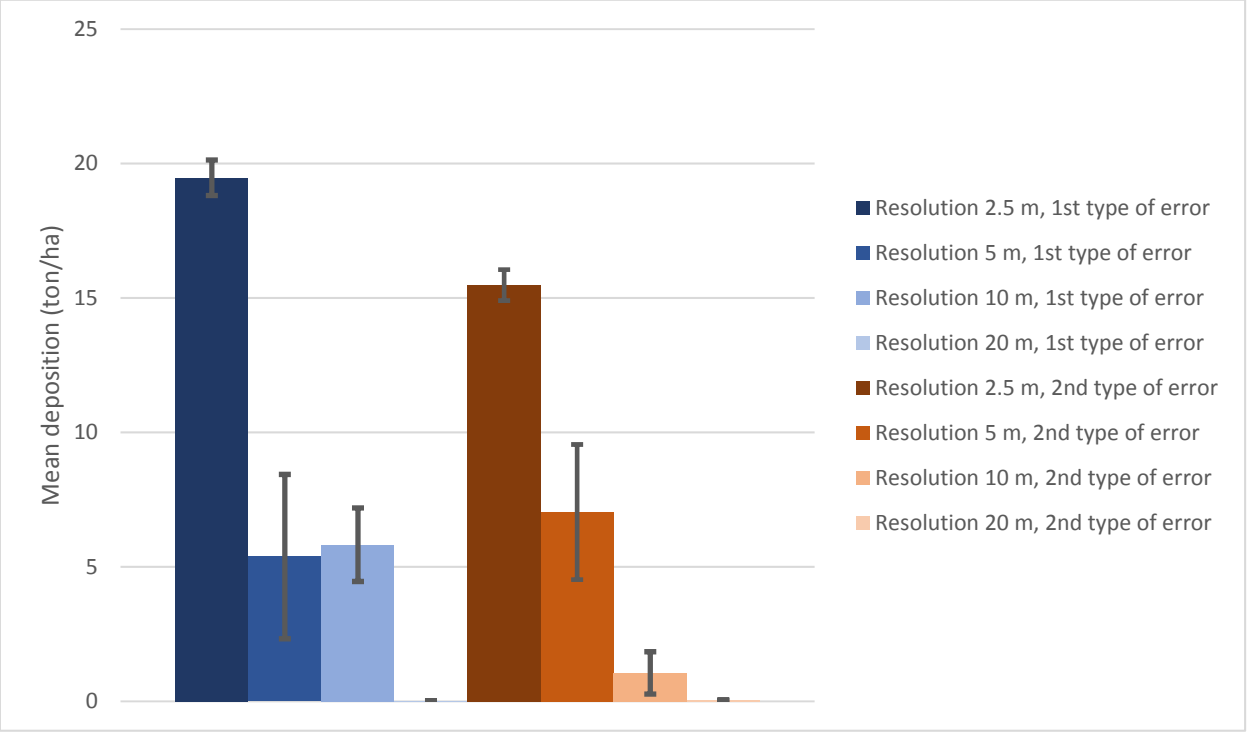

Figure 24 Mean deposition and SD based on simulated error DEMs for 10th year for HCL-scenario

3.3.4. Spatial distribution of erosion and deposition

Let us consider the distribution of the mean for 125 cumulative erosion and deposition simulations for the L scenario. When comparing maps with the first and second type errors, it is seen that there is more spatial erosion differences (see Figure 25). It is also true for both types of DEM error that with increasing resolution, there is an increase in erosion in space. The largest amounts of erosion are characteristic for the bottoms of the gullies.

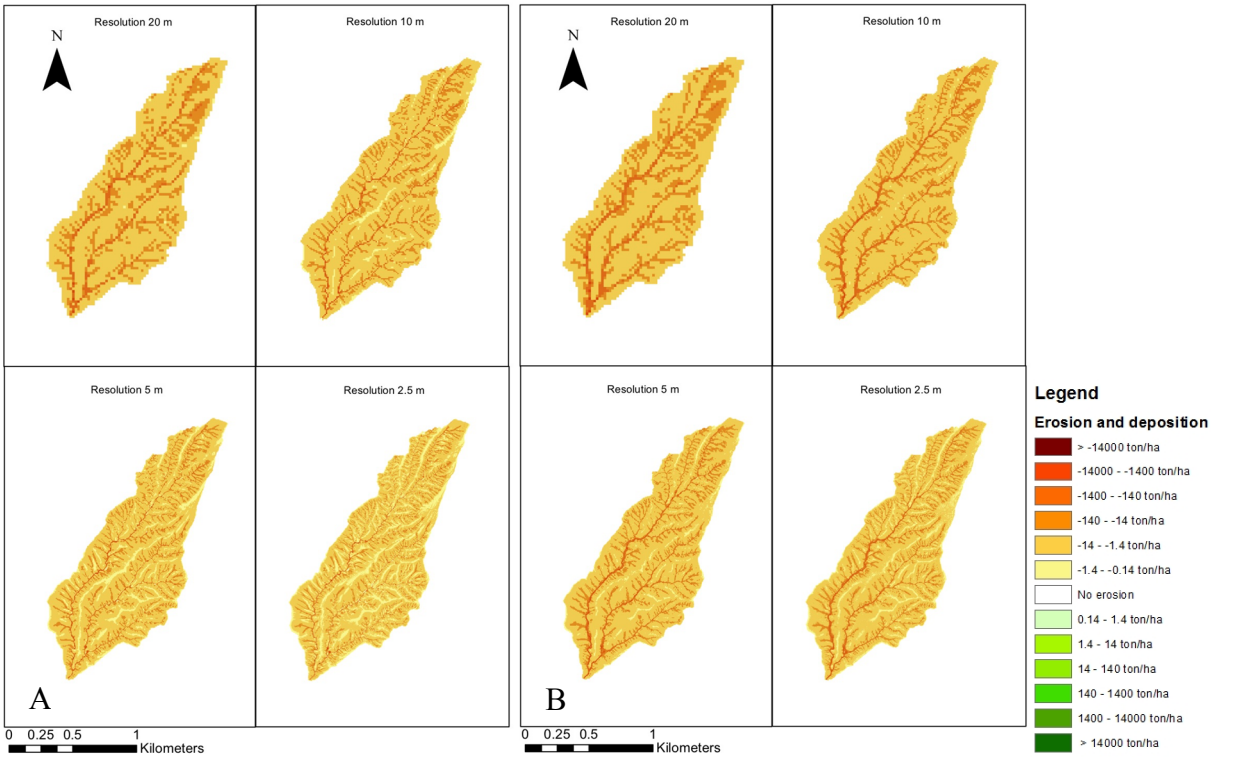

Figure 25 with A - Maps of mean net erosion for the 10 years of simulation for the L scenario with the first type error, B - Maps of mean net erosion for the 10 years of simulation for the L scenario with the second type error

Next, let us consider the distribution of the mean for 125 simulations cumulative erosion and deposition of material for the H scenario (see Figure 26). It should be noted that there is more distribution of erosion in space in the second type of DEM error. For both types of DEM errors, erosion also increases as resolution increases. Another interesting observation to mention is that there is sedimentation at the bottom of the ravines at 2.5 and 5 m resolution DEMs whereas no sedimentation is observed at all at 10 and 20 m resolution DEMs. It should be noted that the sedimentation area is larger for the lowest resolution - 2.5 m.

Figure 26 with A - Maps of mean net erosion for the 10 years of simulation for the H scenario with first type error, B - Maps of mean net erosion for the 10 years of simulation for the H scenario with second type error

The distribution of the mean for 125 simulations cumulative erosion and deposition for the LCL scenario is similar to the L scenario (see figure A.43 and A.44)

The distribution of the mean for 125 simulations cumulative erosion and deposition for the HCL scenario (see figure A.43 and A.44) is similar to the H scenario. The smaller sediments deposition for scenarios with a resolution of 5 m should be noted.

The distribution of cumulative erosion and deposition for the deterministic DEM (see Figure 27) follows the same patterns as for the simulated error DEMs. Thus, erosion increases with increasing resolution, and the highest erosion rates are observed at the bottoms of ravines except for scenarios with high erosion (H and HCL scenarios), where there is deposition of material at the bottoms of ravines at the resolution of 2.5 and 5 m. Moreover, in the H and HCL scenarios, the deposition is greater at the resolution of 2.5 m than at the resolution of 5 m.

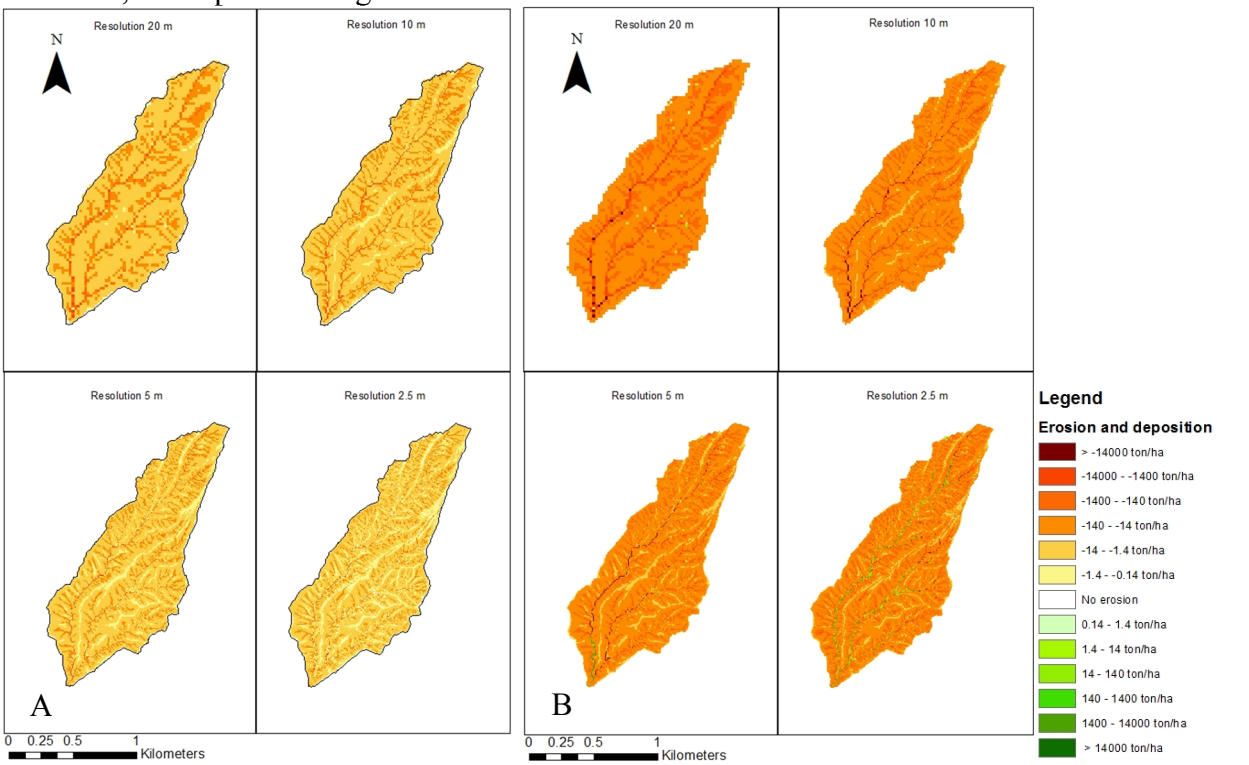

Figure 27 with A - Net erosion maps over 10 years of simulation for the L scenario based on the deterministic DEM, B - Net erosion maps over 10 years of simulation for the H scenario based on the deterministic DEM

Some statistics on the erosion maps for mean erosion of the simulated DEM and the erosion maps of the deterministic DEM, which include: high erosion, standard deviation of erosion and deposition and maximum erosion maximum deposition (see tables A. 5 and A. 6). It should be noted that the maximum erosion per pixel in any scenario is observed at the DEM resolution of 2.5 m, and when the DEM resolution decreases, the maximum erosion decreases, too.

3.3.5. Comparison of cumulative erosion in the deterministic and the simulated DEM scenarios

In order to determine the effect of first and second types of DEM errors on absolute erosion and deposition numbers, a map of the differences between the erosion maps based on the deterministic and the simulated error DEMs was drawn. The least difference between erosion and sediment is typical for low erosion scenarios (L and LCL scenarios). In the same scenarios, the greatest difference is observed in the second type of error (see Figure 28). For all scenarios, the greatest difference in erosion and deposition is observed at the bottoms of gullies.

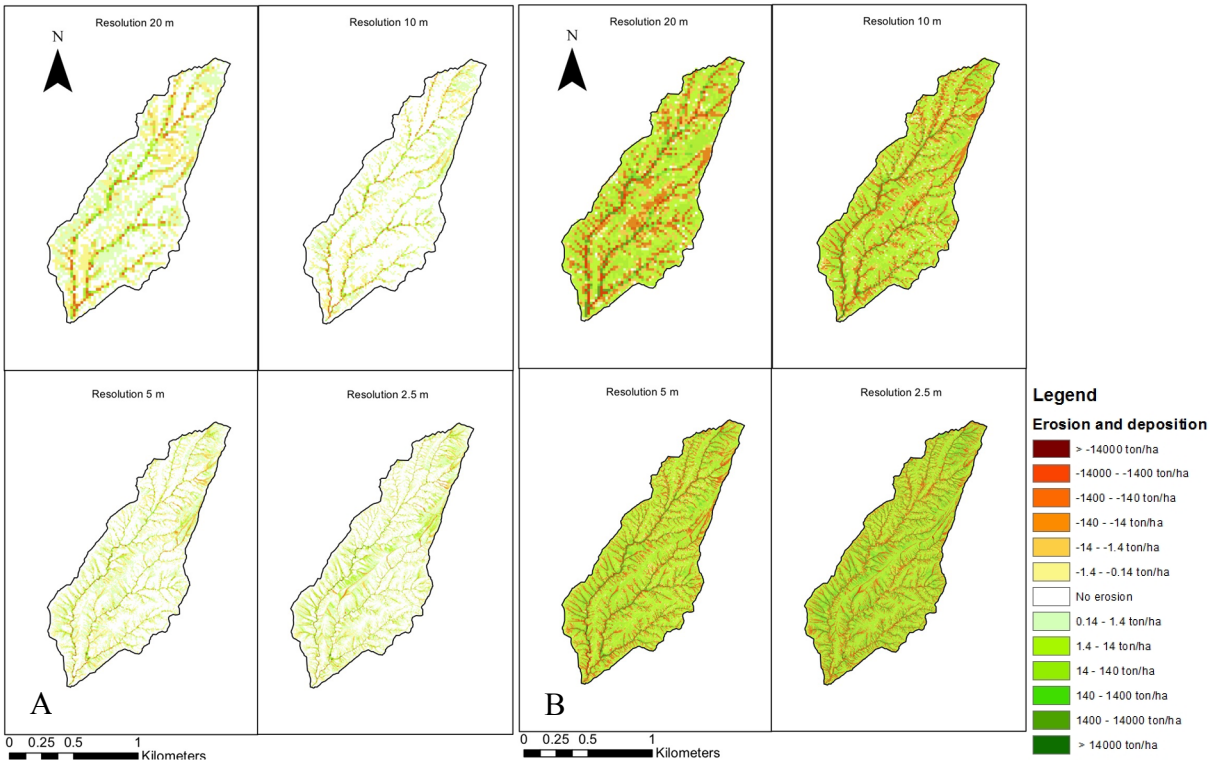

Figure 28 with A - Net erosion difference maps between the deterministic DEM scenarios and the DEMs with the first type of error for the L scenario, B - Net erosion difference maps between the deterministic DEM scenarios and the DEMs with the first type of error for the HCL scenario

3.3.6. RMSE erosion and deposits over 125 simulations in LAPSUS

RMSE (Root-mean-square error) erosion and sediment maps (see Figure 29) were constructed to assess the impact of the first and second types errors DEM on erosion and deposition.

Mean RMSE erosion and deposition ranges from 16.177 to 854.116 ton/ha (see Figure 30 and Figure 31). The smallest mean RMSE is observed for the L and LCL scenarios from 16.177 to 171.742 ton/ha (see table A.7). Moreover, for all scenarios, the lowest mean RMSE erosion and deposition is typical for scenarios with first type of DEM error. Mean RMSE erosion and deposition is minimal for the DEM resolution of 10 m. Minimum mean RMSE erosion and deposition of 16.177 ton/ha was observed in the L scenario for first type of DEM error for the resolution of 10 m. But for second error type of DEM minimum mean RMSE erosion of 54.478 ton/ha was observed in the L scenario for the resolution of 20 m.

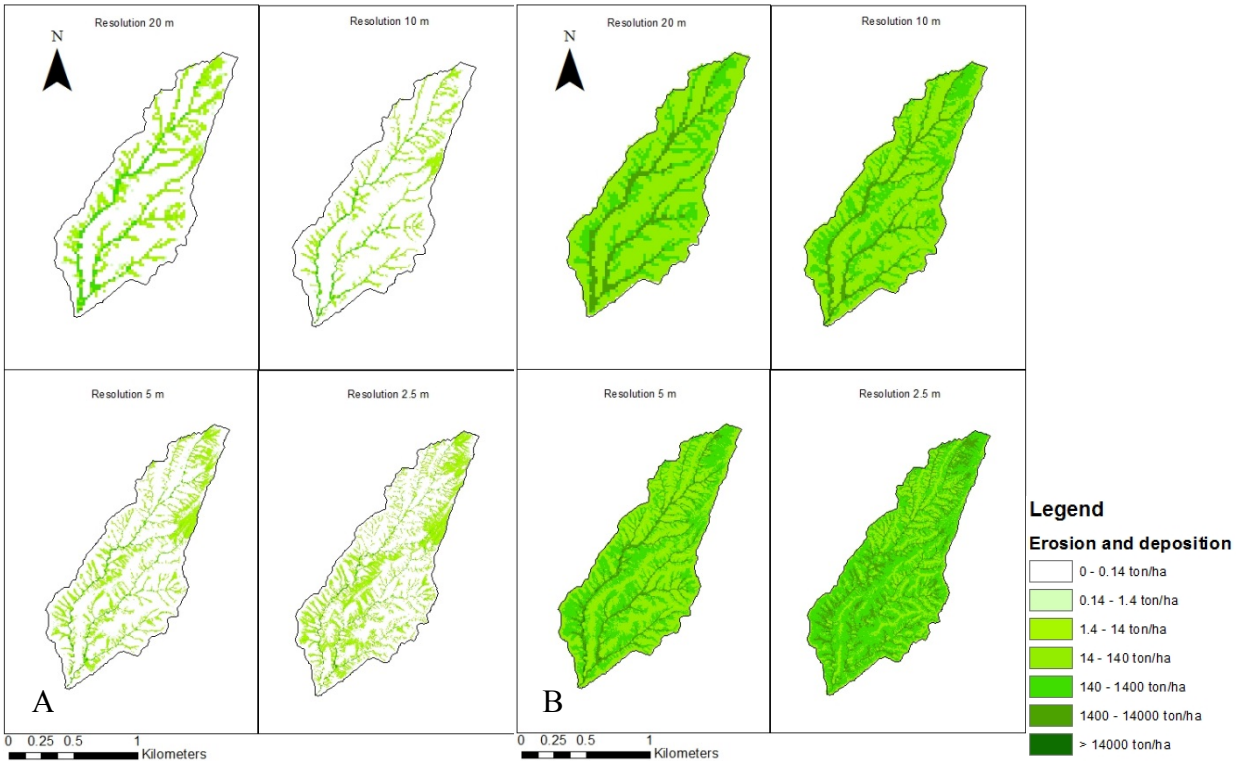

Figure 29 with A - Maps of the RMSE of erosion and deposition with 1st type of error for L scenario, B - Maps of the RMSE of erosion and deposition with 2nd type of error for HCL scenario

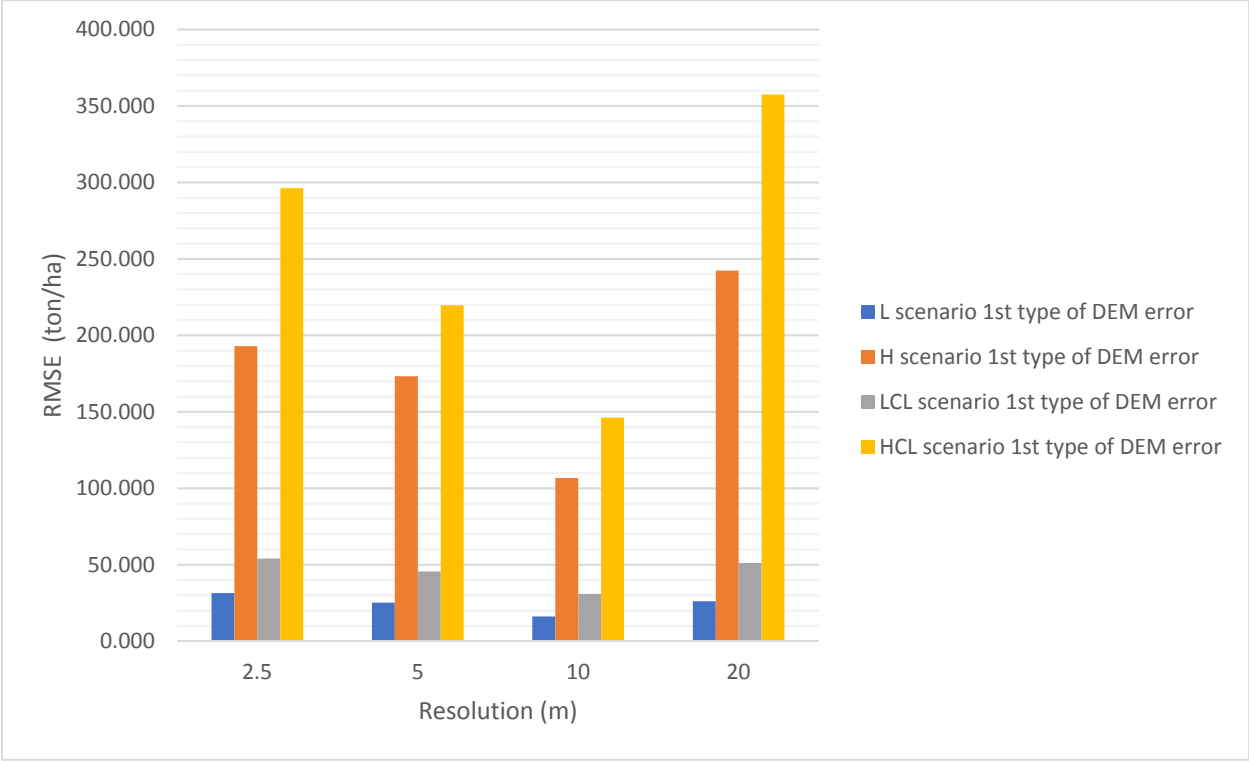

Figure 30 Mean RMSE of erosion and deposition of 125 simulations for the 1st type of DEM error

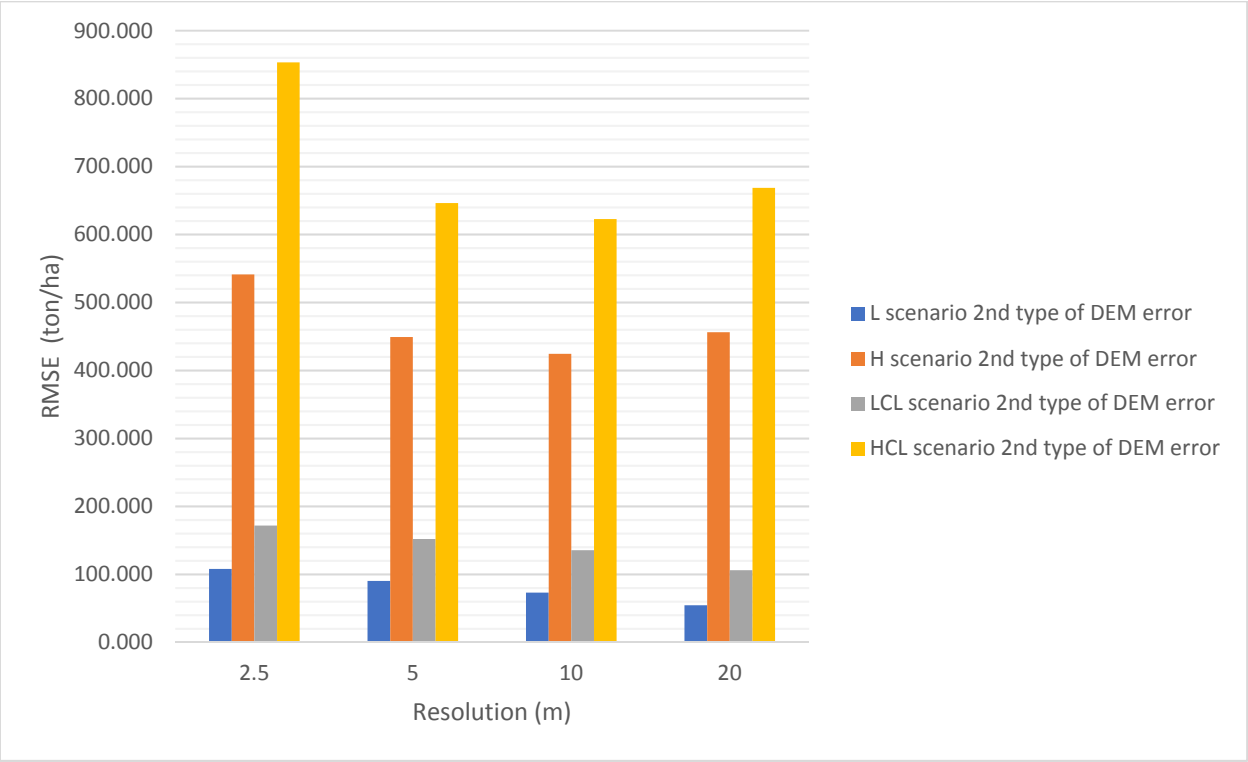

Figure 31 Mean RMSE of erosion and deposition of 125 simulations for the 2nd type of DEM error

4. Discussion

During processing of raw DEM with a high resolution and modeling the evolution of the landscape based on this DEM, taking into account the DEM error, crucial results were obtained, some of them should be analyzed in detail and the possible origin of the results obtained should be revealed.

One of the problems in the building the DEM for the study area was insufficient overlap and sidelap of images (see Figure 10 and Figure 11). The problems with overlapping were caused by strong wind and problems with trigering mechanism of the photocamera. The problem with overlapping images can be solved by repeating flight missions with better meteorological conditions. Since none of these options could be used during the studies, we were forced to significantly cut the DEM used for modeling in LAPSUS. Nevertheless, the area of interest was sufficient to produce representative results in this study.

Another important aspect that strongly affects the DEM accuracy is vegetation. Some authors (Vlachos and Skarlatos, 2018) argue that AgiSoft PhotoScan is capable of eliminating vegetation from the DEM at a satisfactory level. In my opinion, this problem requires additional research that would be able to prove the ability of the AgiSoft PhotoScan program and the like to eliminate vegetation. The result of the accuracy should correspond to the results of studies conducted using LiDAR technology, which has proven itself.

It should be noted that 125 simulations conducted were sufficient to assess the impact of the DEM error. In tables A. 3 and A. 4 it is noted that the standard deviation for 125 simulations of the DEM error differs by no more than 0.15 m from the DEM error obtained by the kriging method. Extreme values (DEM maximum and minimum errors) do not differ more than 0.1 m. From the Figure 17 and Figure 18 it can be seen that the spatial distribution of DEM errors varies. It should be noted that there is noise on the simulated error map. The statement is consistent with the results of the work by Raaflaub et al. (2006), which states that if the change in the standard deviation is insignificant, the addition of new DEM simulations will not provide any new information. Therefore, any new DEM simulations after this point will be unnecessary. It is also worth noting that the spread of the DEM error was taken for the entire research area, because it gave the necessary number of points for kriging. If there were enough GCPs and RPs in the area of interest, it would give completely different semivariograms and according a completely different distribution of the DEM error in space. This is consistent with the work by Sunila and Virrantaus (2011), which states that simulating a semivariogram is an important step in kriging interpolation. Semivariogram models can be built on the basis of all points where the height was measured or only on the basis of points within the study area. Of course, we are interested in understanding how the DEM error is spatially distributed within the study area, but unfortunately the amount of data is not sufficient to build a semivariogram of the area of interest which the LAPSUS modeling was carried out on, as claiming in article of Cameron and Hunter (2002) at least 30-50 data points are recommended for kriging.

I would also like to dwell on the results associated with the difference in erosion and deposition, depending on the terrain error. Despite the fact that the second type DEM error is bigger, erosion both in bottom-line figures and on the distribution maps is lower. This statement is true for all scenarios. This can be explained by the fact that the elevation gradient became relatively smaller than the elevation gradient for fist type error scenarios. Figure 17 and Figure 18 show the spatial distribution of the error of the first and second types. If we compare this distribution with maps of the erosion and deposition difference based on the deterministic DEM between average erosion and deposition based on the simulated DEM, we can see that for resolutions of 10 and 20 m for the first type error, areas in the south and north-east are quite distinct, where the difference in scenarios is much higher than in other areas. This change in erosion could be caused by an increased gradient due to the DEM error addition.

The simulations created are only a presumed reality. Adding an error does not create true terrain. But the created deterministic DEM looks more smoothed than the reality. Because the deterministic DEM is only a reproduction of the real terrain and cannot be considered absolutely

correct terrain model. This is confirmed by the results of Temme et al. 2009, who state that the deterministic DEMs are smoothed representations, which are also not completely untrue. The potential problem with Monte Carlo error simulation described in Temme et al. 2009 is that it does not preserve the spatial structure of the landscape, but at the same time DEM errors are spatially correlated.

It should be noted that DEM errors of the first and second types increase erosion and deposition in the study area in absolute numbers. The simulated DEMs are more characterized by relatively high sediment deposition than the deterministic DEMs, but this can be explained by the fact that the DEM error leads to the unnatural terrain shape formation, whereas in the simulation of erosion and deposition in LAPSUS, the terrain begins to take on more natural shapes. This statement is largely consistent with the results by Temme et al. 2009, which indicate that the simulated DEMs form not natural landscape.

The results of erosion and deposition modelling for LCL and HCL scenarios are generally similar to those for L and H ones, respectively. However, it should be noted that for the LCL and HCL scenarios, values were taken from the climate model (Climate4impact Infrastructure for the European Network of Earth System Modelling, 2018) and the dataset was averaged for a 44 km by 44 km area. Thus, the average annual precipitation for these scenarios was 1123 mm and evaporation was 229 mm, while for the L and H scenarios the average annual precipitation was 700 mm and evaporation was 209 mm. From the above figures it becomes clear why the erosion figures for the LCL and HCL scenarios were higher than for the L and H scenarios respectively. So we can clearly see in the figures (figures 24, 25, A.42, A.43) that the LAPSUS model forms the transport limited conditions (erosion) for scenarios with increased precipitation.

Among the four scenarios, two scenarios, L and LCL, were calibrated with net erosion of 4.25 ton/ha/year. These scenarios were designed to demonstrate the behavior of erosion and deposition depending on the DEM error for conditionally natural conditions. The L and LCL scenarios are characterized by detachment limited conditions (see figures 23, 25, A.41, A.43). In the L and LCL scenarios, gullies are most susceptible to erosion processes which was expected. The H and HCL scenarios with 10 times greater erosion (42.5 ton/ha/year) were expected to show an extreme erosion, where the transport limited conditions (i.e. deposition of material) are more visible compared to other scenarios. The amount of eroded material is greater, therefore more water is needed to move this material. Indeed, the transport limited conditions are visible in the gullies, but only for the DEM resolution of 2.5 and 5 m (figures 24, 25, A.42, A.43). And this distribution is typical for both types of DEM error. Moreover, there is no sediment deposition at 10 and 20 m resolution for the H and HCL scenarios. The above is an indication of the impact of the DEM resolution on the sediment and erosion distribution for transport limited conditions. So it is worth saying that such sediment distribution is typical for the deterministic DEM. Thus, it is possible to say that for the DEM with the resolution of 2.5 and 5 m, small areas of less than 100 m^2 can be formed where transport limited conditions are possible. Such sites can be flattened areas of gullies. Moreover, it is worth noting that the areas with transport limited conditions for the resolution of 2.5 m occupy a larger area than for the DEM resolution of 5 m. This may be due to the fact that the probability of the flattened areas formation for high resolution is much higher.

Differences in cumulative net erosion trends for different scenarios should be noted. For the L scenario, the trend of net erosion is the same for all resolutions and error types except the 2.5 m resolution with the second type error, where the trend shows a decrease in net erosion rates on the 6^{th} year of the simulation. For the H, LCL and HCL scenarios, a pattern is seen; the lower the resolution is, the earlier the trend changes to a lower net erosion. This behavior can be explained by the fact that a variety of rough terrains in high resolution are flattened much easier. For the low DEM resolutions (10 and 20 m) surface smoothing takes a greater amount of time in order to blur the terrain roughness. The trends for the simulated and these deterministic DEM are the same.

Until now, the Kula badlands area has not been modeled in such a way that at least its outlines look like existing in reality relief. But it is obvious that the microterrain, which determines

the high dissection of the terrain plays a huge role in the formation of the badlands. In the LAPSUS results, the deposition of material only for a DEM with high resolution (2.5 and 5 m) is observed in the gullies, which was observed in the field that there are spots with re- deposed sediments. So it is possible to assume that DEM resolutions of 2.5 and 5 m are modelling erosion and deposition more naturally, but more field studies are needed to confirm that statement. Moreover, it is must be taken an account that described situation fair only for short term simulations of the erosion and deposition, and for longer timescale modeling re-deposition of the sediments matter less (van Gorp et al. 2014, van Gorp et al. 2015).

Thus, we can say that the erosion and deposition RMSE is the smallest for DEM resolution of 10 m for most of the scenarios (see Figure 30 and Figure 31). It is also worth noting that the RMSE for first type of DEM error is also lower for 10 m resolution, but of second type of DEM error RMSE is lower for 5 m resolution and for 10 m resolution as well (see Table 3). Despite this, in some works, there is an uncertainty in the choice of resolution for modeling. The work by Claessens et. al (2005), which describes the landslides modeling depending on the DEM resolution, does not provide clear and unambiguous criteria for selecting the DEM resolution. The article states that the choice of the DEM resolution may be limited primarily by the data availability, but should always be made in the context of a particular study. Ideally, the DEM should display topographical and hydrological properties in such a way that ignoring features that may have been "filtered out" (i.e. lost) would not harm the quality of the DEM. The work by Schoorl et al. (2000) claims that the DEM with the highest resolution should be used for modeling sites with the sedimentation deposition, and a lower DEM resolution should be used to model more realistic landscape development for larger areas. Based on the abovementioned arguments, it can be stated that the most optimal DEM resolution for modeling erosion and deposition is a DEM with a resolution of 10 m.

Conclusions

This research was conducted to understand the impact of the DEM error and resolution on changes in the LEM erosion and deposition in the study area of Kula badlands.

Following the fieldwork for aerial photography using UAVs, the raw DEM of the studied area of the Kula Badlands was created. Unfortunately, due to the loss of some data, the DEM did not fully cover the study area, repeated aerial photography of the Kula badlands will be carried out in the course of further studies. It is also worth noting that the method of vegetation elimination used in this study is not perfect, as a result of which an additional inaccuracy was introduced in the DEM, which was not taken into account in this study. In order to further improve the quality of work on the DEM building, it is necessary to conduct the field work with the help of LiDAR or conduct the field work to classify vegetation by height and further eliminate the vegetation from the DEM, taking into account the data obtained.

The DEM accuracy was assessed by identifying errors in GCPs and RPs. It can be confidently stated that the uneven spatial distribution of the two types of DEM errors changes the terrain gradient, which affects the spatial distribution of erosion and sedimentation.

Based on the calulcated DEM errors, a set of 1000 error DEMs was compiled. The number of simulations was chosen to be sufficient to assess the DEM error impact on erosion and deposition modelling in LAPSUS.

Our hypothesis, the spatial variability of the DEM error and the resolution leads to a significant change in erosion and sedimentation for our study area, could not be falsified. If there is an uneven distribution of the DEM error, the terrain gradient may increase which will lead to increased erosion.

A number of scenarios with different erosion parameters and differences in precipitation and evaporation were selected. It should be noted that the scenarios with increased erosion at high resolutions of 2.5 and 5 m gave a result with re-sedimentation, this is more in line with our on-site observations in the Kula Badlands in comparison to the results of erosion and deposition simulations at lower DEM resolutions. According to the results of this work, the DEM resolution of 10 m is the optimal solution for modeling erosion processes in the territory under consideration, because RMSE of the erosion and sedimentation is the lowest in case of 10 m resolution.

References

Agisoft PhotoScan User Manual: Professional Edition, Version 1.4. (2018). Agisoft LLC

Buis E. and Veldkamp A. (2008). Modelling dynamic water redistribution patterns in arid catchments in the Negev Desert of Israel, Earth Surf. Process. Landforms 33, 107–122

Cameron K. and Hunter P. (2002). Using Spatial Models and Kriging Techniques to Optimize Long-Term Ground-Water Monitoring Networks: A Case Study. Environmetrics, 13:629-59.

Cantreul V., Bielders C., Calsamiglia A. and Degré A., (2018). How pixel size affects a sediment connectivity index in central Belgium. Earth Surf. Process. Landforms 43, 884–893

Claessens L., Heuvelink G. B. M., Schoorl J. M. and Veldkamp A., (2005). DEM resolution effects on shallow landslide hazard and soil redistribution modelling, Earth Surf. Process. Landforms 30, 461–477

Climate4impact, Infrastructure for the European Network of Earth System Modelling (2018). IS-ENES2 project, https://climate4impact.eu

Foster G.R. and Meyer L.D. (1975). Mathematical simulation of up- land erosion by fundamental erosion mechanics. p. 190–207. In Anonymous (ed.) Present and perspective technology for predicting sediment yields and sources. Proceedings Sediment Yield Workshop, Oxford (1972). USDA, Washington D.C..

Foster G.R. and Meyer. L.D. (1972). A closed–form soil erosion equation for upland areas. p. 12.1–12.19. In H.W. Shen (ed.) Sedimentation: Symposium to honour professor H.A. Einstein. Colorado State University, Fort Collins, CO.

Fresco L.O. (1995). Agro–ecological knowledge at different scales. p. 133–141. In J. Bouma et al. (ed.) Eco–regional approaches for sustainable land use and food production. Kluwer Academic Publishers, Dordrecht.

Heineke C., Hetzel, R., Akal, C., & Christl, M. (2017). Constraints on water reservoir lifetimes from catchment- wide 10Be erosion rates—A case study from Western Turkey. Water Resources Research, 53, 9206–9224

Höhle M., Höhle M. (2009). Accuracy assessment of digital elevation models by means of robust statistical methods. Journal of Photogrammetry and Remote Sensing 64, 398–406

Holmesa K.W., Chadwicka O.A., Kyriakidisb P.C. (2000). Error in a USGS 30-meter digital elevation model and its impact on terrain modeling, Journal of Hydrology, volume 233, 154-173

Kale S. (2017). Analysis of climatic trends in evaporation for Çanakkale (Turkey) Middle East Journal science, 3(2), 1-13

Kirkby M.J. (1971). Hillslope process-response models based on the continuity equation. p. 15–30. In D. Brunsden (ed.) Slopes, forms and processes. Inst. of Brit. Geographers, Spec. Pub. Institute of British Geographers, London.

Kirkby M.J. (1987). Modelling some influences of soil erosion, land- slides and valley gradient on drainage density and hollow develop- ment. Catena Suppl. 10:1–44.

Leitão J. P., Vitry M. M. de, Scheidegger A. and Rieckermann J. (2016). Assessing the quality of digital elevation models obtained from mini unmanned aerial vehicles for overland flow modelling in urban areas, Hydrol. Earth Syst. Sci., 20, 1637–1653

Lesschen J. P., Schoorl J. M., Cammeraat L. H. (2009). Modelling runoff and erosion for a semi-arid catchment using a multi-scale approach based on hydrological connectivity. Geomorphology, 109(3-4), 174-183.

Lu X., Li Y., Washington-Allen R.A., Li Y., Li H., Hu Q. (2017). The effect of grid size on the quantification of erosion, deposition, and rill network, International Soil and Water Conservation Research, 5, 241–251

Maddy D., Demir T., Bridgland D.R., Veldkamp A., Stemerdin C., van der Schriek T., Westaway R. (2008). The Early Pleistocene development of the Gediz River, Western Turkey: An uplift-driven, climate-controlled system? Quat. Int. 189, 115–128

Maddy D., Schreve D., Demir T., Veldkamp A., Wijbrans J. R., van Gorp W., van Hinsbergen D. J. J., Dekkers M. J., Scaife R., Schoorl J. M., Stemerdink,C., van der Schriek T. (2015). The earliest securely-dated hominin artefact in Anatolia? Quaternary Science Reviews, 109, 68–75.

Maddy D., Veldkamp A., Jongmans A.G., Candy I., Demir T., Schoorl J.M., van der Schriek T., Stemerdink C., Scaife R.G., van Gorp W. (2012). Volcanic disruption and drainage diversion of the palaeo-Hudut River, a tributary of the Early Pleistocene Gediz River, Western Turkey, Geomorphology 165-166, 62–77

Pohjola J., Turunen J., Lipping T. and Ikonen A. (2009). Creation and Error Analysis of High Resolution DEM Based on Source Data Sets of Various Accuracy, Book 3DGeo-Information Sciences, 437

Raaflaub L. D., Collins M. J. (2006). The effect of error in gridded digital elevation models on the estimation of topographic parameters, Environmental Modelling & Software 21, 710-732

Remondino F., Barazzetti L., Nex F., Scaioni M., Sarazzi D. (2011). UAV photogrammetry for mapping and 3D modeling current status and future perspectives. International Archives of the Photogrammetry, Remote Sensing and Spatial Information Sciences, Volume XXXVIII-1/C22, 2011

Ruzgienea B., Berteskab T., Gecytec S., Jakubauskiened E., Aksamitauskas V. (2014). Photogrammetric Processing of UAV Imagery: Checking DTM, The 9th Conference Environmental Engineering, Selected Papers, 242

Sammartano G. and Spanò A. (2016). DEM Generation based on UAV Photogrammetry Data in Critical Areas, In Proceedings of the 2nd International Conference on Geographical Information Systems Theory, Applications and Management (GISTAM), pages 92-98

Schoorl J. M., Sonneveld M. P. W., Veldkamp A. (2000). Three-dimensional landscape process modelling: the effect of DEM resolution. Earth Surf. Process. Landforms PS, 1025-1034

Schoorl J.M., Veldkamp A. (2003). Late Cenozoic landscape development and its tectonic implications for the Guadalhorce valley near Alora (Southern Spain). Geomorphology 50(1-3), 43-57.

Sona G., Pinto L., Pagliari D., Passoni D., Gini R. (2014). Experimental analysis of different software packages for orientation and digital surface modelling from UAV images, Earth Sci Inform, 7:97–107

Sunila R. and Virrantaus K. (2011). Digital Elevation Model Construction Using Geostatistics and Geological Expert Knowledge – A Case Study in Oitti Area in Southern Finland, Nordic Journal of Surveying and Real Estate Research 8:1, 7–

Suzanne P., Kroll W., Kroll C. N. (2006). Quantifying DEM Uncertainty and its Effect on Topographic Parameters, Photogrammetric Engineering & Remote Sensing Vol. 72, No. 9, pp. 1081–1090

Temme A.J.A.M., Heuvelink G.B.M., Schoorl J.M. and Claessens L. (2009). Geostatistical Simulation and Error Propagation in Geomorphometry, Article in Developments in Soil Science

Uysal M., Toprak A.S., Polat N. (2015). DEM generation with UAV Photogrammetry and accuracy analysis in Sahitler hill, Measurement 73, 539–543

van Gorp W. (2014). From Basalts to Badlands Modelling long-term landscape response to lava damming of an upland catchment in western Turkey, PhD thesis

van Gorp W., Temme A. J. A. M., Veldkamp A. and Schoorl J. M. (2015). Modelling long-term (300ka) upland catchment response to multiple lava damming events, Earth Surf. Process. Landforms 40, 888–900

van Sickle J. (2015). GPS for Land Surveyors Fourth Edition, CRC Press, NW

Vaze J., Teng J., Spencer G. (2010). Impact of DEM accuracy and resolution on topographic indices, Environmental Modelling & Software, 25, 1086-1098

Vlachos M., Skarlatos D. (2018). Vegetation removal from UAV derived DSMS, using combination of RGB and NIR imagery, ISPRS Annals of the Photogrammetry, Remote Sensing and Spatial Information Sciences, Volume IV-2

Wang L. and Lui. H. (2006). An efficient method for identifying and filling surface depressions in digital elevation models for hydrologic analysis and modelling, International Journal of Geographical Information Science, 20(2),193-213

Westaway R., Pringle M., Yurtmen S., Demir T., Bridgland D., Rowbotham G., Maddy D. (2004). Pliocene and Quaternary regional uplift in western Turkey: The Gediz River terrace staircase and the volcanism at Kula. Tectonophysics 391, 121–169.

Yilmaz V., Konakoglu B., Serifoglu C., Gungor O. & Gökalp E. (2018). Image classification-based ground filtering of point clouds extracted from UAV-based aerial photographs, Geocarto International, Vol. 33, no. 3, 310–320

Zhang J., Chang K.-T., Wu J. Q. (2008). Effects of DEM resolution and source on soil erosion modelling: a case study using the WEPP model, International Journal of Geographical Information Science, 22:8, 925-942

Annex A

Table A. 1 GCP errors for different resolutions

N	Error (m) in GCP for different resolutions			
	Resolution 2.5 m	Resolution 5 m	Resolution 10 m	Resolution 20 m
1	0.214	-0.416	-0.163	-1.807
2	1.143	2.465	0.889	2.778
3	0.209	0.166	0.256	0.666
4	0.001	-0.067	-0.47	-1.837
5	0.203	0.29	-0.754	-2.032
6	0.2	0.126	-0.447	-1.495
7	-0.302	-0.489	-0.183	0.628
8	0.601	0.764	0.744	0.721
9	0.87	0.671	-0.188	0.493
10	-0.05	-0.324	0.525	-0.436
11	-0.735	-0.486	-1.06	-2.359
12	-0.909	-0.836	-0.669	-0.325
13	-0.531	-0.659	-0.959	-0.624
14	0.64	0.322	0.889	-0.371
15	-0.755	-0.76	-1.26	-2.259
16	-0.404	-0.446	-0.679	-1.407
17	-0.086	-0.136	-0.216	-1.804
18	-1.427	-1.236	-1.421	-2.608
19	0.627	0.699	0.908	0.472
20	-0.286	-0.137	0.147	0.562
21	2.285	2.306	2.009	3.472
22	-0.151	-0.118	-0.188	-0.048
23	0.124	0.304	1.338	4.857
24	-0.147	-0.274	-0.551	-0.164
25	0.14	0.125	0.398	0.891
26	0.159	0.272	1.463	2.244
27	-1.606	-2.162	-1.379	-2.783
28	6.711	6.631	5.195	2.794
Mean	**0.241**	**0.236**	**0.149**	**-0.064**
SD	**1.456**	**1.521**	**1.306**	**1.921**

Table A. 2 RP errors for different resolutions

N	Error (m) in RP for different resolutions			
	Resolution 2.5 m	Resolution 5 m	Resolution 10 m	Resolution 20 m
1	-3.056	-3.267	-3.54	-4.622
2	-1.87	-1.695	-1.042	-0.669
3	-3.949	-3.648	-3.502	-2.033
4	-2.124	-2.098	-2.112	-3.867
5	0.452	0.394	0.406	1.112
6	-0.781	-0.85	-0.763	-0.165
7	-0.046	0.07	-0.446	-0.258
8	-4.2	-4.249	-4.137	-5.028
9	1.635	1.26	0.111	-0.554
10	3.818	3.636	3.362	2.545
11	1.104	1.455	1.905	2.643
12	0.488	0.634	1.149	1.449
13	2.853	3.265	3.992	4.741
14	1.45	1.558	1.92	2.683
15	2.068	2.24	2.369	3.362

N	Error (m) in RP for different resolutions			
	Resolution 2.5 m	Resolution 5 m	Resolution 10 m	Resolution 20 m
16	4.339	4.037	3.983	2.684
17	4.938	4.65	3.062	3.908
18	-0.375	-0.558	-1.2	-1.489
19	-1.788	-1.556	-1.024	-1.016
20	-2.599	-2.675	-3.047	-4.285
21	0.273	0.255	0.257	0.106
22	2.275	1.3	-0.373	-2.311
23	-2.459	-2.26	-2.823	-3.066
24	-0.137	-1.278	-1.334	-1.826
25	-0.323	-0.821	-1.675	-4.461
26	3.403	3.404	3.328	2.51
27	3.768	3.747	3.639	3.754
28	1.184	1.268	1.343	1.061
29	3.406	3.457	3.542	3.69
30	3.016	3.038	2.236	2.041
31	5.136	5.2	5.516	4.56
32	0.275	0.424	0.432	-2.249
33	4.775	4.703	5.471	6.34
34	3.93	4.225	4.435	5.279
35	2.227	1.683	1.956	1.193
36	-0.147	-0.274	-0.551	-0.164
37	4.45	4.182	4.415	3.349
38	-6.105	-5.793	-6.61	-3.778
39	3.805	3.285	2.558	5.143
40	2.87	2.997	1.552	1.396
41	-1.868	-2.129	-1.634	-1.217
42	-1.443	-1.592	-1.509	-2.421
43	-1.528	-1.208	-1.708	-3.544
44	-0.495	-0.211	-0.409	-0.643
45	0.763	0.633	0.13	1.727
46	-1.982	-1.912	-1.24	-1.098
47	4.219	3.922	3.915	2.653
48	2.791	2.935	2.182	1.575
49	5.633	5.919	6.401	6.942
50	-2.997	-2.652	-3.492	-2.317
51	-2.652	-2.287	-2.021	-1.465
52	-0.61	-0.632	-0.803	-1.528
53	4.656	4.739	4.231	1.211
54	6.611	6.108	5.543	2.896
Mean	**0.909**	**0.870**	**0.710**	**0.490**
SD	**2.926**	**2.865**	**2.910**	**3.022**

Table A. 3 Kriging DEM error

Type of DEM error	Resolution (m)	Mean (m)	SD (m)	Min (m)	Max (m)
1st	2.5	0.232	0.524	-0.445	2.281
	5	0.414	0.784	-0.646	2.454
	10	0.176	0.507	-0.760	2.000
	20	0.380	0.910	-1.985	3.396
2nd	2.5	1.061	0.617	-0.594	6.584
	5	1.045	0.604	-0.590	6.031
	10	0.899	0.633	-0.720	5.301
	20	0.761	0.847	-2.278	5.762

Table A. 4 Mean simulated DEM error

Type of DEM error	Resolution (m)	Mean (m)	SD (m)	Min (m)	Max (m)
1st	2.5	0.343	0.432	-0.354	2.280
	5	0.507	0.634	-0.493	2.427
	10	0.248	0.420	-0.738	2.025
	20	0.380	0.901	-1.925	3.408
2nd	2.5	1.112	0.602	-0.618	6.536
	5	1.173	0.623	-0.589	5.973
	10	0.980	0.652	-0.816	5.275
	20	0.908	0.885	-2.102	5.747

Table A. 5 Statistics of erosion based on deterministic DEM

Scenario	Resolution (m)	Mean (ton/ha)	SD (ton/ha)	Min (ton/ha)	Max (ton/ha)
L	2.5	-42.725	501.438	-16823.955	2.072
	5	-43.953	400.701	-15289.133	0.854
	10	-43.893	288.480	-9060.492	0.000
	20	-44.063	209.989	-6672.092	0.000
H	2.5	-213.869	1270.328	-22357.691	32703.092
	5	-290.635	1662.792	-18738.188	21959.461
	10	-379.606	1728.922	-17187.898	10.892
	20	-453.342	1719.220	-17470.740	17.402
LCL	2.5	-76.526	753.858	-17467.745	1.652
	5	-84.365	688.791	-16839.494	0.574
	10	-85.920	544.689	-16199.329	0.000
	20	-86.329	401.507	-12227.418	0.000
HCL	2.5	-386.139	1716.945	-23000.880	32916.408
	5	-510.311	2072.813	-21349.370	6397.874
	10	-601.592	2312.669	-17621.743	25291.251
	20	-781.764	2491.716	-18166.092	0.000

Table A. 6 Statistics of erosion based on simulated DEMs

Scenario	Type of DEM error	Resolution (m)	Mean (ton/ha)	SD (ton/ha)	Min (ton/ha)	Max (ton/ha)
L	1st	2.5	-41.285	423.087	-16801.666	1.666
		5	-42.808	354.158	-14725.229	0.840
		10	-42.836	264.213	-8256.108	0.000
		20	-42.396	181.777	-5603.752	0.000
	2nd	2.5	-37.871	242.476	-10075.016	6.118
		5	-41.780	252.194	-10258.500	-0.056
		10	-42.802	211.019	-5560.940	-0.770
		20	-43.747	164.810	-4569.208	-0.014
H	1st	2.5	-217.250	1037.906	-18470.313	17914.611
		5	-286.001	1358.967	-16892.358	10691.926
		10	-374.151	1628.486	-16846.761	9.478
		20	-431.004	1466.739	-16629.102	6.552
	2nd	2.5	-206.296	584.997	-14931.280	9986.942
		5	-244.308	859.169	-15354.108	7731.332
		10	-324.037	1113.608	-14491.709	-0.350
		20	-412.830	1216.587	-14671.454	-0.112
LCL	1st	2.5	-74.039	637.953	-16845.556	21.980
		5	-82.080	610.336	-16799.986	0.644
		10	-83.853	499.596	-14710.542	0.000
		20	-83.047	348.516	-10320.842	0.000
	2nd	2.5	-64.347	351.436	-11732.056	27.650
		5	-75.847	410.834	-12886.104	-0.924
		10	-82.577	388.742	-9831.738	-1.526
		20	-85.470	312.643	-7816.298	-0.014
HCL	1st	2.5	-394.779	1469.060	-21266.266	21139.467
		5	-480.929	1786.553	-17257.940	7495.572
		10	-597.743	2185.287	-17167.990	22566.096
		20	-744.518	2144.591	-17427.802	0.000
	2nd	2.5	-374.444	867.185	-16084.333	10618.328
		5	-407.922	1131.109	-16384.732	6710.326
		10	-528.138	1511.304	-16600.921	6986.308
		20	-691.270	1736.926	-16024.204	-0.210

Table A. 7 Statistics of erosion and deposition RMSE

Scenario	Type of DEM error	Resolution (m)	Mean (ton/ha)	SD (ton/ha)	Min (ton/ha)	Max (ton/ha)
L	1st	2.5	31.435	310.943	0.000	15614.409
		5	25.185	212.829	0.000	9199.764
		10	16.177	109.275	0.000	2919.700
		20	26.092	114.415	0.000	2133.614
	2nd	2.5	107.968	593.076	0.000	16286.284
		5	90.367	482.347	0.000	12711.496
		10	73.176	335.595	0.000	7183.862
		20	54.478	208.446	0.000	4486.664
H	1st	2.5	192.986	819.256	0.000	25990.692
		5	173.304	1045.630	0.000	25180.974
		10	106.682	578.161	0.000	10494.428
		20	242.372	938.837	0.000	11763.668
	2nd	2.5	541.267	1263.784	2.800	28772.968
		5	449.129	1537.423	0.000	24442.068
		10	424.379	1408.332	2.800	14573.595
		20	456.175	1404.777	1.246	12998.734
LCL	1st	2.5	54.052	466.360	0.000	15599.850
		5	45.557	354.120	0.000	12621.434
		10	30.910	201.366	0.000	5365.276
		20	51.109	219.045	0.000	3878.056
	2nd	2.5	171.742	831.257	0.000	16343.964
		5	152.091	734.778	0.000	15219.385
		10	135.672	588.476	0.000	12523.154
		20	106.128	393.331	0.000	7559.286
HCL	1st	2.5	296.259	1006.473	0.000	27813.687
		5	219.611	1060.722	0.000	17771.712
		10	146.174	713.604	0.000	12086.312
		20	357.405	1244.732	0.000	11380.684
	2nd	2.5	853.116	1604.695	8.946	31698.282
		5	646.273	1804.100	6.510	20073.634
		10	622.665	1812.562	9.618	28013.719
		20	668.709	1815.223	2.506	13163.934

Table A. 8 Data for yearly mean cumulative erosion based on simulates DEMs

Scenario	Type of DEM error	Resolution of DEM (m)	Time (year)	Mean net erosion (ton/ha)	SD net erosion (ton/ha)	Mean erosion (ton/ha)	SD erosion (ton/ha)	Mean deposition (ton/ha)	SD Deposition (ton/ha)	Cumulative net erosion (ton/ha)	Mean deposition+ Sd (ton/ha)	Mean deposition- sd (ton/ha)	SDR (-)
L-scenario	1st type of DEM error	2.5	1	-4.275	0.041	-4.276	0.041	0.001	0.000	-4.275	0.001	0.001	1.000
			2	-4.287	0.041	-4.288	0.041	0.001	0.000	-8.562	0.001	0.001	1.000
			3	-4.280	0.040	-4.281	0.040	0.001	0.000	-12.843	0.001	0.001	1.000
			4	-4.236	0.040	-4.237	0.040	0.001	0.000	-17.079	0.001	0.001	1.000
			5	-4.188	0.043	-4.189	0.043	0.001	0.000	-21.267	0.001	0.001	1.000
			6	-4.129	0.045	-4.130	0.045	0.001	0.000	-25.396	0.001	0.001	1.000
			7	-4.070	0.046	-4.071	0.046	0.001	0.000	-29.466	0.001	0.001	1.000
			8	-4.005	0.048	-4.005	0.048	0.001	0.000	-33.471	0.001	0.001	1.000
			9	-3.937	0.049	-3.938	0.049	0.001	0.000	-37.408	0.001	0.001	1.000
			10	-3.876	0.050	-3.877	0.050	0.001	0.000	-41.285	0.001	0.001	1.000
		5	1	-4.285	0.044	-4.285	0.044	0.000	0.000	-4.285	0.000	0.000	1.000
			2	-4.286	0.043	-4.286	0.043	0.000	0.000	-8.571	0.001	0.000	1.000
			3	-4.285	0.043	-4.285	0.043	0.001	0.000	-12.855	0.001	0.000	1.000
			4	-4.283	0.043	-4.284	0.043	0.001	0.000	-17.138	0.001	0.000	1.000
			5	-4.281	0.043	-4.281	0.043	0.000	0.000	-21.419	0.001	0.000	1.000
			6	-4.279	0.043	-4.279	0.043	0.000	0.000	-25.698	0.001	0.000	1.000
			7	-4.276	0.043	-4.277	0.043	0.000	0.000	-29.974	0.000	0.000	1.000
			8	-4.274	0.043	-4.274	0.043	0.000	0.000	-34.248	0.000	0.000	1.000
			9	-4.269	0.043	-4.269	0.043	0.000	0.000	-38.517	0.000	0.000	1.000
			10	-4.261	0.044	-4.261	0.044	0.000	0.000	-42.778	0.000	0.000	1.000
		10	1	-4.286	0.032	-4.286	0.032	0.000	0.000	-4.286	0.000	0.000	1.000
			2	-4.286	0.032	-4.286	0.032	0.000	0.000	-8.572	0.000	0.000	1.000
			3	-4.285	0.032	-4.286	0.032	0.000	0.000	-12.858	0.000	0.000	1.000
			4	-4.285	0.032	-4.285	0.032	0.000	0.000	-17.143	0.000	0.000	1.000
			5	-4.284	0.032	-4.284	0.032	0.000	0.000	-21.427	0.000	0.000	1.000
			6	-4.283	0.032	-4.284	0.032	0.000	0.000	-25.710	0.000	0.000	1.000
			7	-4.283	0.032	-4.283	0.032	0.000	0.000	-29.993	0.000	0.000	1.000
			8	-4.282	0.032	-4.282	0.032	0.000	0.000	-34.275	0.000	0.000	1.000
			9	-4.281	0.032	-4.281	0.032	0.000	0.000	-38.556	0.000	0.000	1.000
			10	-4.280	0.032	-4.280	0.032	0.000	0.000	-42.836	0.000	0.000	1.000
		20	1	-4.241	0.062	-4.241	0.062	0.000	0.000	-4.241	0.000	0.000	1.000
			2	-4.241	0.062	-4.241	0.062	0.000	0.000	-8.482	0.000	0.000	1.000
			3	-4.241	0.062	-4.241	0.062	0.000	0.000	-12.723	0.000	0.000	1.000
			4	-4.240	0.062	-4.241	0.062	0.000	0.000	-16.963	0.000	0.000	1.000
			5	-4.240	0.062	-4.240	0.062	0.000	0.000	-21.203	0.000	0.000	1.000
			6	-4.240	0.062	-4.240	0.062	0.000	0.000	-25.442	0.000	0.000	1.000
			7	-4.239	0.061	-4.239	0.061	0.000	0.000	-29.681	0.000	0.000	1.000
			8	-4.239	0.061	-4.239	0.061	0.000	0.000	-33.920	0.000	0.000	1.000
			9	-4.238	0.061	-4.239	0.061	0.000	0.000	-38.158	0.000	0.000	1.000
			10	-4.238	0.061	-4.238	0.061	0.000	0.000	-42.396	0.000	0.000	1.000
	2nd type of DEM error	2.5	1	-4.268	0.162	-4.271	0.162	0.003	0.000	-4.268	0.003	0.002	0.999
			2	-4.269	0.164	-4.272	0.164	0.003	0.000	-8.537	0.003	0.003	0.999
			3	-4.174	0.163	-4.177	0.163	0.003	0.000	-12.712	0.003	0.002	0.999
			4	-4.021	0.154	-4.024	0.154	0.003	0.001	-16.733	0.003	0.002	0.999
			5	-3.853	0.147	-3.856	0.147	0.002	0.001	-20.586	0.003	0.002	0.999
			6	-3.703	0.141	-3.705	0.141	0.002	0.001	-24.289	0.003	0.001	0.999
			7	-3.567	0.134	-3.570	0.134	0.002	0.001	-27.857	0.003	0.001	0.999
			8	-3.442	0.127	-3.444	0.127	0.002	0.001	-31.299	0.003	0.001	0.999
			9	-3.334	0.122	-3.336	0.122	0.002	0.001	-34.633	0.003	0.001	0.999
			10	-3.238	0.118	-3.240	0.118	0.002	0.001	-37.871	0.003	0.001	0.999
		5	1	-4.298	0.150	-4.300	0.150	0.002	0.000	-4.298	0.002	0.002	1.000
			2	-4.304	0.149	-4.306	0.149	0.002	0.000	-8.602	0.002	0.002	1.000
			3	-4.297	0.146	-4.299	0.146	0.002	0.000	-12.898	0.002	0.002	1.000
			4	-4.280	0.142	-4.282	0.142	0.002	0.000	-17.178	0.002	0.002	1.000
			5	-4.244	0.140	-4.246	0.140	0.002	0.000	-21.422	0.002	0.002	1.000
			6	-4.202	0.139	-4.204	0.139	0.002	0.000	-25.624	0.002	0.002	1.000
			7	-4.145	0.139	-4.147	0.139	0.002	0.000	-29.769	0.002	0.002	1.000
			8	-4.071	0.135	-4.072	0.135	0.002	0.000	-33.840	0.002	0.002	1.000
			9	-3.994	0.128	-3.996	0.128	0.002	0.000	-37.834	0.002	0.002	0.999
			10	-3.917	0.124	-3.918	0.124	0.002	0.000	-41.751	0.002	0.001	1.000
		10	1	-4.284	0.157	-4.285	0.157	0.001	0.000	-4.284	0.001	0.001	1.000
			2	-4.285	0.157	-4.286	0.157	0.001	0.000	-8.569	0.002	0.001	1.000
			3	-4.286	0.157	-4.287	0.157	0.001	0.000	-12.855	0.002	0.001	1.000
			4	-4.287	0.156	-4.288	0.156	0.001	0.000	-17.142	0.002	0.001	1.000
			5	-4.288	0.156	-4.289	0.156	0.001	0.000	-21.429	0.002	0.001	1.000
			6	-4.288	0.155	-4.289	0.155	0.001	0.000	-25.717	0.002	0.001	1.000
			7	-4.285	0.156	-4.286	0.156	0.001	0.000	-30.002	0.002	0.001	1.000
			8	-4.275	0.153	-4.277	0.153	0.002	0.000	-34.277	0.002	0.001	1.000
			9	-4.267	0.150	-4.269	0.149	0.002	0.000	-38.544	0.002	0.001	1.000
			10	-4.258	0.143	-4.260	0.143	0.002	0.000	-42.803	0.002	0.001	1.000
		20	1	-4.376	0.205	-4.377	0.205	0.001	0.000	-4.376	0.001	0.001	1.000

Scenario	Type of DEM error	Resolution of DEM (m)	Time (year)	Mean net erosion (ton/ha)	SD net erosion (ton/ha)	Mean erosion (ton/ha)	SD erosion (ton/ha)	Mean deposition (ton/ha)	SD Deposition (ton/ha)	Cumulative net erosion (ton/ha)	Mean deposition+ Sd (ton/ha)	Mean deposition- sd (ton/ha)	SDR (-)
			2	-4.376	0.205	-4.377	0.205	0.001	0.000	-8.752	0.001	0.001	1.000
			3	-4.376	0.204	-4.377	0.204	0.001	0.000	-13.127	0.001	0.001	1.000
			4	-4.375	0.204	-4.376	0.204	0.001	0.000	-17.503	0.001	0.001	1.000
			5	-4.375	0.204	-4.376	0.204	0.001	0.000	-21.878	0.001	0.001	1.000
			6	-4.375	0.203	-4.376	0.203	0.001	0.000	-26.252	0.001	0.001	1.000
			7	-4.374	0.203	-4.375	0.203	0.001	0.000	-30.627	0.001	0.001	1.000
			8	-4.374	0.203	-4.375	0.203	0.001	0.000	-35.001	0.001	0.001	1.000
			9	-4.374	0.202	-4.375	0.202	0.001	0.000	-39.374	0.001	0.001	1.000
			10	-4.373	0.202	-4.374	0.202	0.001	0.000	-43.747	0.001	0.001	1.000
H-scenario	1st type of DEM error	2.5	1	-42.265	0.383	-42.676	0.381	0.411	0.014	-42.265	0.424	0.397	0.990
			2	-36.907	0.844	-38.824	0.330	1.916	0.671	-79.172	2.588	1.245	0.951
			3	-25.817	2.643	-35.710	0.527	9.893	2.243	-104.989	12.136	7.651	0.723
			4	-15.157	2.761	-34.204	0.488	19.047	2.438	-120.146	21.485	16.609	0.443
			5	-12.144	2.677	-33.847	0.519	21.703	2.397	-132.290	24.101	19.306	0.359
			6	-15.450	2.533	-34.163	0.448	18.713	2.296	-147.741	21.009	16.416	0.452
			7	-16.919	1.277	-33.710	0.421	16.791	1.223	-164.659	18.015	15.568	0.502
			8	-17.483	1.079	-33.342	0.363	15.859	1.035	-182.142	16.894	14.824	0.524
			9	-17.372	0.951	-32.733	0.449	15.361	0.939	-199.514	16.300	14.422	0.531
			10	-17.736	1.068	-32.353	0.362	14.617	1.017	-217.250	15.634	13.601	0.548
		5	1	-43.013	0.322	-43.084	0.322	0.070	0.005	-43.013	0.075	0.066	0.998
			2	-40.874	0.355	-40.934	0.362	0.060	0.033	-83.888	0.093	0.028	0.999
			3	-38.708	0.434	-38.747	0.434	0.039	0.008	-122.596	0.046	0.031	0.999
			4	-35.167	0.963	-35.830	0.554	0.663	0.664	-157.762	1.327	-0.001	0.981
			5	-29.886	2.897	-32.909	0.639	3.024	2.492	-187.648	5.516	0.532	0.908
			6	-24.299	4.494	-30.796	0.623	6.497	4.238	-211.947	10.734	2.259	0.789
			7	-20.150	4.894	-29.061	0.698	8.911	5.063	-232.097	13.974	3.848	0.693
			8	-18.368	4.436	-28.065	1.269	9.697	4.957	-250.465	14.654	4.740	0.654
			9	-17.867	4.115	-27.015	1.461	9.148	4.800	-268.332	13.948	4.348	0.661
			10	-17.468	3.760	-26.216	1.725	8.748	4.640	-285.801	13.388	4.108	0.666
		10	1	-42.988	0.326	-43.013	0.326	0.025	0.004	-42.988	0.029	0.021	0.999
			2	-42.883	0.346	-42.905	0.346	0.022	0.004	-85.871	0.026	0.019	0.999
			3	-42.001	0.441	-42.019	0.442	0.018	0.003	-127.871	0.022	0.015	1.000
			4	-40.428	0.537	-40.440	0.537	0.012	0.002	-168.299	0.014	0.010	1.000
			5	-38.523	0.593	-38.533	0.593	0.010	0.001	-206.822	0.011	0.008	1.000
			6	-36.647	0.609	-36.655	0.609	0.008	0.001	-243.469	0.009	0.007	1.000
			7	-34.965	0.537	-34.971	0.537	0.007	0.001	-278.434	0.007	0.006	1.000
			8	-33.424	0.538	-33.429	0.538	0.006	0.001	-311.858	0.006	0.005	1.000
			9	-31.911	0.567	-31.916	0.567	0.005	0.001	-343.769	0.006	0.004	1.000
			10	-30.382	0.562	-30.387	0.562	0.005	0.001	-374.151	0.005	0.004	1.000
		20	1	-45.387	0.662	-45.421	0.663	0.034	0.011	-45.387	0.045	0.023	0.999
			2	-45.328	0.649	-45.357	0.650	0.028	0.010	-90.716	0.038	0.018	0.999
			3	-44.739	0.919	-44.764	0.920	0.024	0.009	-135.455	0.033	0.016	0.999
			4	-44.360	0.899	-44.382	0.899	0.022	0.008	-179.815	0.030	0.014	1.000
			5	-44.152	0.878	-44.172	0.879	0.020	0.008	-223.967	0.028	0.013	1.000
			6	-43.633	1.023	-43.652	1.022	0.019	0.007	-267.600	0.026	0.012	1.000
			7	-42.773	1.070	-42.791	1.069	0.018	0.007	-310.374	0.025	0.011	1.000
			8	-41.602	1.147	-41.619	1.146	0.017	0.007	-351.976	0.024	0.009	1.000
			9	-40.229	1.157	-40.243	1.155	0.015	0.006	-392.205	0.021	0.009	1.000
			10	-38.799	1.159	-38.812	1.157	0.013	0.006	-431.004	0.019	0.008	1.000
	2nd type of DEM error	2.5	1	-39.798	0.843	-40.903	0.827	1.105	0.079	-39.798	1.183	1.026	0.973
			2	-33.603	0.910	-35.495	0.645	1.892	0.532	-73.401	2.424	1.360	0.947
			3	-23.428	2.131	-31.517	0.719	8.089	1.730	-96.829	9.819	6.358	0.743
			4	-14.324	2.000	-29.988	0.644	15.664	1.914	-111.154	17.578	13.750	0.478
			5	-12.565	2.524	-30.087	0.730	17.523	2.125	-123.718	19.648	15.397	0.418
			6	-15.870	1.693	-30.819	0.630	14.949	1.624	-139.589	16.573	13.325	0.515
			7	-16.470	1.082	-30.480	0.584	14.010	1.081	-156.059	15.091	12.929	0.540
			8	-16.822	0.977	-30.248	0.642	13.426	0.948	-172.880	14.375	12.478	0.556
			9	-16.627	0.875	-29.752	0.594	13.124	0.924	-189.508	14.049	12.200	0.559
			10	-16.789	0.850	-29.497	0.610	12.709	0.895	-206.296	13.604	11.814	0.569
		5	1	-41.588	1.192	-41.872	1.185	0.284	0.035	-41.588	0.319	0.249	0.993
			2	-35.729	1.077	-36.006	1.054	0.277	0.169	-77.316	0.447	0.108	0.992
			3	-31.490	1.111	-31.798	1.029	0.308	0.338	-108.807	0.645	-0.030	0.990
			4	-27.371	1.654	-28.633	1.081	1.262	1.004	-136.178	2.266	0.257	0.956
			5	-22.794	2.736	-26.384	1.040	3.590	2.401	-158.971	5.991	1.190	0.864
			6	-18.880	3.230	-25.083	1.005	6.202	3.286	-177.852	9.488	2.916	0.753
			7	-17.008	3.333	-24.774	1.267	7.767	3.495	-194.859	11.261	4.272	0.687
			8	-16.444	3.251	-24.508	1.446	8.064	3.305	-211.304	11.368	4.759	0.671
			9	-16.323	2.993	-24.262	1.417	7.938	3.142	-227.627	11.081	4.796	0.673
			10	-16.510	2.941	-24.067	1.475	7.557	3.139	-244.137	10.696	4.418	0.686
		10	1	-42.581	1.481	-42.753	1.477	0.171	0.027	-42.581	0.199	0.144	0.996
			2	-41.059	1.277	-41.226	1.271	0.167	0.028	-83.640	0.195	0.139	0.996
			3	-37.760	1.456	-37.900	1.450	0.140	0.027	-121.400	0.167	0.114	0.996
			4	-34.561	1.373	-34.678	1.366	0.117	0.024	-155.961	0.141	0.093	0.997

Scenario	Type of DEM error	Resolution of DEM (m)	Time (year)	Mean net erosion (ton/ha)	SD net erosion (ton/ha)	Mean erosion (ton/ha)	SD erosion (ton/ha)	Mean deposition (ton/ha)	SD Deposition (ton/ha)	Cumulative net erosion (ton/ha)	Mean deposition+ Sd (ton/ha)	Mean deposition-sd (ton/ha)	SDR (-)
			5	-31.984	1.325	-32.084	1.319	0.100	0.021	-187.946	0.121	0.079	0.997
			6	-30.003	1.207	-30.089	1.201	0.087	0.018	-217.948	0.104	0.069	0.997
			7	-28.340	1.115	-28.417	1.110	0.077	0.016	-246.289	0.092	0.061	0.997
			8	-26.999	1.023	-27.068	1.019	0.069	0.015	-273.287	0.084	0.054	0.997
			9	-25.854	0.990	-25.917	0.986	0.063	0.014	-299.141	0.077	0.049	0.998
			10	-24.896	0.912	-24.954	0.908	0.058	0.014	-324.037	0.072	0.045	0.998
		20	1	-46.695	2.205	-46.829	2.200	0.134	0.039	-46.695	0.173	0.094	0.997
			2	-46.281	1.854	-46.404	1.846	0.123	0.038	-92.976	0.161	0.085	0.997
			3	-45.531	1.804	-45.648	1.794	0.117	0.038	-138.507	0.156	0.079	0.997
			4	-44.570	1.780	-44.680	1.770	0.111	0.037	-183.076	0.148	0.073	0.998
			5	-42.939	1.818	-43.041	1.807	0.102	0.035	-226.016	0.137	0.066	0.998
			6	-41.018	1.716	-41.112	1.707	0.094	0.033	-267.034	0.127	0.061	0.998
			7	-39.030	1.770	-39.117	1.760	0.087	0.031	-306.064	0.118	0.056	0.998
			8	-37.185	1.645	-37.266	1.637	0.081	0.028	-343.248	0.109	0.052	0.998
			9	-35.534	1.606	-35.608	1.598	0.075	0.027	-378.782	0.101	0.048	0.998
			10	-34.048	1.545	-34.116	1.537	0.068	0.024	-412.830	0.092	0.045	0.998
LCL-scenario	1st type of DEM error	2.5	1	-4.275	0.041	-4.276	0.041	0.001	0.000	-4.275	0.001	0.001	1.000
			2	-8.462	0.063	-8.463	0.063	0.001	0.000	-12.737	0.001	0.001	1.000
			3	-9.843	0.080	-9.844	0.080	0.001	0.000	-22.580	0.001	0.001	1.000
			4	-7.700	0.078	-7.701	0.078	0.001	0.000	-30.280	0.001	0.001	1.000
			5	-7.707	0.087	-7.708	0.087	0.001	0.000	-37.987	0.001	0.001	1.000
			6	-10.069	0.116	-10.070	0.116	0.001	0.000	-48.057	0.001	0.000	1.000
			7	-3.780	0.058	-3.781	0.058	0.001	0.001	-51.837	0.002	-0.001	1.000
			8	-6.763	0.099	-6.764	0.099	0.001	0.002	-58.599	0.003	-0.001	1.000
			9	-9.165	0.123	-9.166	0.123	0.001	0.002	-67.764	0.004	-0.001	1.000
			10	-6.275	0.095	-6.276	0.095	0.001	0.001	-74.039	0.002	-0.001	1.000
		5	1	-4.285	0.044	-4.285	0.044	0.000	0.000	-4.285	0.000	0.000	1.000
			2	-8.639	0.087	-8.639	0.087	0.000	0.000	-12.923	0.000	0.000	1.000
			3	-10.496	0.106	-10.496	0.106	0.000	0.000	-23.419	0.001	0.000	1.000
			4	-8.183	0.083	-8.184	0.083	0.000	0.000	-31.602	0.001	0.000	1.000
			5	-8.473	0.086	-8.473	0.086	0.000	0.000	-40.075	0.000	0.000	1.000
			6	-11.944	0.127	-11.945	0.127	0.000	0.000	-52.020	0.000	0.000	1.000
			7	-4.189	0.054	-4.189	0.054	0.000	0.000	-56.208	0.000	0.000	1.000
			8	-7.677	0.103	-7.677	0.103	0.000	0.000	-63.885	0.000	0.000	1.000
			9	-10.956	0.147	-10.956	0.147	0.000	0.000	-74.841	0.000	0.000	1.000
			10	-7.181	0.100	-7.181	0.100	0.000	0.000	-82.023	0.000	0.000	1.000
		10	1	-4.286	0.032	-4.286	0.032	0.000	0.000	-4.286	0.000	0.000	1.000
			2	-8.639	0.065	-8.639	0.065	0.000	0.000	-12.925	0.000	0.000	1.000
			3	-10.500	0.079	-10.500	0.079	0.000	0.000	-23.425	0.000	0.000	1.000
			4	-8.194	0.062	-8.195	0.062	0.000	0.000	-31.619	0.000	0.000	1.000
			5	-8.498	0.064	-8.498	0.064	0.000	0.000	-40.117	0.000	0.000	1.000
			6	-12.074	0.091	-12.074	0.091	0.000	0.000	-52.191	0.000	0.000	1.000
			7	-4.299	0.032	-4.299	0.032	0.000	0.000	-56.490	0.000	0.000	1.000
			8	-7.973	0.060	-7.973	0.060	0.000	0.000	-64.463	0.000	0.000	1.000
			9	-11.620	0.087	-11.621	0.087	0.000	0.000	-76.083	0.000	0.000	1.000
			10	-7.769	0.065	-7.769	0.065	0.000	0.000	-83.853	0.000	0.000	1.000
		20	1	-4.241	0.062	-4.241	0.062	0.000	0.000	-4.241	0.000	0.000	1.000
			2	-8.548	0.125	-8.549	0.125	0.000	0.000	-12.789	0.000	0.000	1.000
			3	-10.391	0.151	-10.391	0.151	0.000	0.000	-23.180	0.000	0.000	1.000
			4	-8.111	0.118	-8.111	0.118	0.000	0.000	-31.292	0.000	0.000	1.000
			5	-8.413	0.122	-8.413	0.122	0.000	0.000	-39.705	0.000	0.000	1.000
			6	-11.957	0.172	-11.957	0.172	0.000	0.000	-51.662	0.000	0.000	1.000
			7	-4.258	0.061	-4.259	0.061	0.000	0.000	-55.920	0.000	0.000	1.000
			8	-7.900	0.113	-7.900	0.113	0.000	0.000	-63.820	0.000	0.000	1.000
			9	-11.518	0.165	-11.518	0.165	0.000	0.000	-75.337	0.000	0.000	1.000
			10	-7.710	0.110	-7.710	0.110	0.000	0.000	-83.047	0.000	0.000	1.000
	2nd type of DEM error	2.5	1	-4.268	0.162	-4.271	0.162	0.003	0.000	-4.268	0.003	0.002	0.999
			2	-8.288	0.296	-8.290	0.296	0.003	0.000	-12.556	0.003	0.002	1.000
			3	-9.147	0.321	-9.150	0.321	0.002	0.000	-21.703	0.003	0.002	1.000
			4	-6.804	0.255	-6.807	0.255	0.003	0.001	-28.507	0.004	0.001	1.000
			5	-6.602	0.251	-6.605	0.251	0.002	0.001	-35.110	0.003	0.001	1.000
			6	-8.458	0.285	-8.460	0.285	0.002	0.001	-43.568	0.003	0.001	1.000
			7	-3.061	0.113	-3.064	0.113	0.003	0.002	-46.629	0.004	0.001	0.999
			8	-5.445	0.190	-5.447	0.191	0.002	0.001	-52.074	0.003	0.001	1.000
			9	-7.358	0.236	-7.360	0.236	0.002	0.002	-59.431	0.004	0.001	1.000
			10	-4.915	0.176	-4.918	0.176	0.002	0.001	-64.347	0.004	0.001	0.999
		5	1	-4.298	0.150	-4.300	0.150	0.002	0.000	-4.298	0.002	0.002	1.000
			2	-8.662	0.294	-8.664	0.294	0.002	0.000	-12.960	0.002	0.001	1.000
			3	-10.407	0.337	-10.409	0.337	0.002	0.000	-23.368	0.002	0.002	1.000
			4	-7.922	0.263	-7.924	0.263	0.002	0.000	-31.289	0.002	0.002	1.000
			5	-7.936	0.249	-7.938	0.249	0.002	0.000	-39.225	0.002	0.002	1.000
			6	-10.782	0.357	-10.783	0.357	0.002	0.000	-50.007	0.002	0.001	1.000
			7	-3.685	0.127	-3.686	0.127	0.002	0.000	-53.692	0.002	0.001	1.000

Scenario	Type of DEM error	Resolution of DEM (m)	Time (year)	Mean net erosion (ton/ha)	SD net erosion (ton/ha)	Mean erosion (ton/ha)	SD erosion (ton/ha)	Mean deposition (ton/ha)	SD Deposition (ton/ha)	Cumulative net erosion (ton/ha)	Mean deposition+ Sd (ton/ha)	Mean deposition-sd (ton/ha)	SDR (-)
			8	-6.676	0.238	-6.677	0.238	0.001	0.000	-60.368	0.002	0.001	1.000
			9	-9.376	0.330	-9.378	0.330	0.001	0.000	-69.744	0.001	0.001	1.000
			10	-6.049	0.217	-6.051	0.217	0.001	0.000	-75.794	0.001	0.001	1.000
		10	1	-4.284	0.157	-4.285	0.157	0.001	0.000	-4.284	0.001	0.001	1.000
			2	-8.639	0.316	-8.640	0.316	0.001	0.000	-12.923	0.001	0.001	1.000
			3	-10.508	0.383	-10.509	0.383	0.001	0.000	-23.431	0.001	0.001	1.000
			4	-8.195	0.295	-8.196	0.295	0.001	0.000	-31.625	0.002	0.001	1.000
			5	-8.471	0.296	-8.473	0.296	0.001	0.000	-40.097	0.002	0.001	1.000
			6	-11.966	0.387	-11.967	0.387	0.001	0.000	-52.063	0.002	0.001	1.000
			7	-4.228	0.141	-4.229	0.141	0.001	0.000	-56.291	0.002	0.001	1.000
			8	-7.782	0.261	-7.783	0.261	0.001	0.000	-64.072	0.002	0.001	1.000
			9	-11.170	0.378	-11.171	0.378	0.001	0.000	-75.242	0.002	0.001	1.000
			10	-7.335	0.253	-7.337	0.253	0.001	0.000	-82.577	0.002	0.001	1.000
		20	1	-4.376	0.205	-4.377	0.205	0.001	0.000	-4.376	0.001	0.001	1.000
			2	-8.822	0.412	-8.822	0.412	0.001	0.000	-13.198	0.001	0.001	1.000
			3	-10.724	0.500	-10.725	0.500	0.001	0.000	-23.922	0.001	0.001	1.000
			4	-8.371	0.389	-8.372	0.389	0.001	0.000	-32.292	0.001	0.001	1.000
			5	-8.683	0.402	-8.684	0.402	0.001	0.000	-40.976	0.001	0.001	1.000
			6	-12.337	0.564	-12.338	0.564	0.001	0.000	-53.312	0.001	0.001	1.000
			7	-4.388	0.198	-4.389	0.198	0.001	0.000	-57.700	0.001	0.001	1.000
			8	-8.118	0.343	-8.119	0.342	0.001	0.000	-65.818	0.001	0.001	1.000
			9	-11.791	0.488	-11.792	0.488	0.001	0.000	-77.609	0.001	0.001	1.000
			10	-7.861	0.309	-7.862	0.309	0.001	0.000	-85.470	0.001	0.001	1.000
HCL-scenario	1st type of DEM error	2.5	1	-42.265	0.383	-42.676	0.381	0.411	0.014	-42.265	0.424	0.397	0.990
			2	-63.900	0.856	-65.763	0.433	1.864	0.672	-106.164	2.535	1.192	0.972
			3	-60.649	3.559	-71.590	0.649	10.941	3.113	-166.813	14.054	7.828	0.847
			4	-33.154	3.547	-55.297	0.580	22.143	3.186	-199.967	25.329	18.957	0.600
			5	-31.694	3.291	-55.786	0.659	24.092	2.945	-231.661	27.037	21.147	0.568
			6	-49.399	2.556	-73.129	0.590	23.730	2.410	-281.060	26.140	21.320	0.676
			7	-11.237	0.924	-31.406	0.449	20.169	0.956	-292.297	21.125	19.213	0.358
			8	-30.196	1.426	-50.438	0.561	20.242	1.394	-322.493	21.636	18.848	0.599
			9	-44.986	1.457	-66.032	0.615	21.046	1.543	-367.479	22.589	19.503	0.681
			10	-27.300	1.214	-46.773	0.567	19.473	1.318	-394.779	20.791	18.155	0.584
		5	1	-43.013	0.322	-43.084	0.322	0.070	0.005	-43.013	0.075	0.066	0.998
			2	-65.768	0.555	-65.828	0.561	0.059	0.033	-108.782	0.092	0.027	0.999
			3	-70.136	0.732	-70.175	0.711	0.039	0.087	-178.918	0.126	-0.048	0.999
			4	-54.874	0.940	-55.221	0.722	0.347	0.484	-233.792	0.831	-0.137	0.994
			5	-51.067	2.124	-52.316	0.716	1.249	1.777	-284.859	3.026	-0.528	0.976
			6	-61.253	3.702	-63.841	0.840	2.588	3.520	-346.112	6.109	-0.932	0.959
			7	-22.090	4.407	-25.799	0.629	3.709	4.555	-368.202	8.264	-0.846	0.856
			8	-35.370	4.967	-40.715	1.246	5.345	5.719	-403.572	11.064	-0.374	0.869
			9	-47.189	5.342	-52.710	1.649	5.521	6.305	-450.761	11.826	-0.784	0.895
			10	-29.830	4.745	-35.214	1.894	5.384	6.113	-480.591	11.497	-0.729	0.847
		10	1	-42.988	0.326	-43.013	0.326	0.025	0.004	-42.988	0.029	0.021	0.999
			2	-85.020	0.718	-85.043	0.718	0.023	0.004	-128.008	0.027	0.019	1.000
			3	-94.642	1.276	-94.654	1.276	0.013	0.002	-222.649	0.015	0.010	1.000
			4	-67.112	1.065	-67.217	0.973	0.105	0.328	-289.761	0.433	-0.223	0.998
			5	-62.298	2.056	-64.218	1.077	1.919	1.538	-352.060	3.458	0.381	0.970
			6	-81.710	1.435	-81.799	1.424	0.090	0.037	-433.769	0.127	0.052	0.999
			7	-26.262	0.421	-26.499	0.444	0.237	0.245	-460.031	0.482	-0.008	0.991
			8	-45.680	1.629	-47.035	0.697	1.354	1.449	-505.711	2.803	-0.095	0.971
			9	-58.243	2.460	-63.772	0.880	5.529	2.212	-563.954	7.741	3.318	0.913
			10	-33.789	2.845	-39.616	0.584	5.827	2.736	-597.743	8.563	3.091	0.853
		20	1	-45.387	0.662	-45.421	0.663	0.034	0.011	-45.387	0.045	0.023	0.999
			2	-90.741	1.480	-90.769	1.481	0.028	0.010	-136.128	0.038	0.018	1.000
			3	-108.196	2.066	-108.219	2.067	0.023	0.009	-244.324	0.032	0.015	1.000
			4	-81.769	1.951	-81.788	1.950	0.019	0.008	-326.093	0.027	0.011	1.000
			5	-80.136	2.148	-80.152	2.147	0.016	0.007	-406.229	0.023	0.009	1.000
			6	-104.864	3.203	-104.878	3.202	0.014	0.005	-511.093	0.019	0.008	1.000
			7	-34.760	1.154	-34.775	1.153	0.015	0.006	-545.853	0.021	0.009	1.000
			8	-61.874	2.087	-61.885	2.086	0.011	0.004	-607.727	0.015	0.007	1.000
			9	-84.148	2.682	-84.158	2.680	0.010	0.004	-691.875	0.014	0.006	1.000
			10	-52.643	1.737	-52.653	1.736	0.010	0.003	-744.518	0.014	0.007	1.000
	2nd type of DEM error	2.5	1	-39.798	0.843	-40.903	0.827	1.105	0.079	-39.798	1.183	1.026	0.973
			2	-58.250	1.155	-60.091	0.939	1.840	0.525	-98.048	2.365	1.316	0.969
			3	-55.336	2.932	-63.790	1.144	8.454	2.256	-153.385	10.710	6.198	0.867
			4	-31.007	2.508	-48.675	0.954	17.669	2.185	-184.391	19.854	15.483	0.637
			5	-29.944	2.888	-49.494	0.909	19.550	2.530	-214.335	22.080	17.020	0.605
			6	-47.342	2.090	-65.503	0.945	18.161	1.916	-261.677	20.077	16.245	0.723
			7	-12.735	1.059	-28.502	0.613	15.768	1.192	-274.411	16.960	14.576	0.447
			8	-30.163	1.259	-45.595	0.793	15.433	1.296	-304.574	16.729	14.137	0.662
			9	-42.853	1.369	-59.364	0.924	16.511	1.282	-347.427	17.793	15.229	0.722
			10	-27.017	1.040	-42.498	0.694	15.481	1.154	-374.444	16.635	14.327	0.636

Scenario	Type of DEM error	Resolution of DEM (m)	Time (year)	Mean net erosion (ton/ha)	SD net erosion (ton/ha)	Mean erosion (ton/ha)	SD erosion (ton/ha)	Mean deposition (ton/ha)	SD Deposition (ton/ha)	Cumulative net erosion (ton/ha)	Mean deposition+ Sd (ton/ha)	Mean deposition- sd (ton/ha)	SDR (-)
		5	1	-41.588	1.192	-41.872	1.185	0.284	0.035	-41.588	0.319	0.249	0.993
			2	-58.254	1.477	-58.521	1.459	0.267	0.163	-99.842	0.430	0.104	0.995
			3	-58.752	1.575	-59.019	1.552	0.267	0.309	-158.594	0.576	-0.042	0.995
			4	-44.045	1.677	-44.768	1.396	0.723	0.705	-202.638	1.429	0.018	0.984
			5	-40.556	2.916	-42.811	1.377	2.255	2.282	-243.194	4.537	-0.026	0.947
			6	-49.422	4.266	-53.783	1.533	4.361	3.990	-292.616	8.350	0.371	0.919
			7	-16.844	3.710	-22.211	1.036	5.367	4.005	-309.460	9.372	1.362	0.758
			8	-29.998	4.215	-36.431	1.486	6.433	4.686	-339.457	11.119	1.747	0.823
			9	-41.114	4.533	-48.466	1.822	7.352	5.344	-380.571	12.696	2.009	0.848
			10	-27.065	3.921	-34.104	1.953	7.039	5.027	-407.635	12.067	2.012	0.794
		10	1	-42.581	1.481	-42.753	1.477	0.171	0.027	-42.581	0.199	0.144	0.996
			2	-78.845	2.367	-79.008	2.360	0.163	0.027	-121.426	0.190	0.136	0.998
			3	-80.077	3.088	-80.430	3.088	0.354	0.794	-201.503	1.148	-0.441	0.996
			4	-54.175	2.775	-54.828	2.142	0.654	1.501	-255.678	2.155	-0.848	0.988
			5	-51.350	2.592	-52.079	2.036	0.729	1.485	-307.028	2.214	-0.755	0.986
			6	-67.476	2.983	-68.325	2.434	0.849	1.822	-374.503	2.671	-0.973	0.988
			7	-22.111	1.465	-22.790	0.857	0.679	1.373	-396.614	2.052	-0.695	0.970
			8	-40.397	2.042	-41.094	1.455	0.697	1.570	-437.011	2.267	-0.873	0.983
			9	-55.860	2.575	-56.848	1.784	0.988	1.956	-492.871	2.944	-0.968	0.983
			10	-35.267	1.715	-36.324	1.226	1.057	1.576	-528.138	2.633	-0.519	0.971
		20	1	-46.695	2.205	-46.829	2.200	0.134	0.039	-46.695	0.173	0.094	0.997
			2	-92.683	3.518	-92.800	3.510	0.117	0.037	-139.378	0.154	0.080	0.999
			3	-106.213	4.063	-106.323	4.051	0.111	0.037	-245.591	0.148	0.074	0.999
			4	-74.992	3.228	-75.083	3.218	0.091	0.033	-320.583	0.124	0.058	0.999
			5	-71.100	3.087	-71.178	3.079	0.078	0.028	-391.683	0.106	0.050	0.999
			6	-92.190	3.934	-92.255	3.926	0.065	0.022	-483.872	0.087	0.042	0.999
			7	-30.536	1.275	-30.591	1.270	0.055	0.017	-514.408	0.072	0.038	0.998
			8	-54.470	2.095	-54.519	2.090	0.049	0.017	-568.878	0.065	0.032	0.999
			9	-74.904	2.757	-74.949	2.753	0.045	0.015	-643.782	0.060	0.030	0.999
			10	-47.488	1.796	-47.529	1.793	0.042	0.014	-691.270	0.055	0.028	0.999

Table A. 9 Data for yearly cumulative erosion based on deterministic DEMs

Scenario	Resolution (m)	Time (year)	Net erosion (ton/ha)	Erosion (ton/ha)	Deposition (ton/ha)	Cumulative net erosion (ton/ha)	SDR (-)
L-scenario	2.5	1	-4.429	-4.430	0.001	-4.429	1.000
		2	-4.446	-4.447	0.001	-8.875	1.000
		3	-4.437	-4.438	0.001	-13.313	1.000
		4	-4.393	-4.394	0.001	-17.706	1.000
		5	-4.330	-4.331	0.001	-22.036	1.000
		6	-4.266	-4.267	0.001	-26.302	1.000
		7	-4.212	-4.213	0.001	-30.514	1.000
		8	-4.143	-4.143	0.001	-34.657	1.000
		9	-4.066	-4.067	0.001	-38.723	1.000
		10	-4.001	-4.002	0.001	-42.725	1.000
	5	1	-4.398	-4.399	0.000	-4.398	1.000
		2	-4.398	-4.398	0.000	-8.796	1.000
		3	-4.397	-4.397	0.000	-13.192	1.000
		4	-4.395	-4.396	0.000	-17.588	1.000
		5	-4.393	-4.394	0.000	-21.981	1.000
		6	-4.392	-4.392	0.000	-26.373	1.000
		7	-4.390	-4.390	0.000	-30.763	1.000
		8	-4.388	-4.389	0.000	-35.151	1.000
		9	-4.386	-4.387	0.000	-39.538	1.000
		10	-4.384	-4.385	0.000	-43.922	1.000
	10	1	-4.393	-4.393	0.000	-4.393	1.000
		2	-4.392	-4.393	0.000	-8.785	1.000
		3	-4.392	-4.392	0.000	-13.177	1.000
		4	-4.391	-4.391	0.000	-17.568	1.000
		5	-4.390	-4.390	0.000	-21.958	1.000
		6	-4.389	-4.389	0.000	-26.347	1.000
		7	-4.388	-4.388	0.000	-30.735	1.000
		8	-4.387	-4.387	0.000	-35.122	1.000
		9	-4.386	-4.386	0.000	-39.508	1.000
		10	-4.385	-4.385	0.000	-43.893	1.000
	20	1	-4.407	-4.408	0.000	-4.407	1.000
		2	-4.407	-4.407	0.000	-8.815	1.000
		3	-4.407	-4.407	0.000	-13.221	1.000
		4	-4.407	-4.407	0.000	-17.628	1.000
		5	-4.406	-4.406	0.000	-22.034	1.000
		6	-4.406	-4.406	0.000	-26.440	1.000
		7	-4.406	-4.406	0.000	-30.846	1.000
		8	-4.406	-4.406	0.000	-35.252	1.000
		9	-4.405	-4.406	0.000	-39.658	1.000
		10	-4.405	-4.405	0.000	-44.063	1.000
H-scenario	2.5	1	-43.697	-44.077	0.379	-43.697	0.991
		2	-36.845	-39.471	2.626	-80.542	0.933
		3	-23.369	-36.144	12.775	-103.912	0.647
		4	-10.644	-34.664	24.020	-114.556	0.307
		5	-12.297	-34.909	22.611	-126.854	0.352
		6	-17.283	-35.525	18.242	-144.136	0.487

Scenario	Resolution (m)	Time (year)	Net erosion (ton/ha)	Erosion (ton/ha)	Deposition (ton/ha)	Cumulative net erosion (ton/ha)	SDR (-)
		7	-17.372	-34.666	17.294	-161.508	0.501
		8	-18.311	-34.162	15.850	-179.819	0.536
		9	-17.582	-33.171	15.589	-197.401	0.530
		10	-16.468	-32.478	16.010	-213.869	0.507
	5	1	-43.996	-44.057	0.061	-43.996	0.999
		2	-42.045	-42.089	0.044	-86.041	0.999
		3	-40.008	-40.042	0.034	-126.048	0.999
		4	-37.096	-37.122	0.026	-163.144	0.999
		5	-33.581	-34.438	0.858	-196.725	0.975
		6	-25.486	-31.534	6.048	-222.211	0.808
		7	-20.052	-30.033	9.981	-242.263	0.668
		8	-15.197	-28.231	13.034	-257.460	0.538
		9	-17.030	-28.593	11.563	-274.491	0.596
		10	-15.941	-26.717	10.776	-290.431	0.597
	10	1	-44.073	-44.091	0.018	-44.073	1.000
		2	-43.926	-43.942	0.016	-87.999	1.000
		3	-42.897	-42.911	0.014	-130.896	1.000
		4	-41.050	-41.061	0.010	-171.946	1.000
		5	-39.147	-39.155	0.008	-211.093	1.000
		6	-37.047	-37.054	0.008	-248.140	1.000
		7	-35.009	-35.015	0.007	-283.148	1.000
		8	-33.700	-33.705	0.005	-316.848	1.000
		9	-32.225	-32.230	0.005	-349.073	1.000
		10	-30.533	-30.538	0.005	-379.606	1.000
	20	1	-47.212	-47.232	0.019	-47.212	1.000
		2	-47.201	-47.218	0.017	-94.413	1.000
		3	-46.409	-46.422	0.014	-140.822	1.000
		4	-45.754	-45.769	0.014	-186.577	1.000
		5	-45.850	-45.864	0.014	-232.426	1.000
		6	-45.935	-45.950	0.015	-278.362	1.000
		7	-45.505	-45.518	0.013	-323.866	1.000
		8	-44.126	-44.133	0.007	-367.992	1.000
		9	-43.389	-43.394	0.005	-411.381	1.000
		10	-41.961	-41.965	0.004	-453.341	1.000
LCL-scenario	2.5	1	-4.429	-4.430	0.001	-4.429	1.000
		2	-8.779	-8.780	0.001	-13.209	1.000
		3	-10.181	-10.182	0.001	-23.390	1.000
		4	-7.967	-7.968	0.001	-31.357	1.000
		5	-7.945	-7.945	0.001	-39.302	1.000
		6	-10.392	-10.393	0.001	-49.694	1.000
		7	-3.913	-3.913	0.000	-53.607	1.000
		8	-6.982	-6.982	0.000	-60.588	1.000
		9	-9.434	-9.435	0.000	-70.023	1.000
		10	-6.503	-6.503	0.000	-76.526	1.000
	5	1	-4.398	-4.399	0.000	-4.398	1.000
		2	-8.864	-8.864	0.000	-13.262	1.000
		3	-10.771	-10.771	0.000	-24.033	1.000

Scenario	Resolution (m)	Time (year)	Net erosion (ton/ha)	Erosion (ton/ha)	Deposition (ton/ha)	Cumulative net erosion (ton/ha)	SDR (-)
		4	-8.399	-8.400	0.000	-32.432	1.000
		5	-8.706	-8.707	0.000	-41.138	1.000
		6	-12.324	-12.324	0.000	-53.462	1.000
		7	-4.308	-4.308	0.000	-57.770	1.000
		8	-7.888	-7.888	0.000	-65.658	1.000
		9	-11.245	-11.246	0.000	-76.903	1.000
		10	-7.403	-7.403	0.000	-84.306	1.000
	10	1	-4.393	-4.393	0.000	-4.393	1.000
		2	-8.853	-8.853	0.000	-13.246	1.000
		3	-10.759	-10.759	0.000	-24.005	1.000
		4	-8.396	-8.396	0.000	-32.401	1.000
		5	-8.707	-8.707	0.000	-41.108	1.000
		6	-12.370	-12.370	0.000	-53.478	1.000
		7	-4.404	-4.404	0.000	-57.881	1.000
		8	-8.167	-8.168	0.000	-66.049	1.000
		9	-11.904	-11.904	0.000	-77.953	1.000
		10	-7.968	-7.968	0.000	-85.920	1.000
	20	1	-4.407	-4.408	0.000	-4.407	1.000
		2	-8.883	-8.883	0.000	-13.290	1.000
		3	-10.798	-10.798	0.000	-24.089	1.000
		4	-8.430	-8.430	0.000	-32.518	1.000
		5	-8.744	-8.745	0.000	-41.263	1.000
		6	-12.429	-12.429	0.000	-53.691	1.000
		7	-4.427	-4.427	0.000	-58.119	1.000
		8	-8.213	-8.213	0.000	-66.332	1.000
		9	-11.976	-11.976	0.000	-78.308	1.000
		10	-8.021	-8.021	0.000	-86.329	1.000
LCL-scenario	2.5	1	-43.697	-44.077	0.379	-43.697	0.991
		2	-64.257	-66.849	2.592	-107.955	0.961
		3	-56.977	-72.361	15.384	-164.931	0.787
		4	-28.621	-55.999	27.378	-193.552	0.511
		5	-29.632	-57.856	28.224	-223.184	0.512
		6	-49.752	-75.075	25.323	-272.936	0.663
		7	-10.061	-32.474	22.413	-282.997	0.310
		8	-29.078	-52.218	23.140	-312.075	0.557
		9	-47.644	-67.793	20.149	-359.719	0.703
		10	-26.420	-47.505	21.085	-386.139	0.556
	5	1	-43.996	-44.057	0.061	-43.996	0.999
		2	-67.300	-67.342	0.042	-111.295	0.999
		3	-72.145	-72.172	0.027	-183.440	1.000
		4	-57.006	-57.021	0.015	-240.446	1.000
		5	-54.382	-54.392	0.011	-294.827	1.000
		6	-65.387	-65.397	0.009	-360.214	1.000
		7	-26.071	-26.078	0.007	-386.285	1.000
		8	-39.410	-40.369	0.959	-425.696	0.976
		9	-51.517	-51.553	0.036	-477.213	0.999
		10	-32.740	-32.769	0.029	-509.953	0.999

Scenario	Resolution (m)	Time (year)	Net erosion (ton/ha)	Erosion (ton/ha)	Deposition (ton/ha)	Cumulative net erosion (ton/ha)	SDR (-)
	10	1	-44.073	-44.091	0.018	-44.073	1.000
		2	-87.040	-87.056	0.016	-131.113	1.000
		3	-96.278	-96.289	0.011	-227.391	1.000
		4	-67.552	-67.560	0.008	-294.943	1.000
		5	-62.067	-64.757	2.689	-357.011	0.958
		6	-81.788	-81.891	0.103	-438.799	0.999
		7	-26.654	-26.769	0.115	-465.452	0.996
		8	-46.051	-48.036	1.984	-511.504	0.959
		9	-56.700	-64.316	7.616	-568.203	0.882
		10	-33.389	-39.145	5.757	-601.592	0.853
	20	1	-47.212	-47.232	0.019	-47.212	1.000
		2	-94.062	-94.079	0.017	-141.274	1.000
		3	-112.208	-112.224	0.016	-253.482	1.000
		4	-86.791	-86.804	0.013	-340.273	1.000
		5	-86.154	-86.160	0.005	-426.427	1.000
		6	-113.543	-113.549	0.006	-539.970	1.000
		7	-36.793	-36.806	0.013	-576.763	1.000
		8	-64.269	-64.276	0.007	-641.032	1.000
		9	-86.733	-86.740	0.006	-727.765	1.000
		10	-53.999	-54.006	0.007	-781.764	1.000

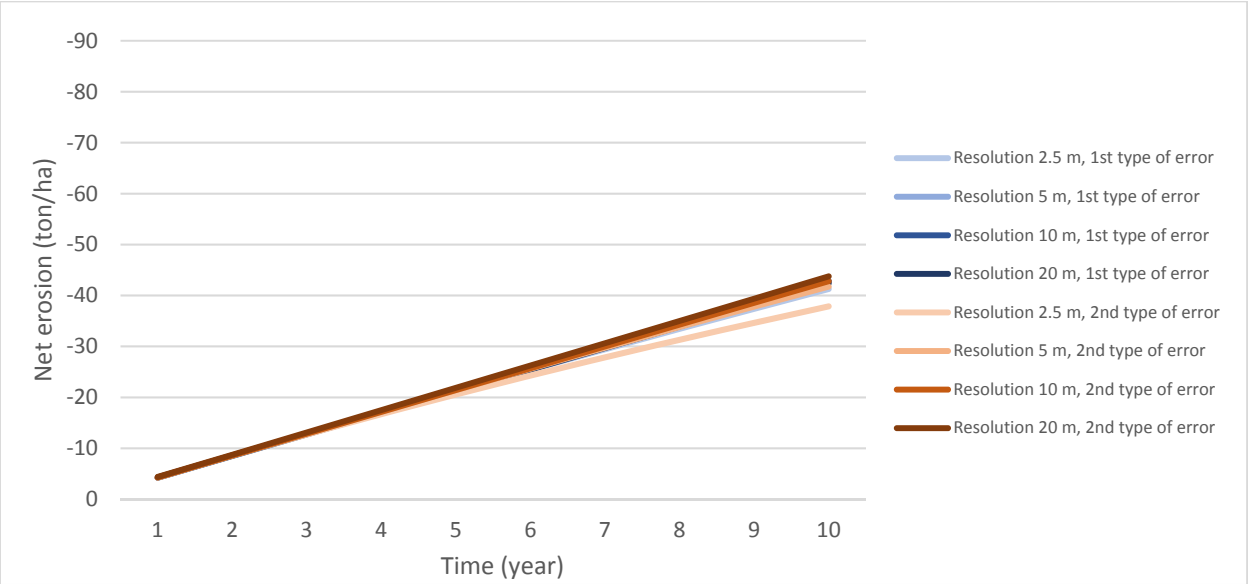

Figure A. 1 Mean cumulative net erosion based on simulated error DEMs for L-scenario

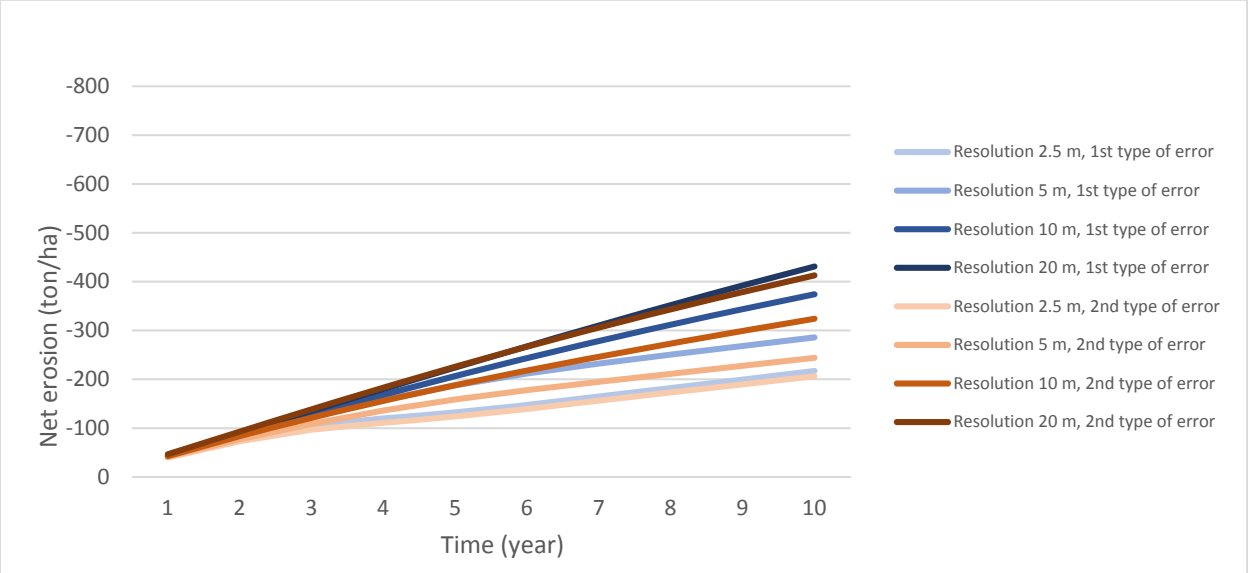

Figure A. 2 Mean cumulative net erosion based on simulated error DEMs for H-scenario

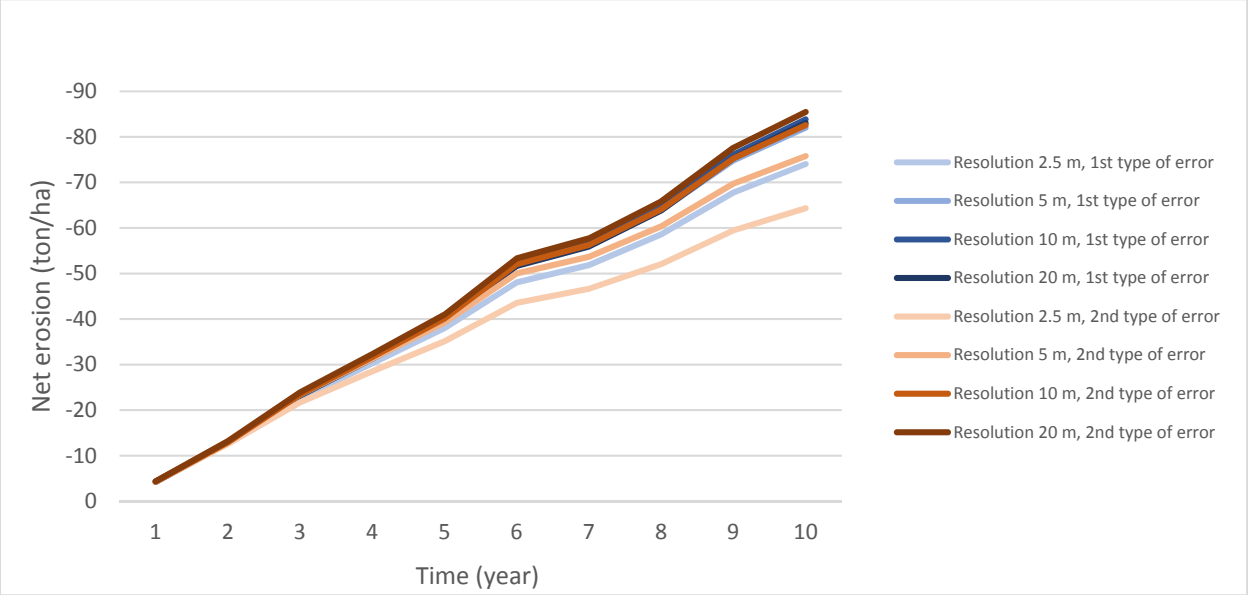

Figure A. 3 Mean cumulative net erosion based on simulated error DEMs for LCL-scenario

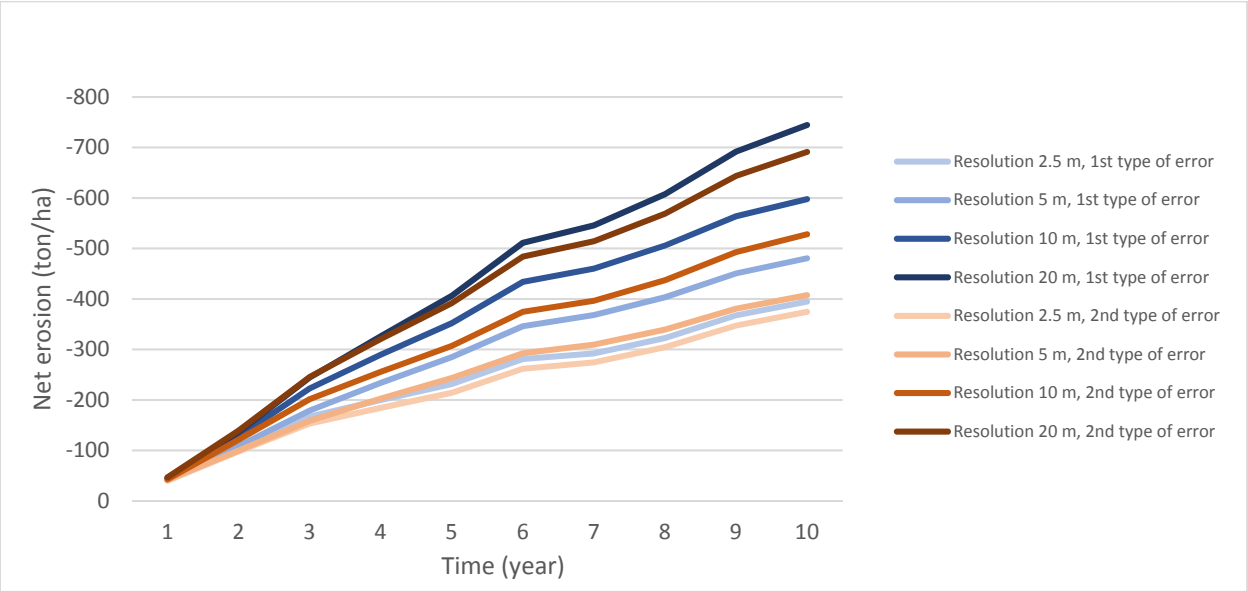

Figure A. 4 Mean cumulative net erosion based on simulated error DEMs for HCL-scenario

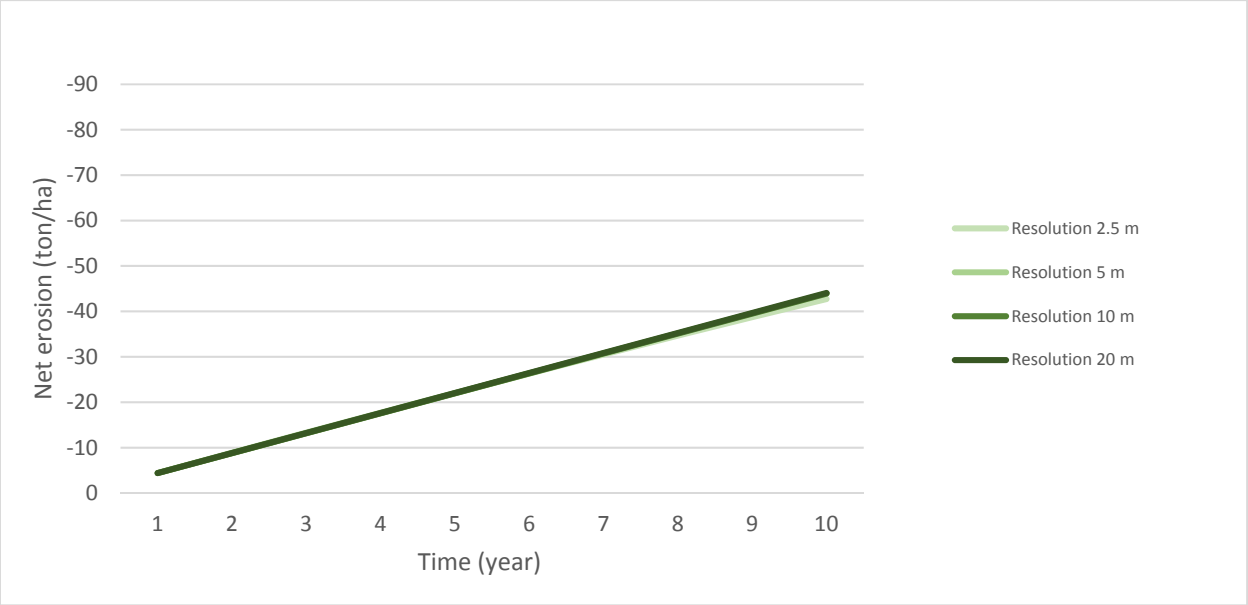

Figure A. 5 Cumulative net erosion based on deterministic DEM for L-scenario

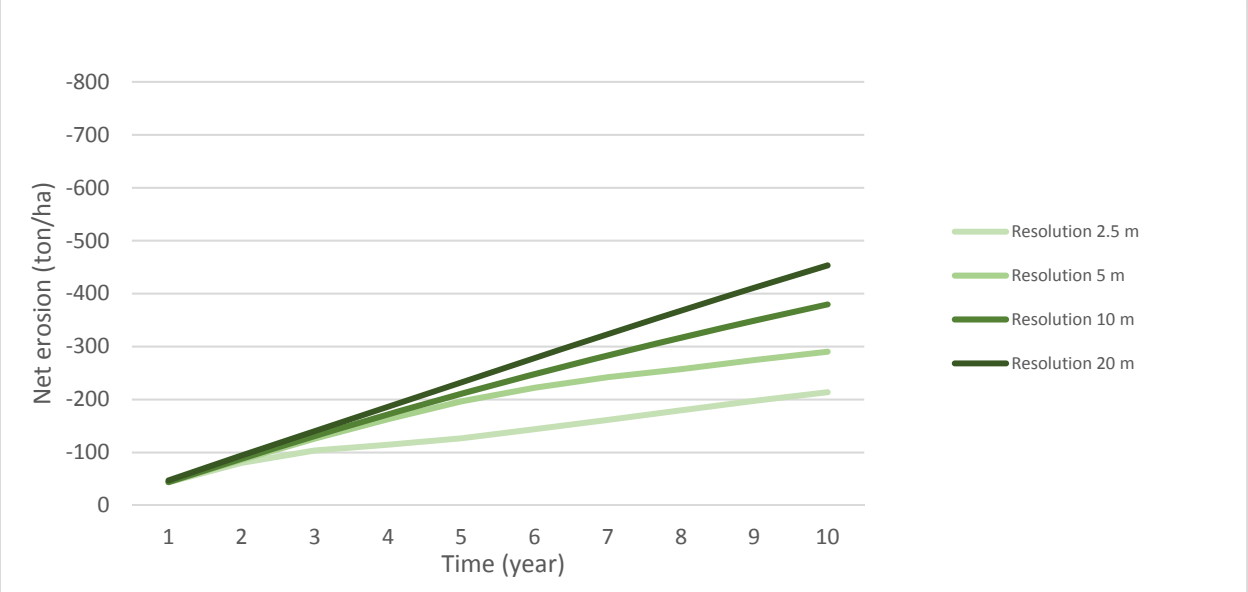

Figure A. 6 Cumulative net erosion based on simulated DEMs for H-scenario

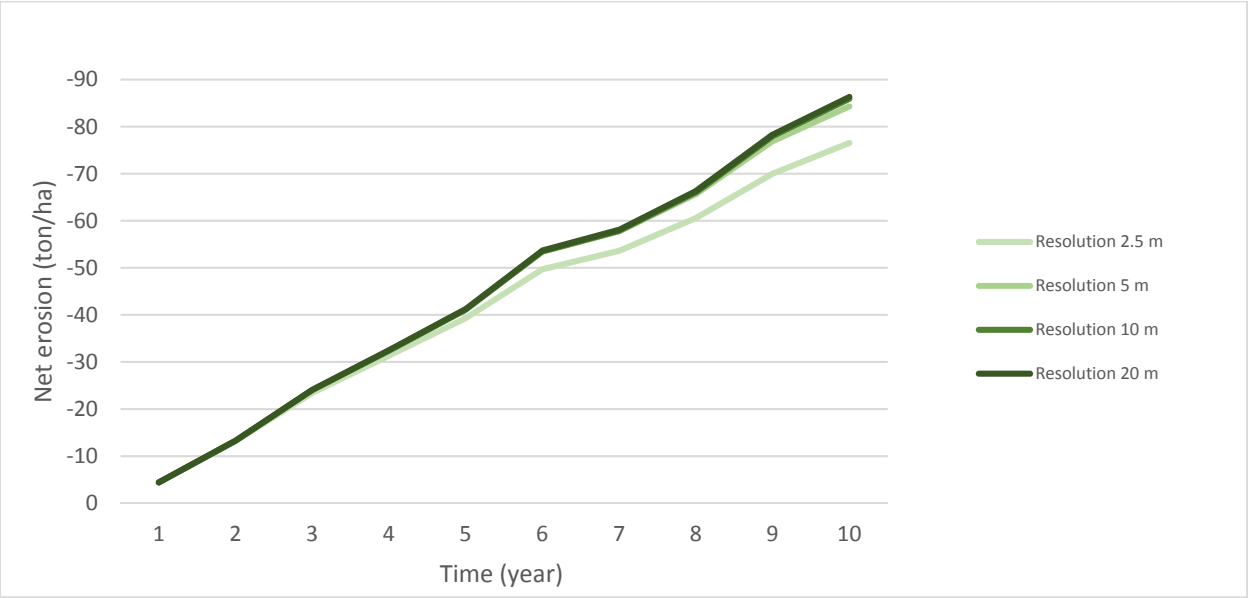

Figure A. 7 Cumulative net erosion based on deterministic DEM for LCL-scenario

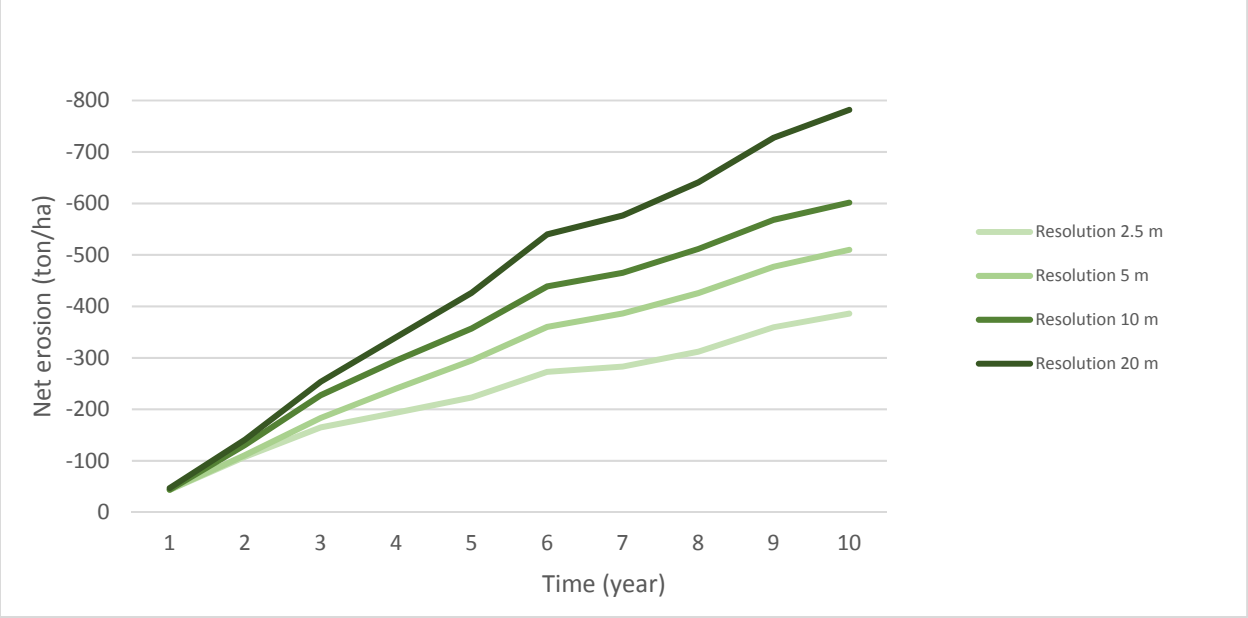

Figure A. 8 Cumulative net erosion based on deterministic DEM for HCL-scenario

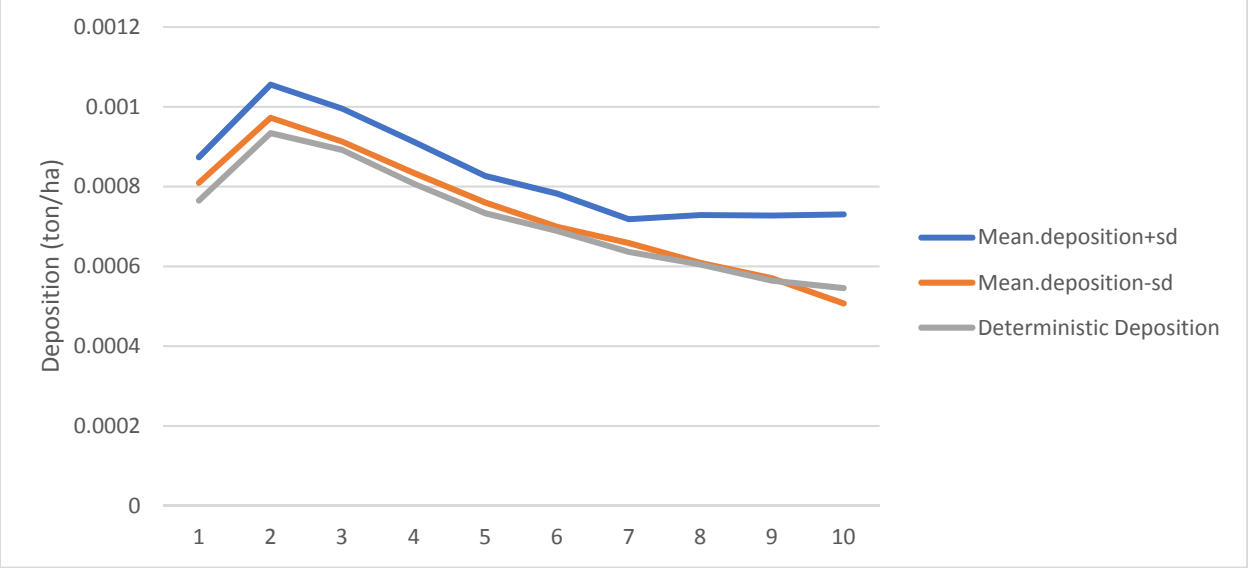

Figure A. 9 Deposition and standard deviation for DEMs with resolution of 2.5 m, 1st type of error for L-scenario

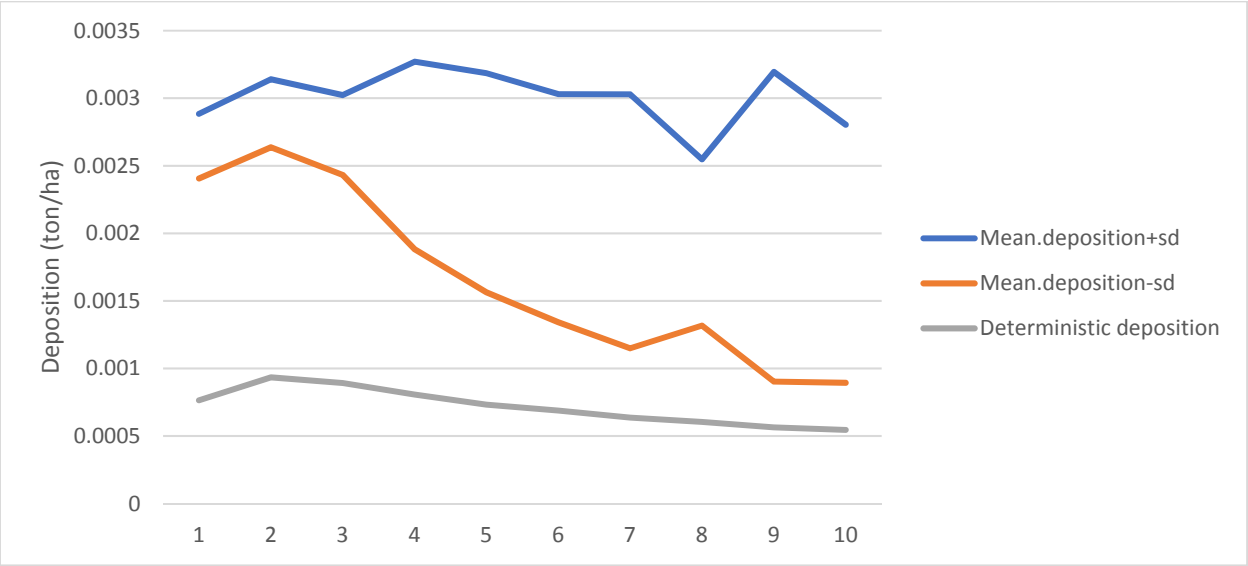

Figure A. 10 Deposition and standard deviation for DEMs with resolution of 2.5 m, 2nd type of error for L-scenario

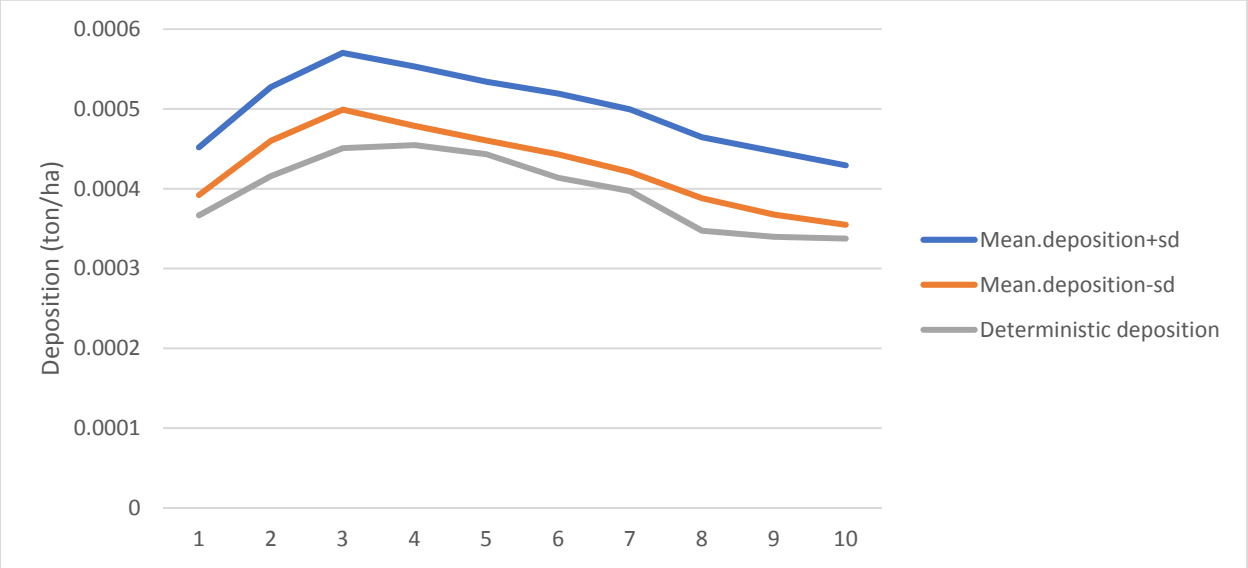

Figure A. 11 Deposition and standard deviation for DEMs with resolution of 5 m, 1st type of error for L-scenario

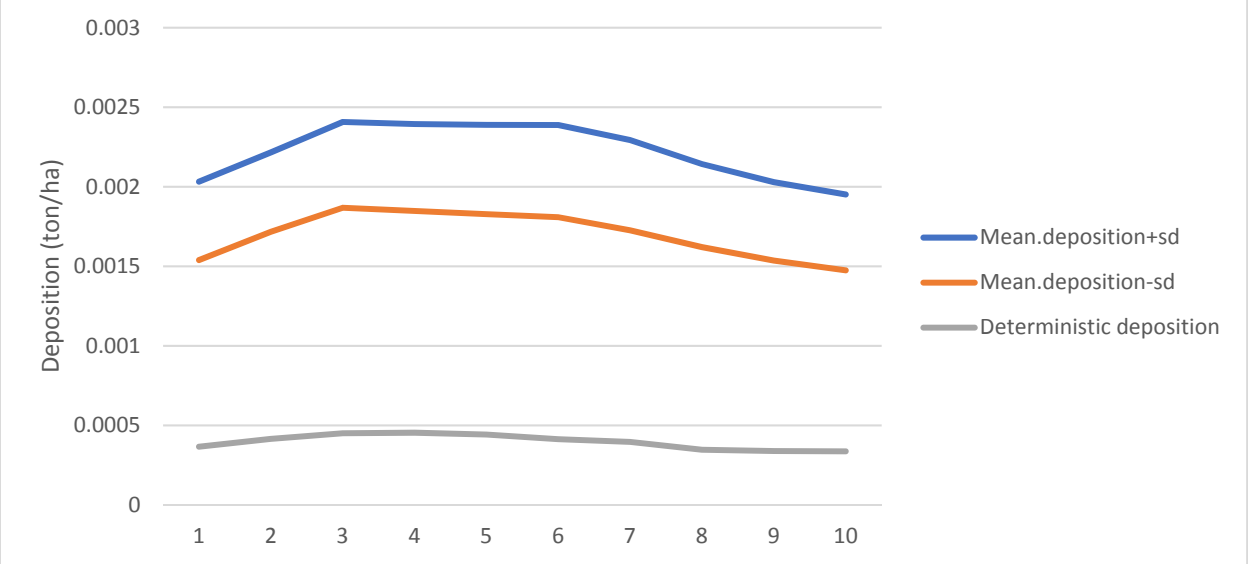

Figure A. 12 Deposition and standard deviation for DEMs with resolution of 5 m, 2st type of error for L-scenario

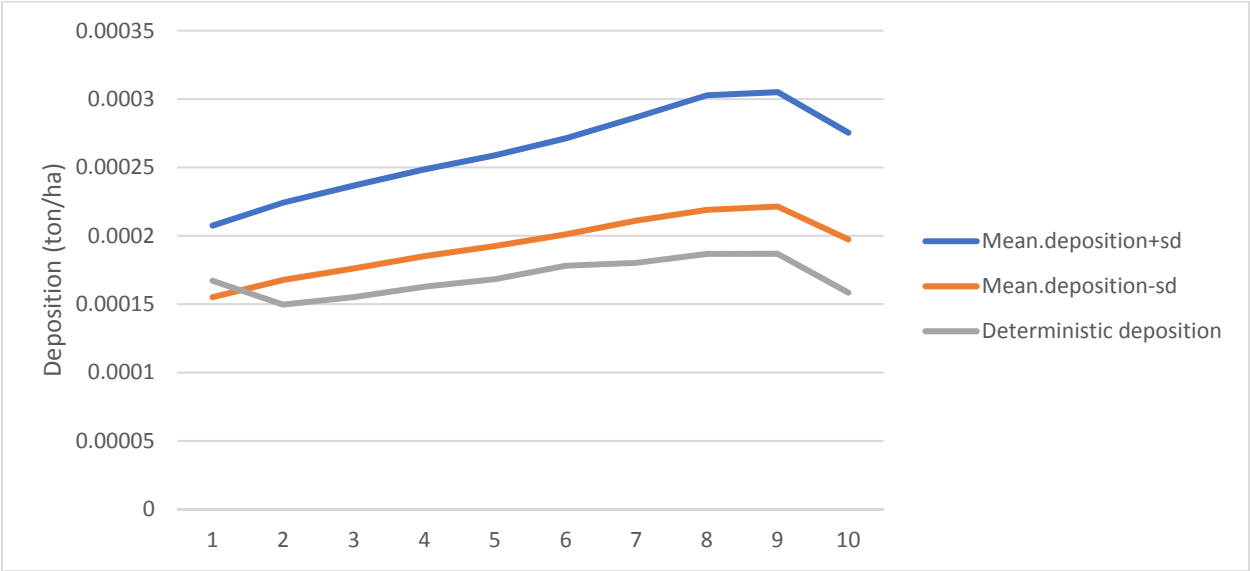

Figure A. 13 Deposition and standard deviation for DEMs with resolution of 10 m, 1st type of error for L-scenario

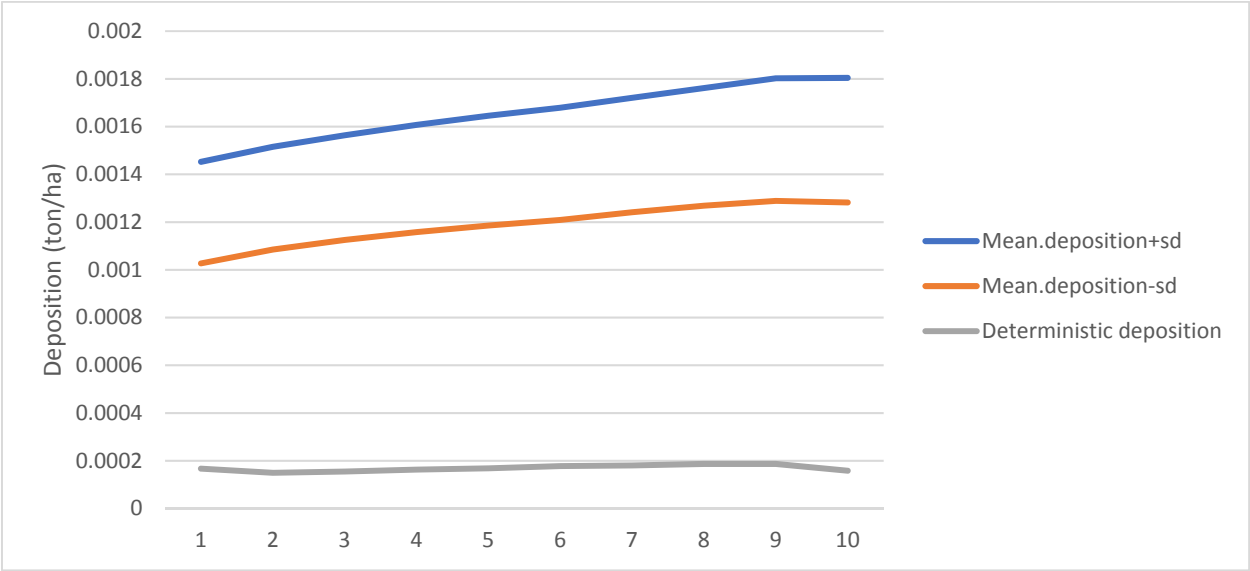

Figure A. 14 Deposition and standard deviation for DEMs with resolution of 10 m, 2st type of error for L-scenario

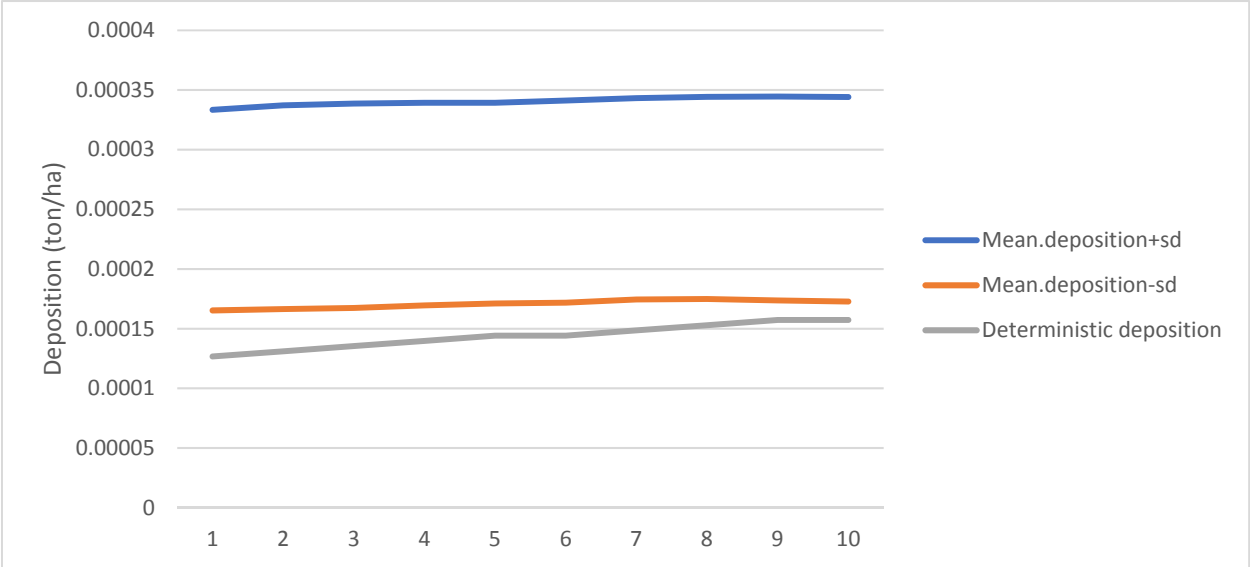

Figure A. 15 Deposition and standard deviation for DEMs with resolution of 20 m, 1st type of error for L-scenario

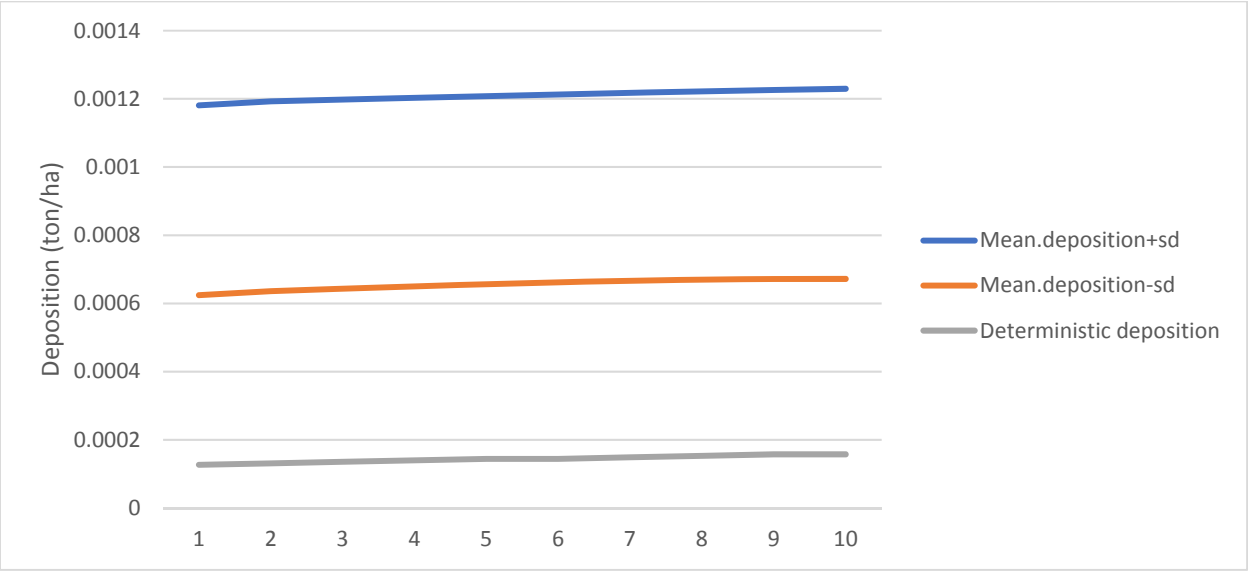

Figure A. 16 Deposition and standard deviation for DEMs with resolution of 20 m, 2st type of error for L-scenario

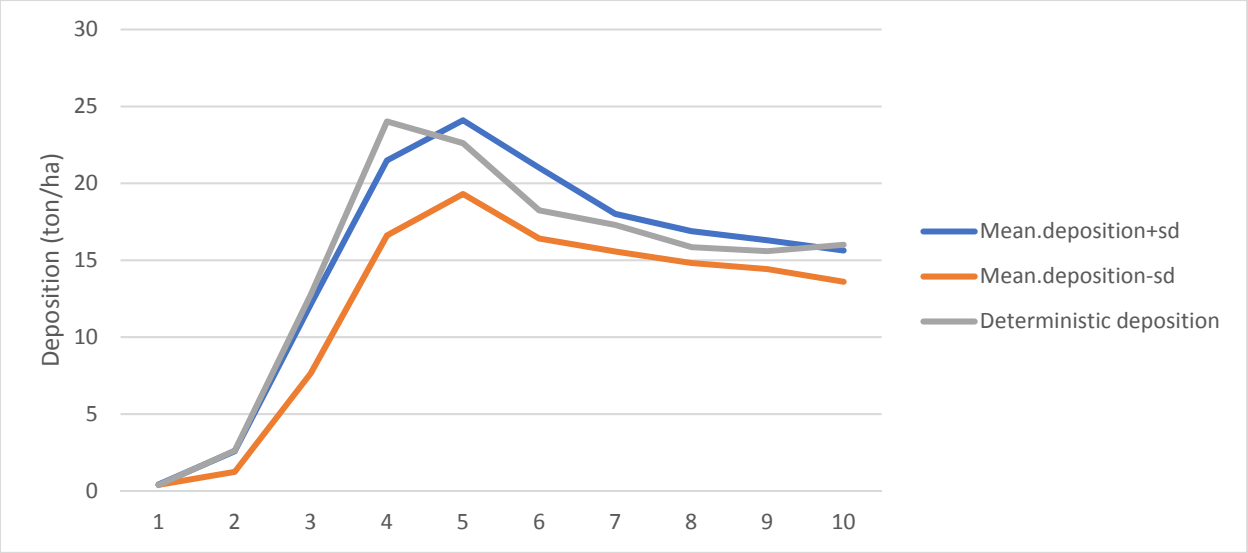

Figure A. 17 Deposition and standard deviation for DEMs with resolution of 2.5 m, 1st type of error for H-scenario

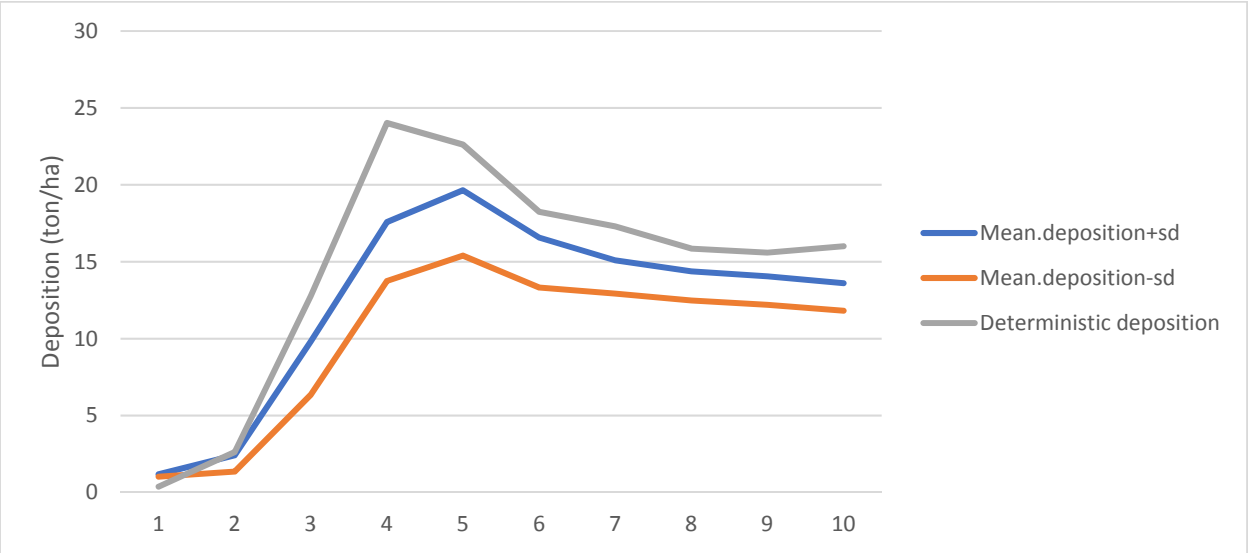

Figure A. 18 Deposition and standard deviation for DEMs with resolution of 2.5 m, 2st type of error for H-scenario

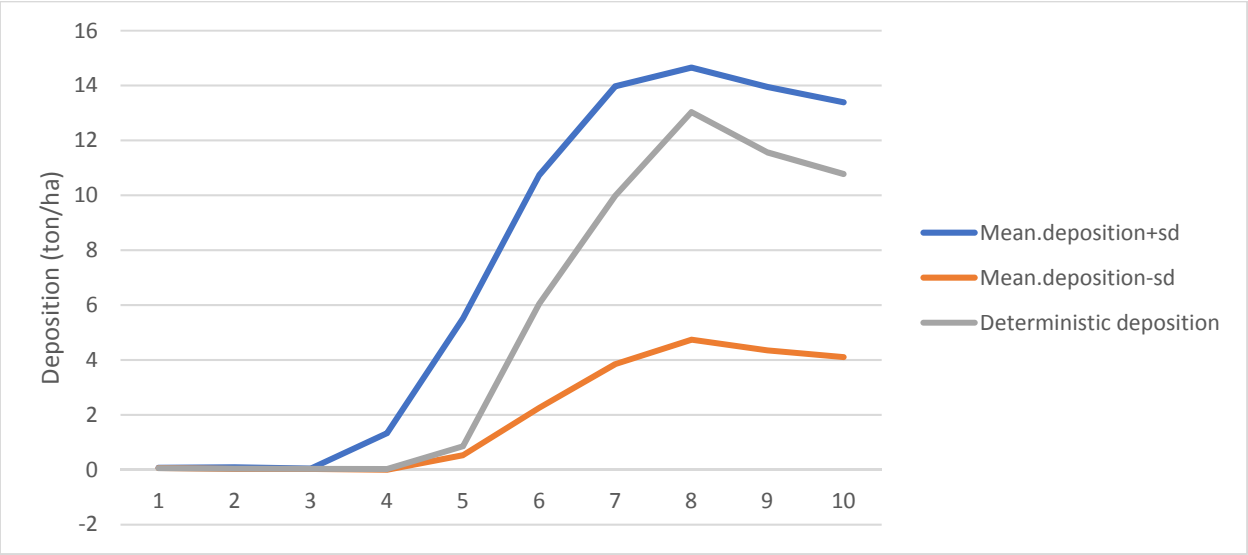

Figure A. 19 Deposition and standard deviation for DEMs with resolution of 5 m, 1st type of error for H-scenario

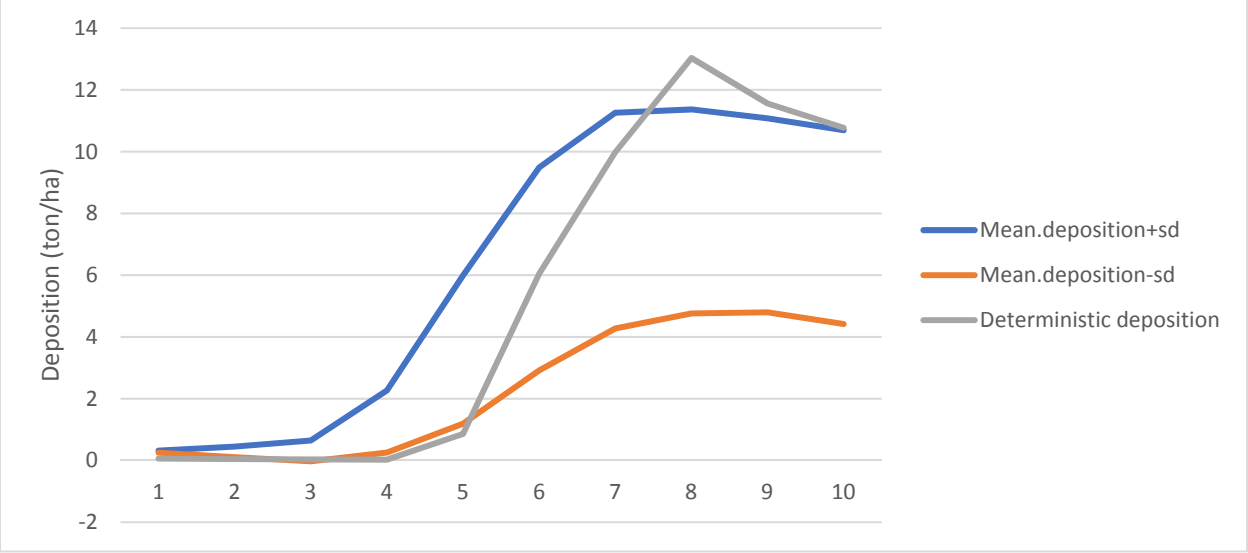

Figure A. 20 Deposition and standard deviation for DEMs with resolution of 5 m, 2st type of error for H-scenario

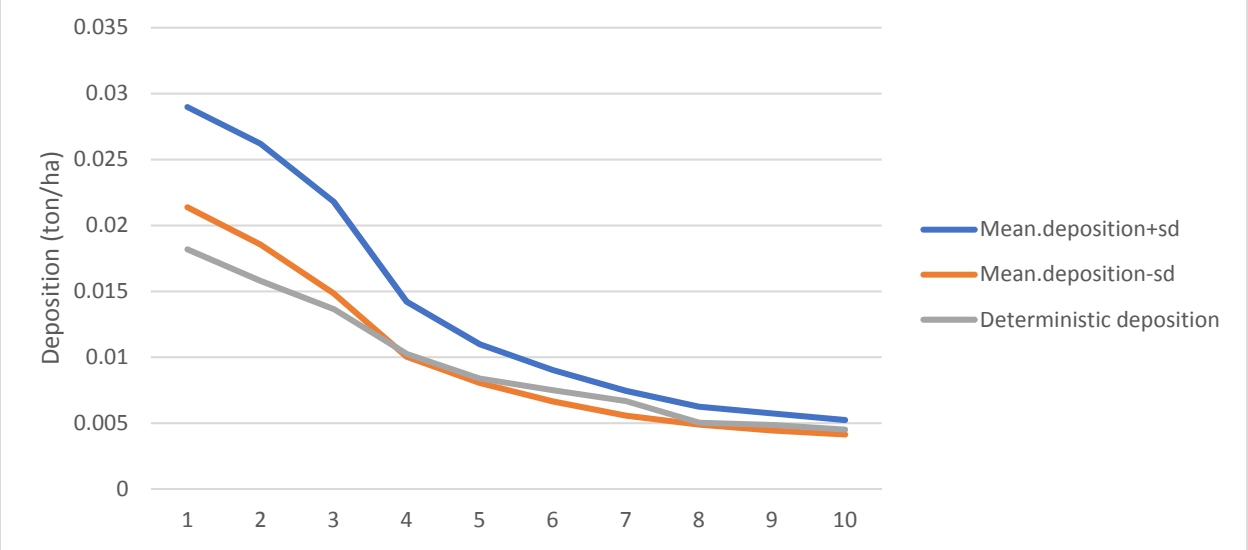

Figure A. 21 Deposition and standard deviation for DEMs with resolution of 10 m, 1st type of error for H-scenario

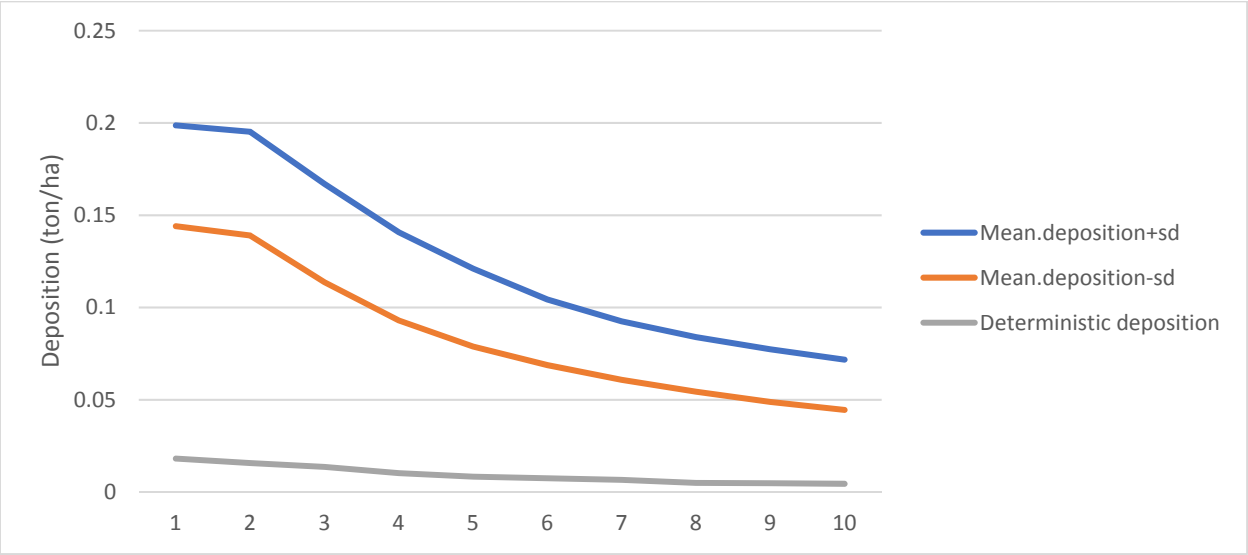

Figure A. 22 Deposition and standard deviation for DEMs with resolution of 10 m, 2st type of error for H-scenario

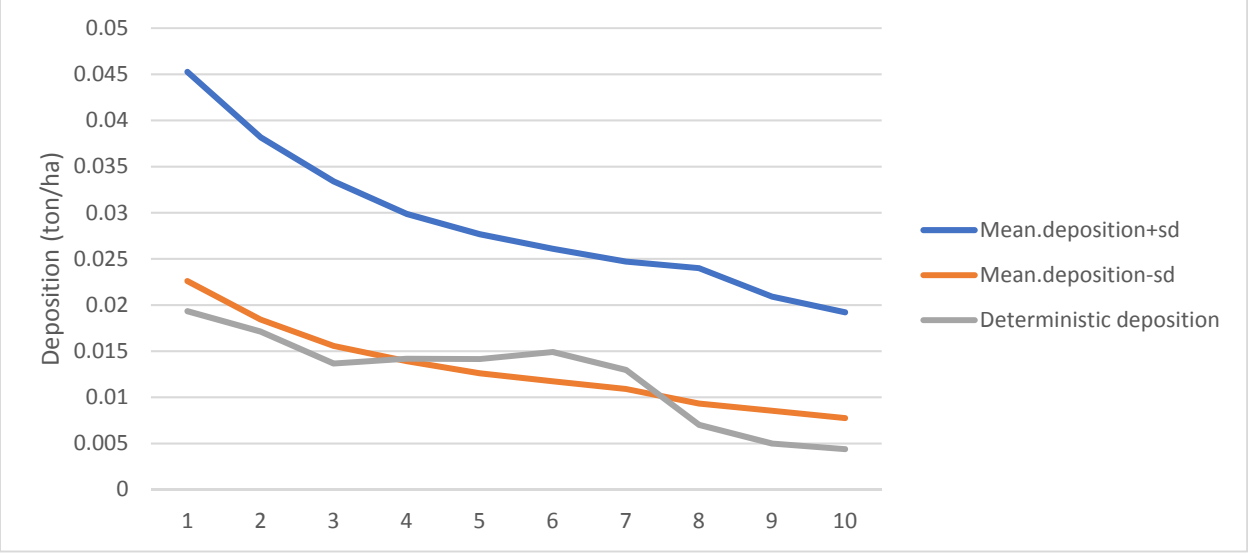

Figure A. 23 Deposition and standard deviation for DEMs with resolution of 20 m, 1st type of error for H-scenario

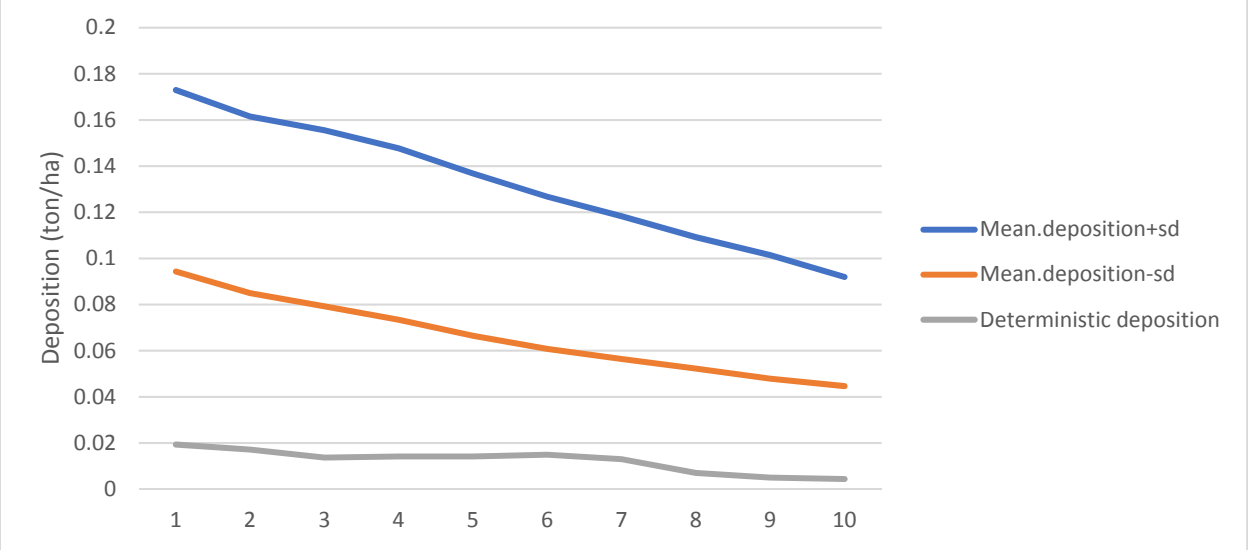

Figure A. 24 Deposition and standard deviation for DEMs with resolution of 20 m, 2st type of error for H-scenario

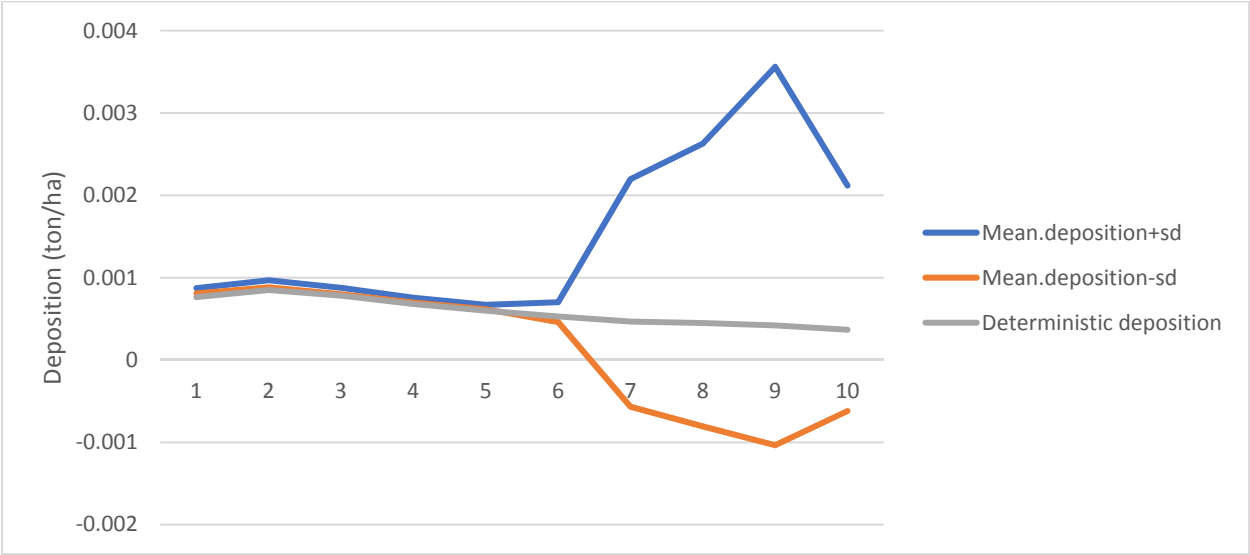

Figure A. 25 Deposition and standard deviation for DEMs with resolution of 2.5 m, 1st type of error for LCL-scenario

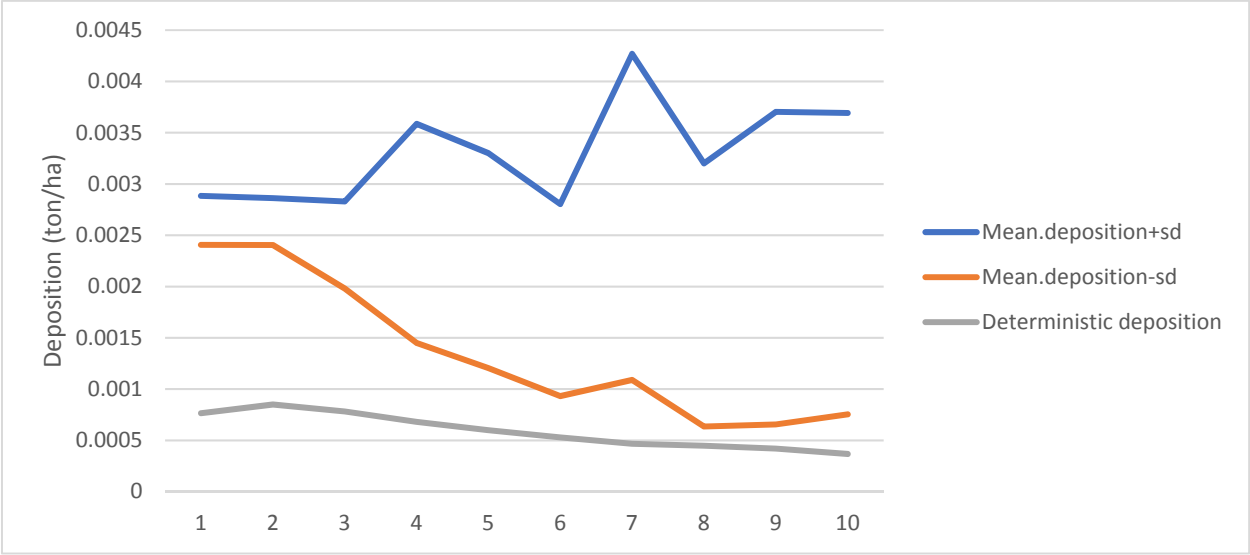

Figure A. 26 Deposition and standard deviation for DEMs with resolution of 2.5 m, 2st type of error for LCL-scenario

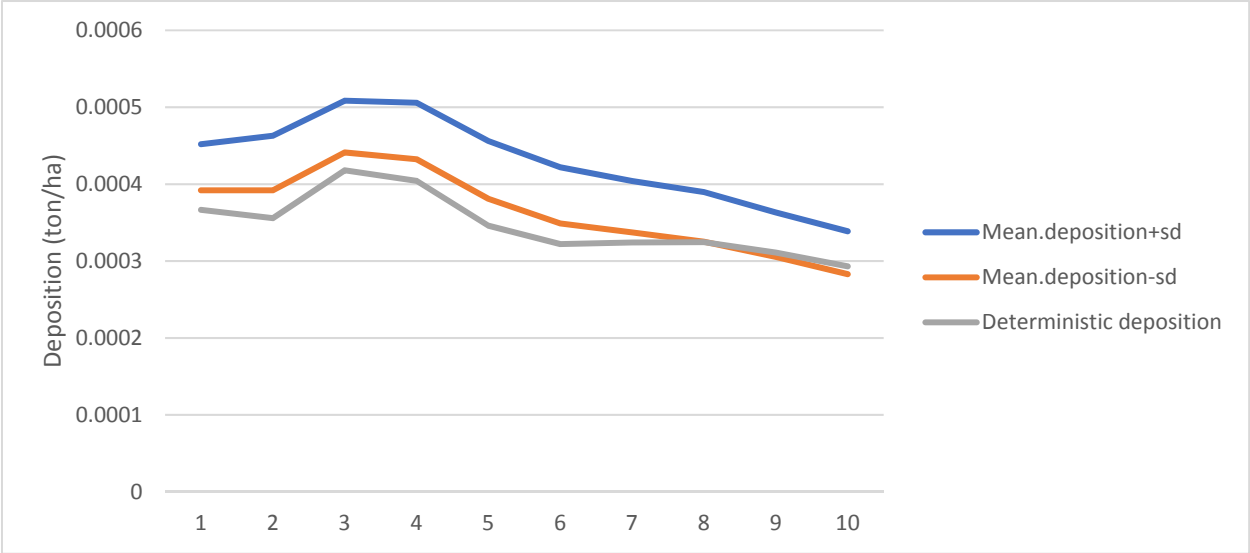

Figure A. 27 Deposition and standard deviation for DEMs with resolution of 5 m, 1st type of error for LCL-scenario

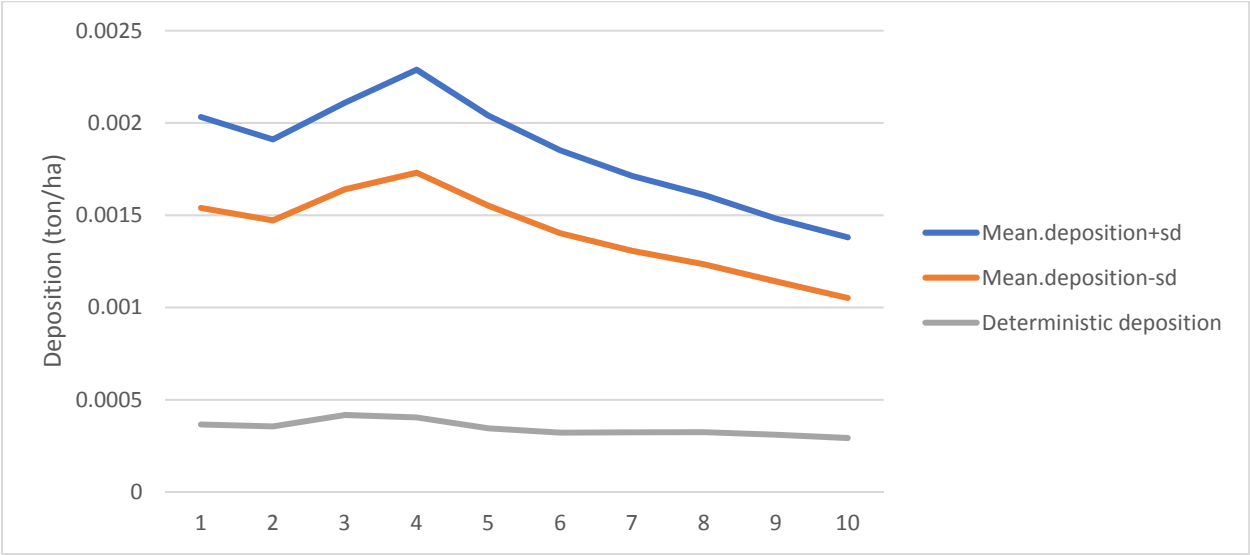

Figure A. 28 Deposition and standard deviation for DEMs with resolution of 5 m, 2st type of error for LCL-scenario

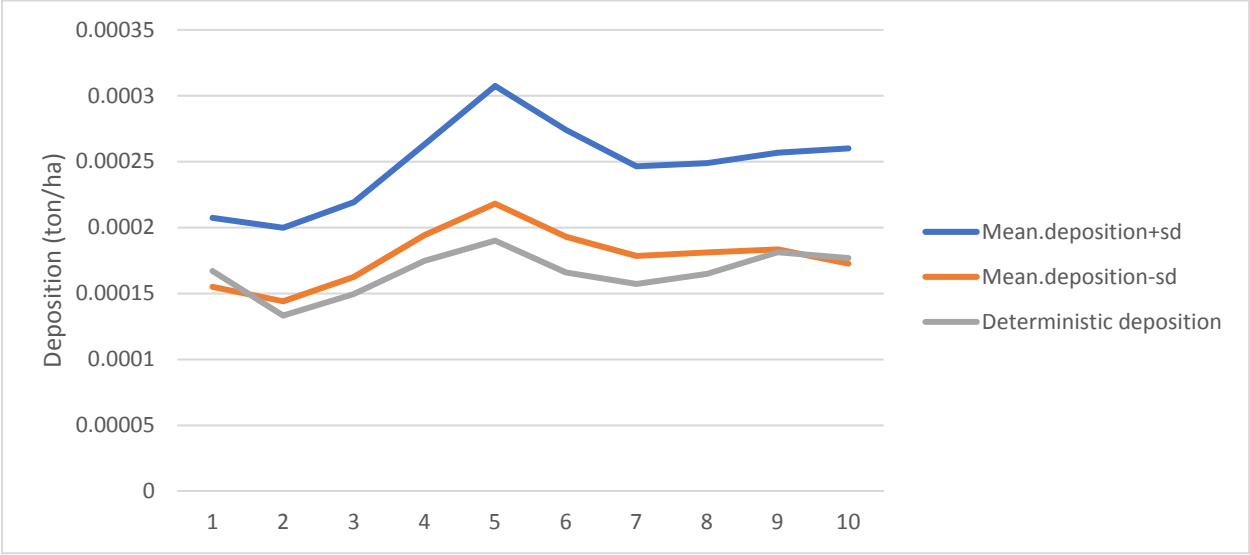

Figure A. 29 Deposition and standard deviation for DEMs with resolution of 10 m, 1st type of error for LCL-scenario

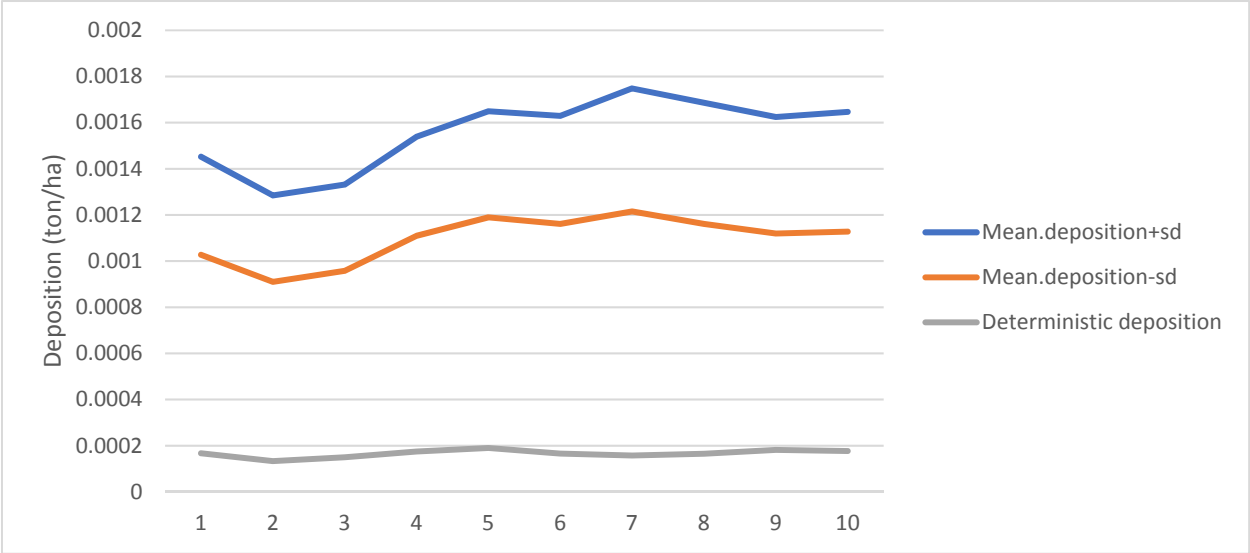

Figure A. 30 Deposition and standard deviation for DEMs with resolution of 10 m, 2st type of error for LCL-scenario

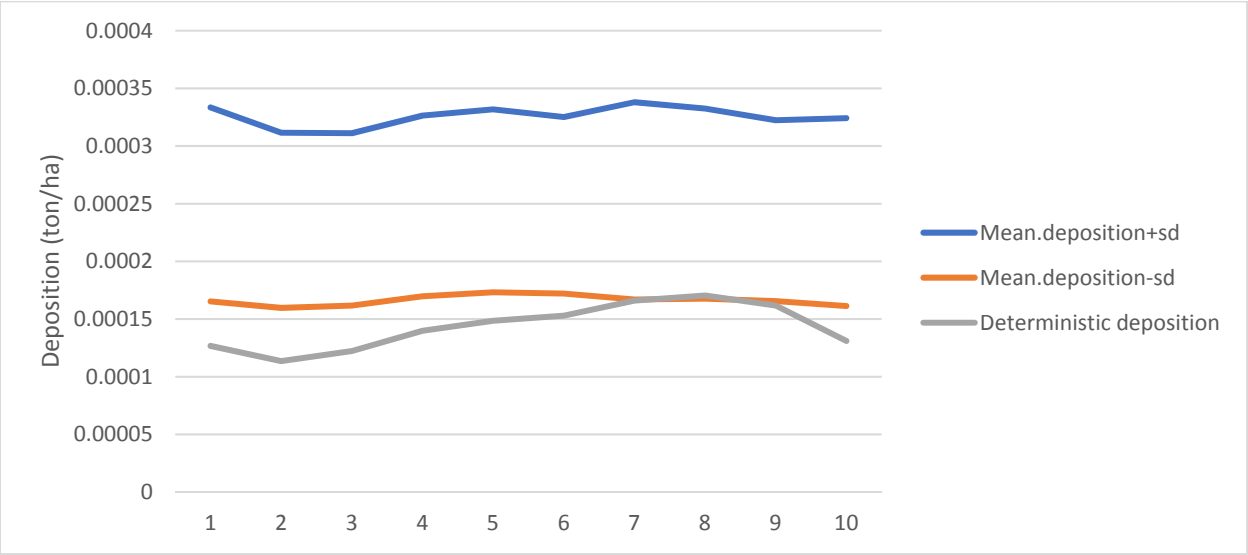

Figure A. 31 Deposition and standard deviation for DEMs with resolution of 20 m, 1st type of error for LCL-scenario

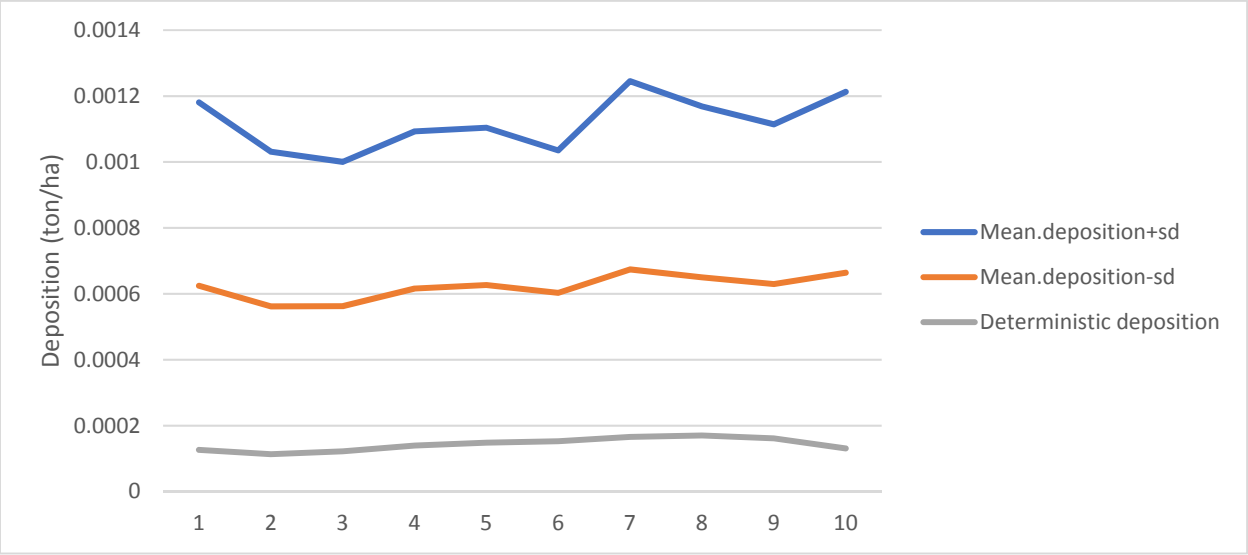

Figure A. 32 Deposition and standard deviation for DEMs with resolution of 20 m, 2st type of error for LCL-scenario

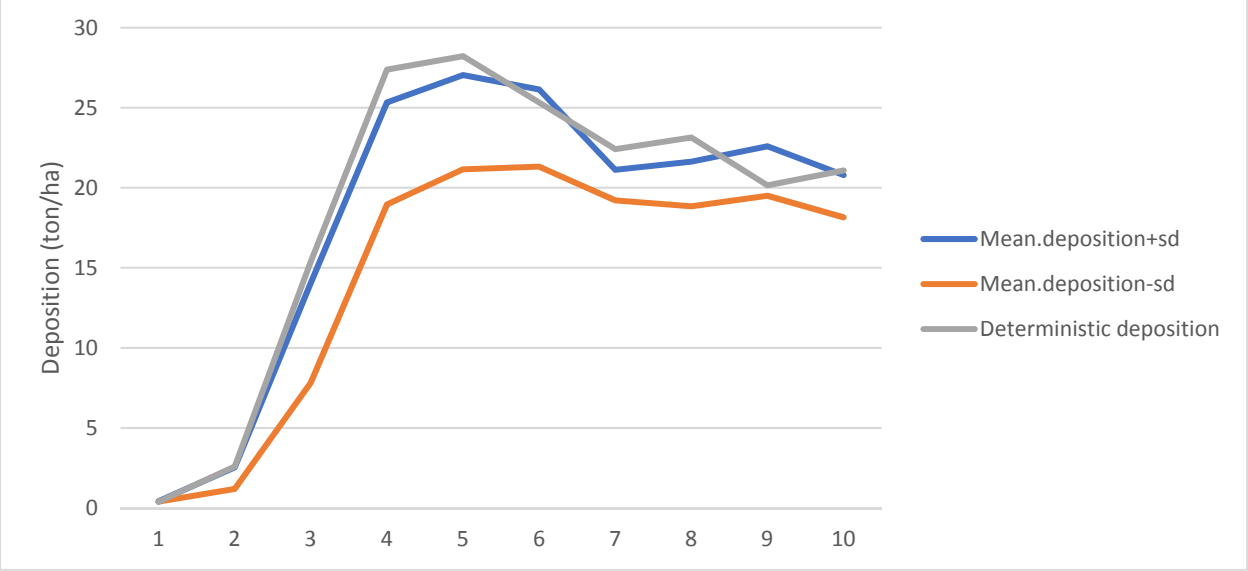

Figure A. 33 Deposition and standard deviation for DEMs with resolution of 2.5 m, 1st type of error for HCL-scenario

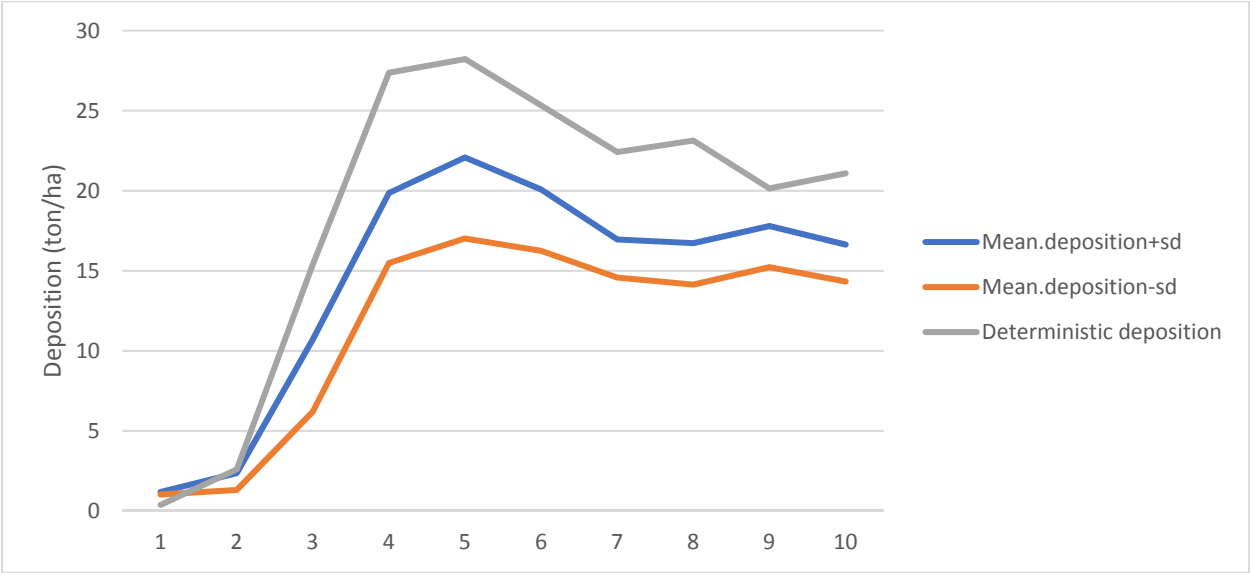

Figure A. 34 Deposition and standard deviation for DEMs with resolution of 2.5 m, 2st type of error for HCL-scenario

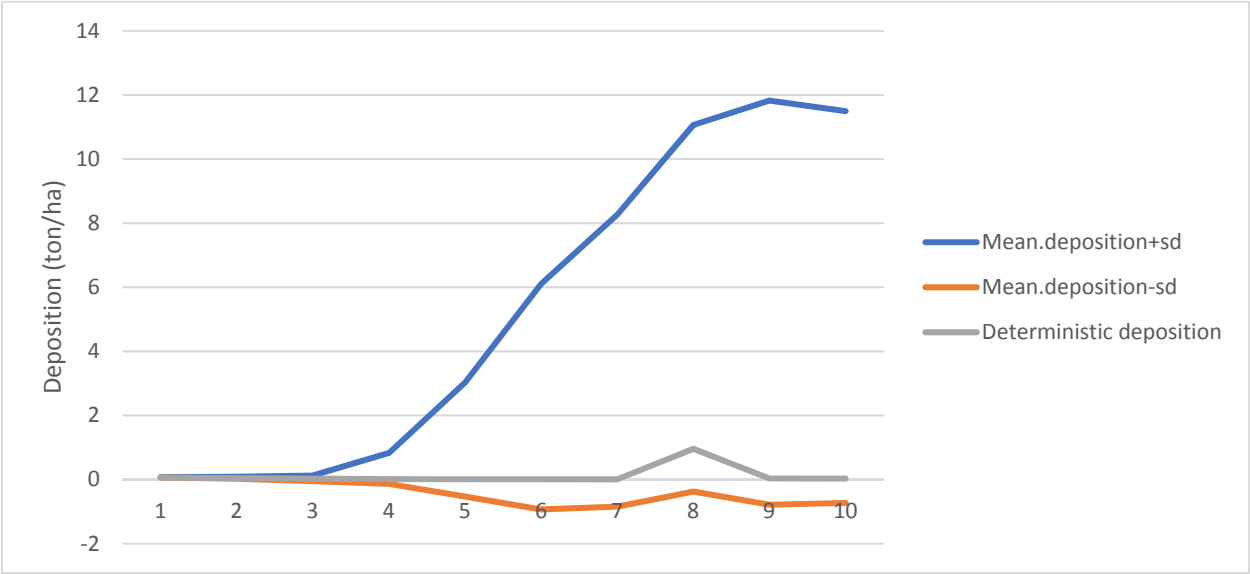

Figure A. 35 Deposition and standard deviation for DEMs with resolution of 5 m, 1st type of error for HCL-scenario

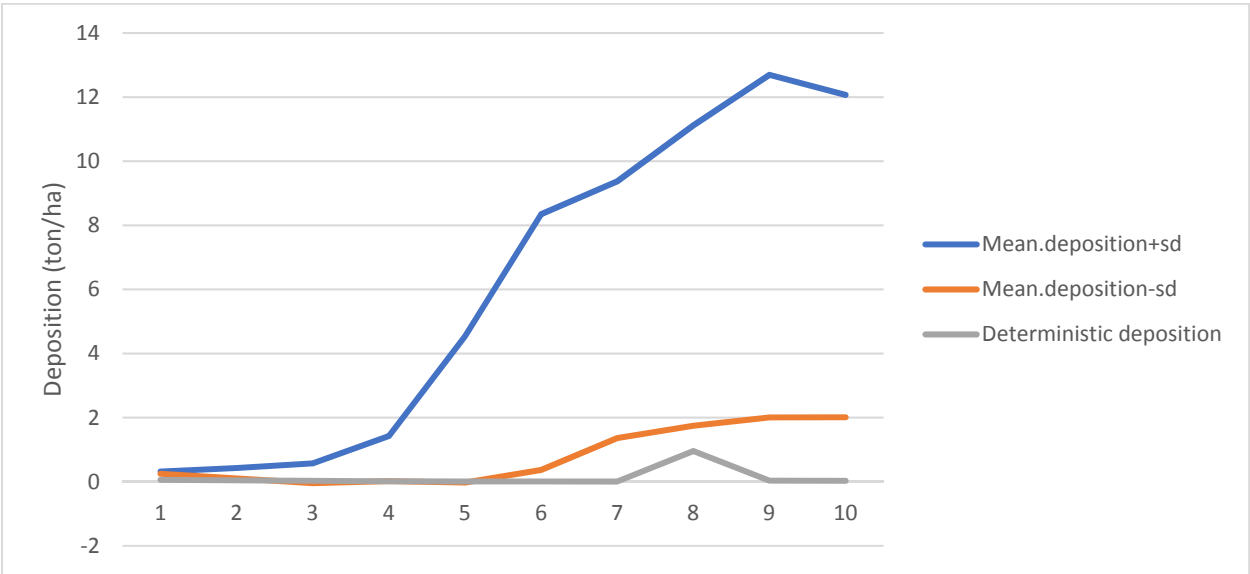

Figure A. 36 Deposition and standard deviation for DEMs with resolution of 5 m, 2st type of error for HCL-scenario

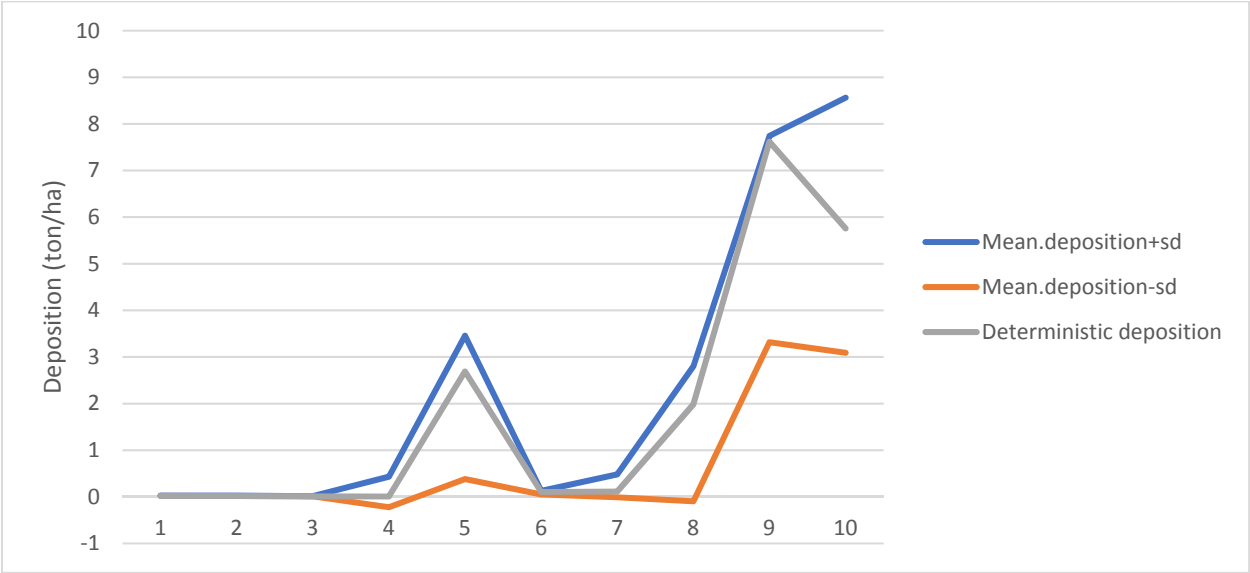

Figure A. 37 Deposition and standard deviation for DEMs with resolution of 10 m, 1st type of error for HCL-scenario

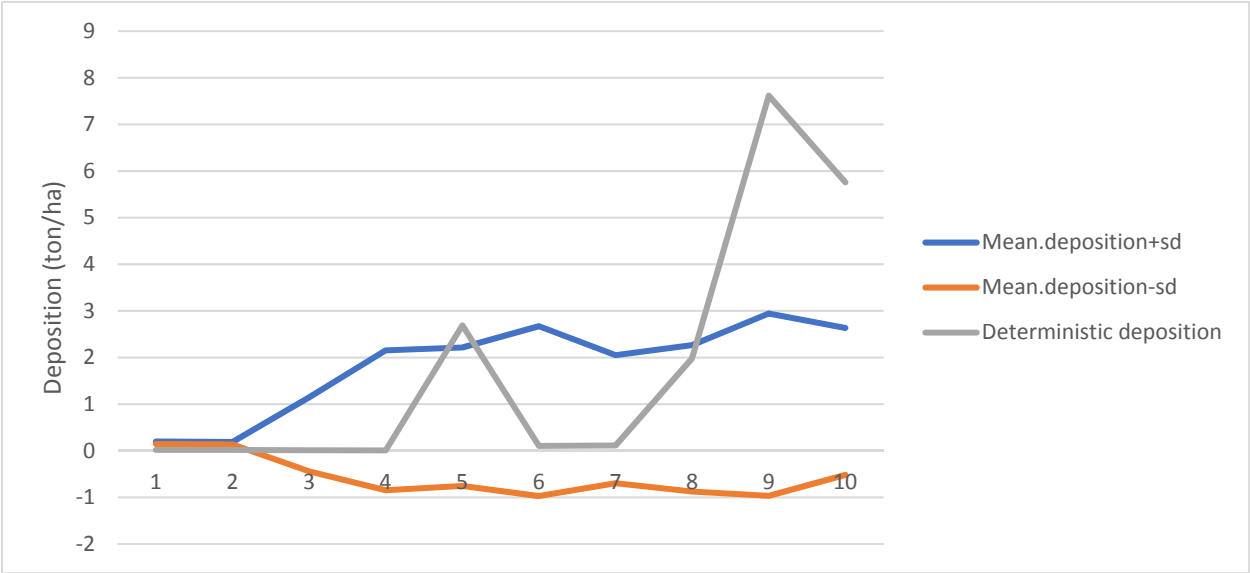

Figure A. 38 Deposition and standard deviation for DEMs with resolution of 10 m, 2st type of error for HCL-scenario

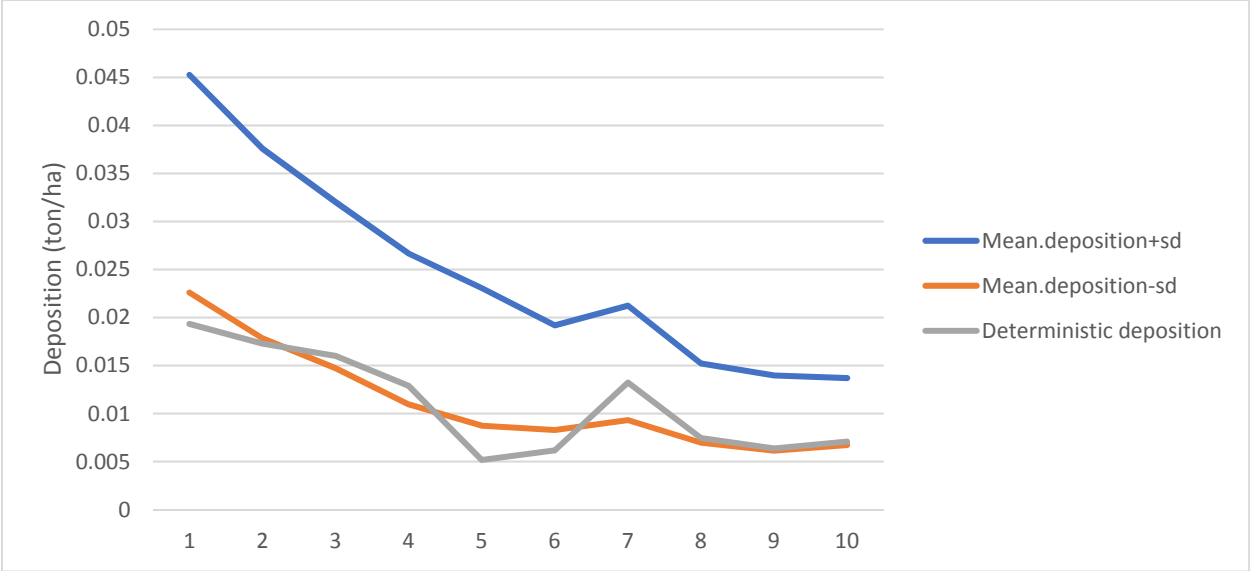

Figure A. 39 Deposition and standard deviation for DEMs with resolution of 20 m, 1st type of error for HCL-scenario

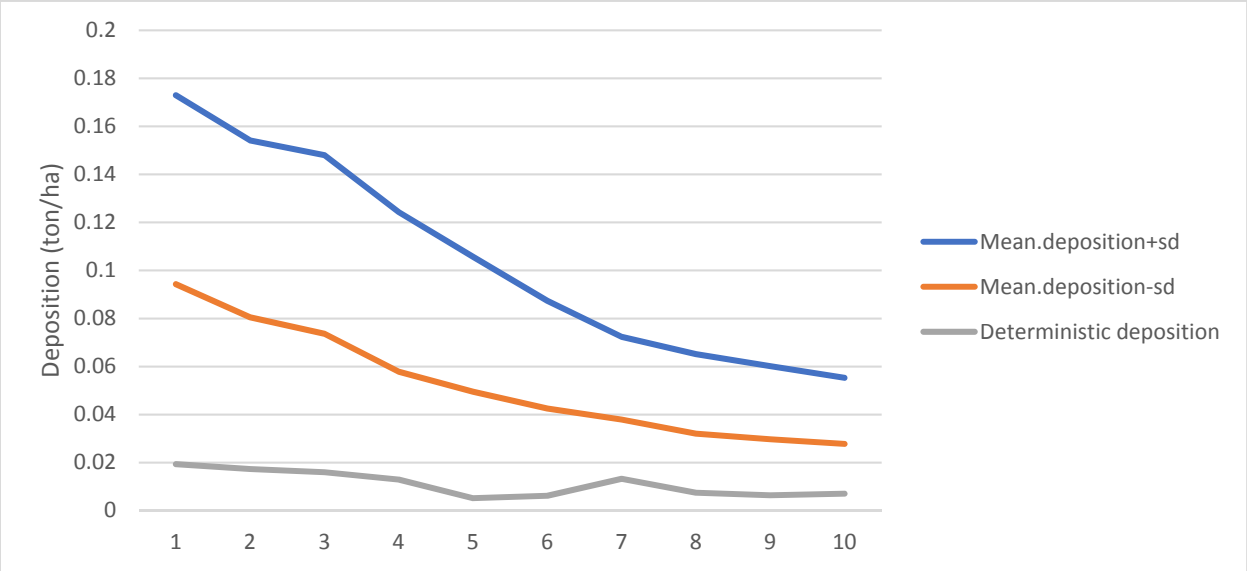

Figure A. 40 Deposition and standard deviation for DEMs with resolution of 20 m, 2st type of error for HCL-scenario

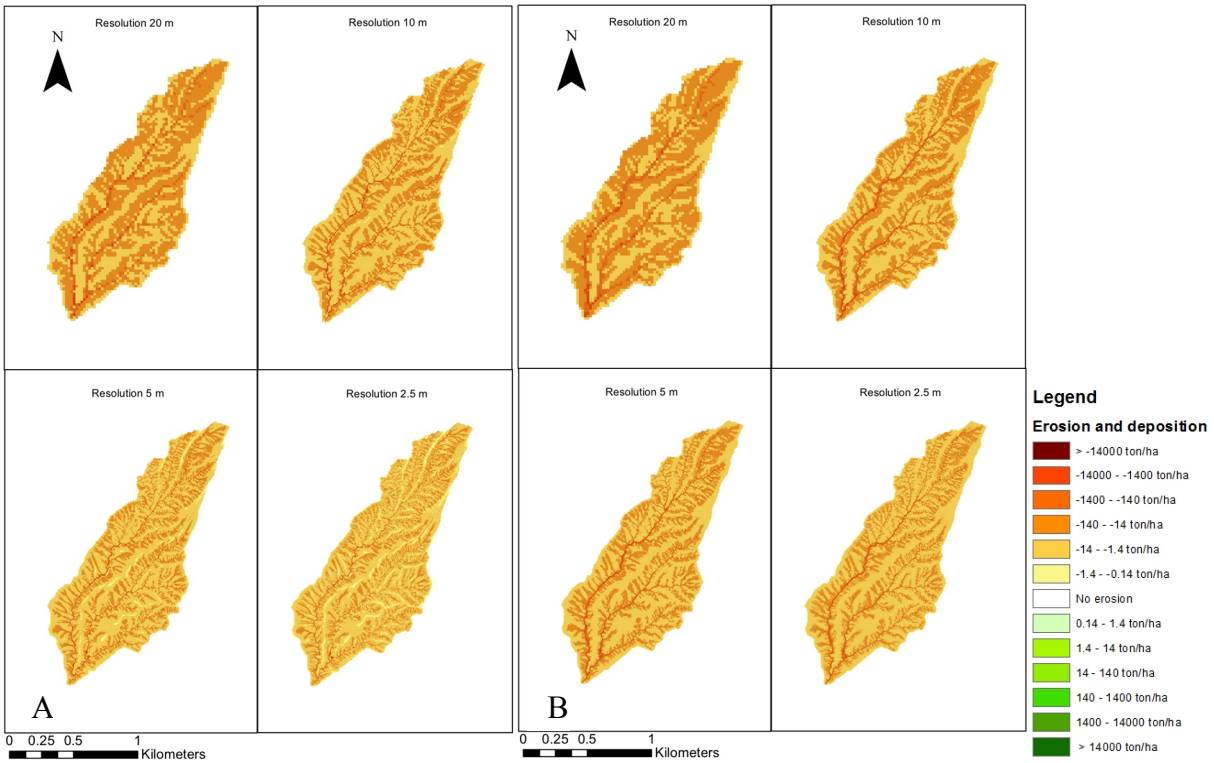

Figure A. 41 with A - Maps of the mean net cumulative erosion (10 years of modelling) for LCL scenario with 1st type of error, B - Maps of the mean net cumulative erosion (10 years of modelling) for LCL scenario with 2nd type of error

Figure A. 42 with A - Maps of the mean net cumulative erosion (10 years of modelling) for HCL scenario with 1st type of error, B - Maps of the mean net cumulative erosion (10 years of modelling) for HCL scenario with 2nd type of error

Figure A. 43 with A - Maps of the mean net cumulative erosion (10 years of modelling) for LCL scenario for deterministic DEM, B - Maps of the mean net cumulative erosion (10 years of modelling) for HCL scenario for deterministic DEM

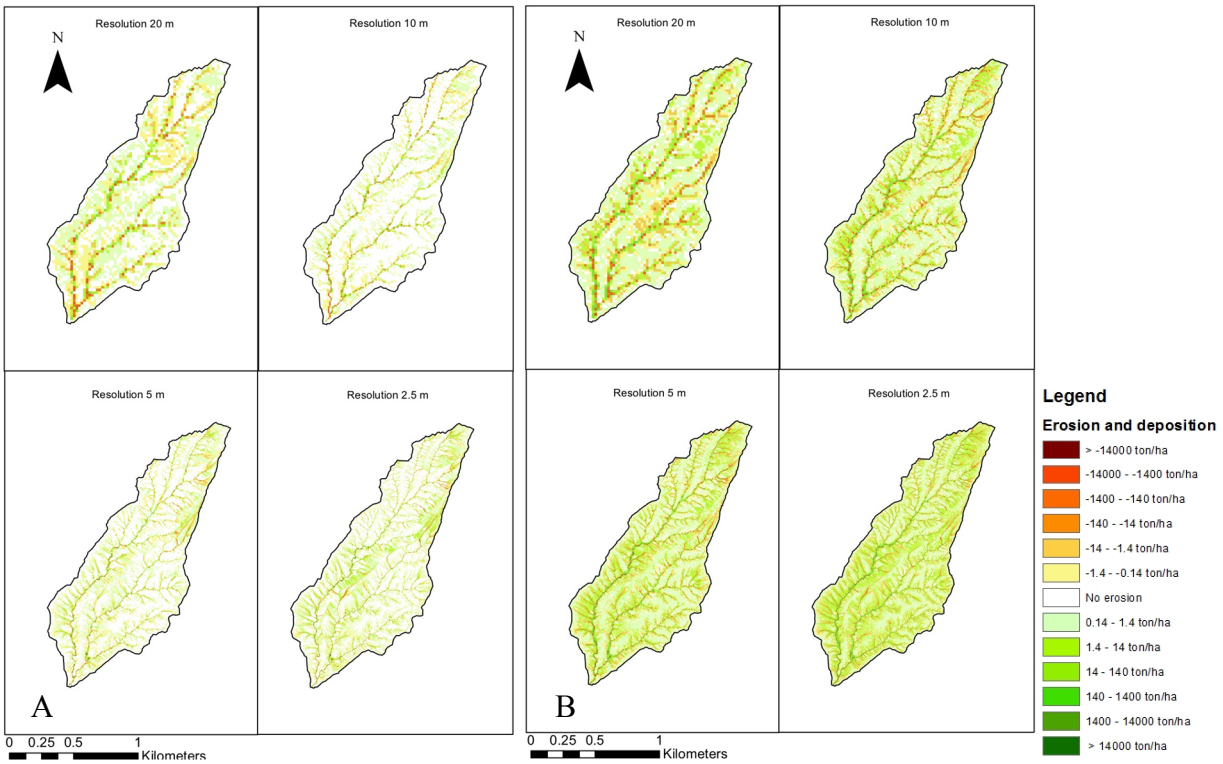

Figure A. 44 with A - Maps of the difference between net erosion based on deterministic DEM and mean net erotion of 125 simulated DEM with 1st type of error, for L scenario, B - Maps of the difference between net erosion based on deterministic DEM and mean net erotion of 125 simulated DEM with 2nd type of error, for L scenario

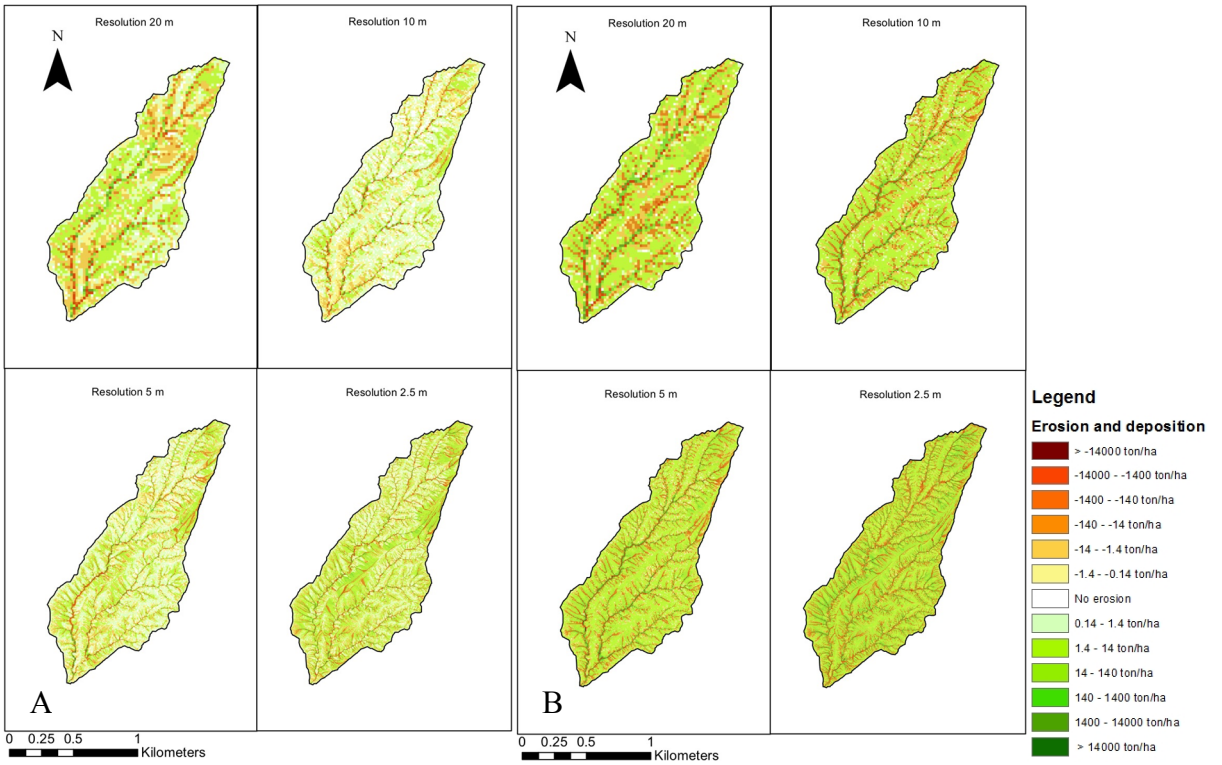

Figure A. 45 with A - Maps of the difference between net erosion based on deterministic DEM and mean net erotion of 125 simulated DEM with 1st type of error, for H scenario, B - Maps of the difference between net erosion based on deterministic DEM and mean net erotion of 125 simulated DEM with 2nd type of error, for H scenario

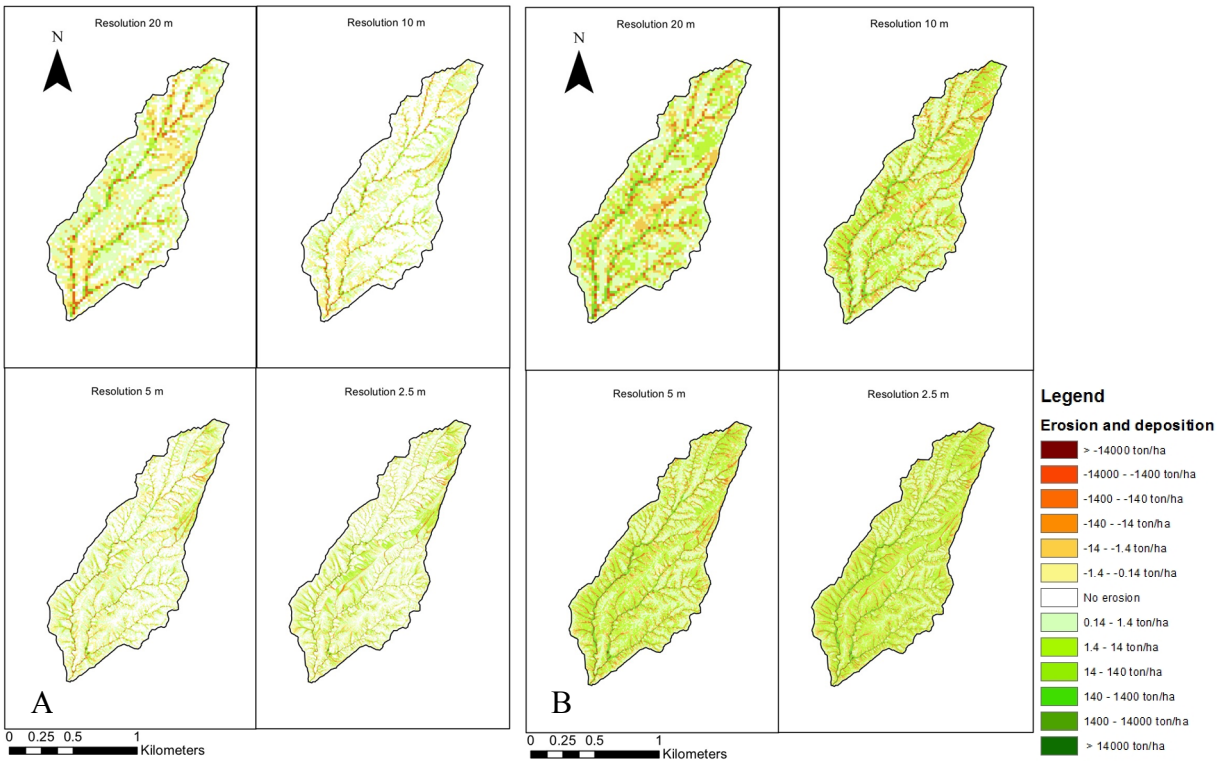

Figure A. 46 with A - Maps of the difference between net erosion based on deterministic DEM and mean net erotion of 125 simulated DEM with 1st type of error, for LCL scenario, B - Maps of the difference between net erosion based on deterministic DEM and mean net erotion of 125 simulated DEM with 2nd type of error, for LCL scenario

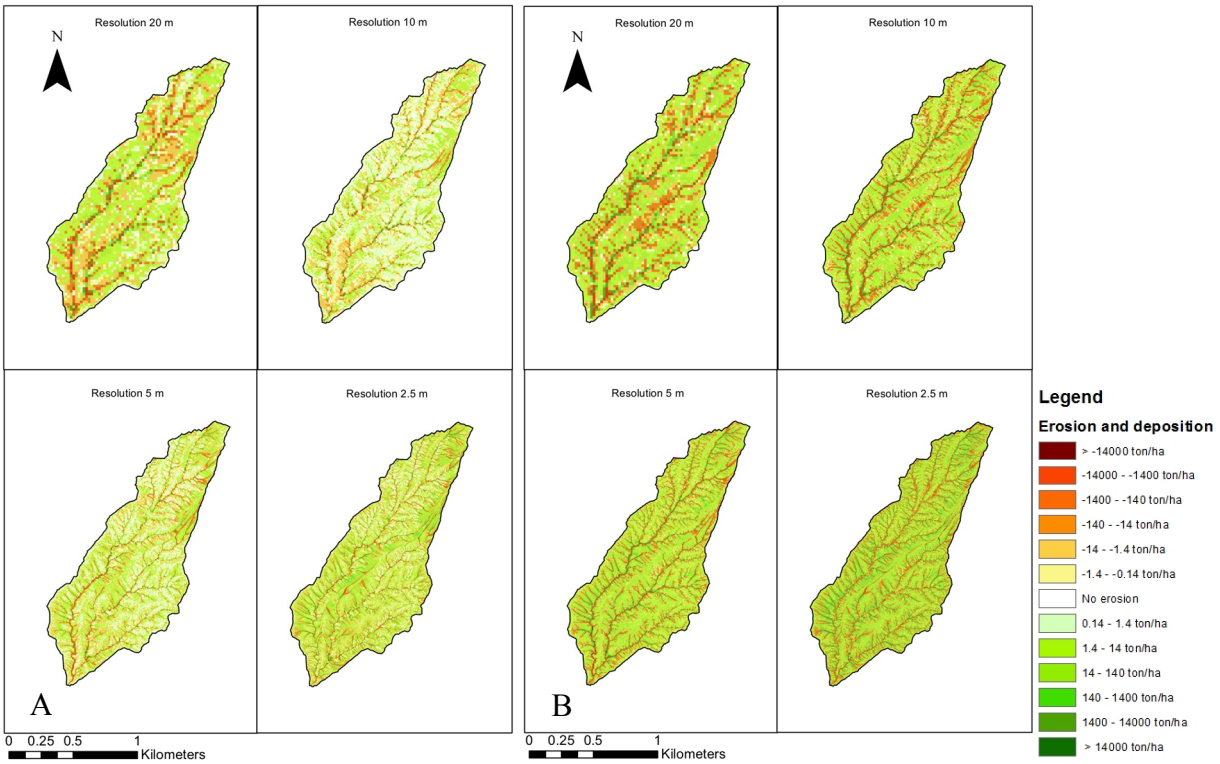

Figure A. 47 with A - Maps of the difference between net erosion based on deterministic DEM and mean net erotion of 125 simulated DEM with 1st type of error, for HCL scenario, B - Maps of the difference between net erosion based on deterministic DEM and mean net erotion of 125 simulated DEM with 2nd type of error, for HCL scenario

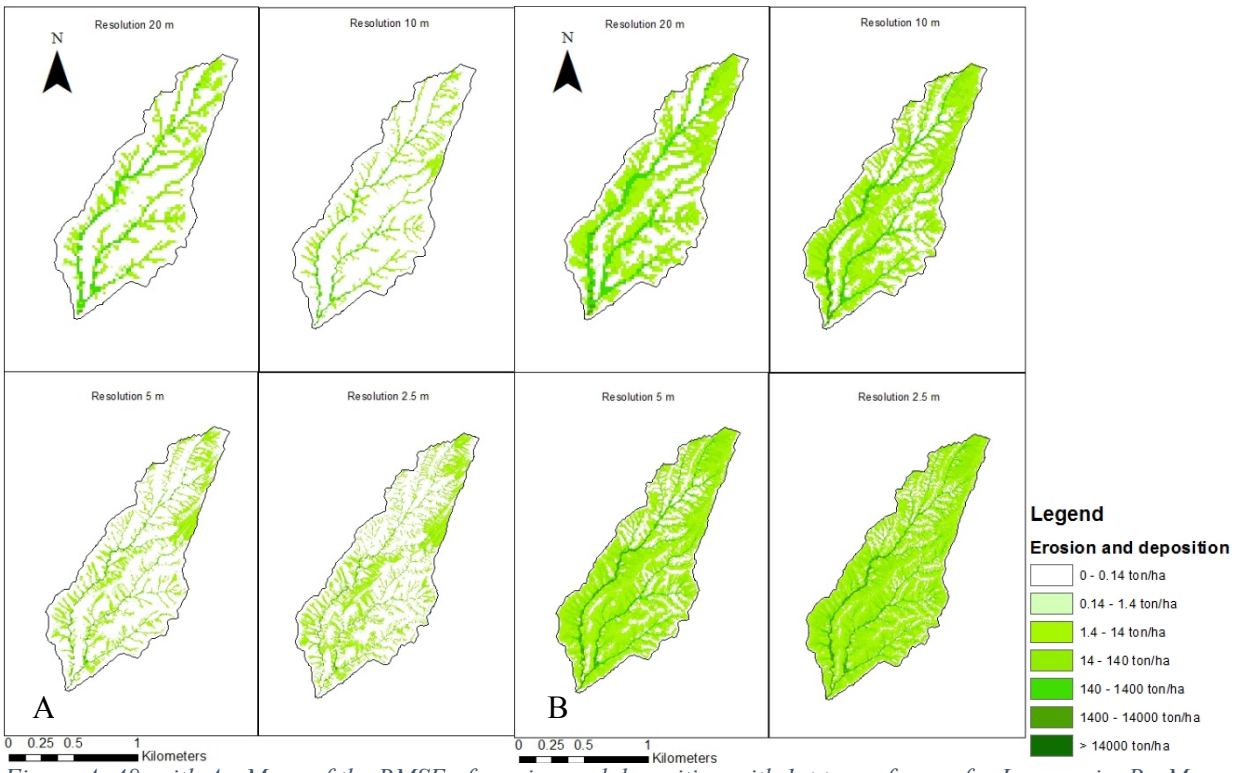

Figure A. 48 with A - Maps of the RMSE of erosion and deposition with 1st type of error for L scenario, B - Maps of the RMSE of erosion and deposition with 2nd type of error for L scenario

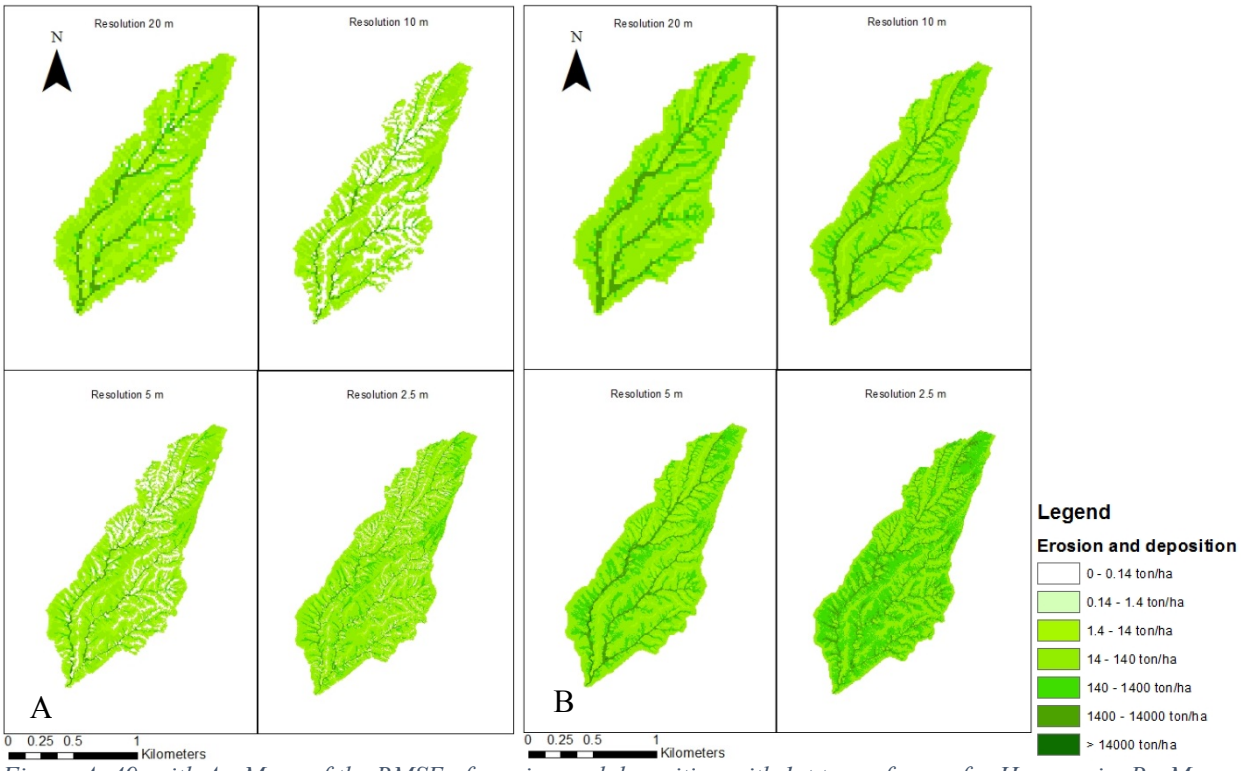

Figure A. 49 with A - Maps of the RMSE of erosion and deposition with 1st type of error for H scenario, B - Maps of the RMSE of erosion and deposition with 2nd type of error for H scenario

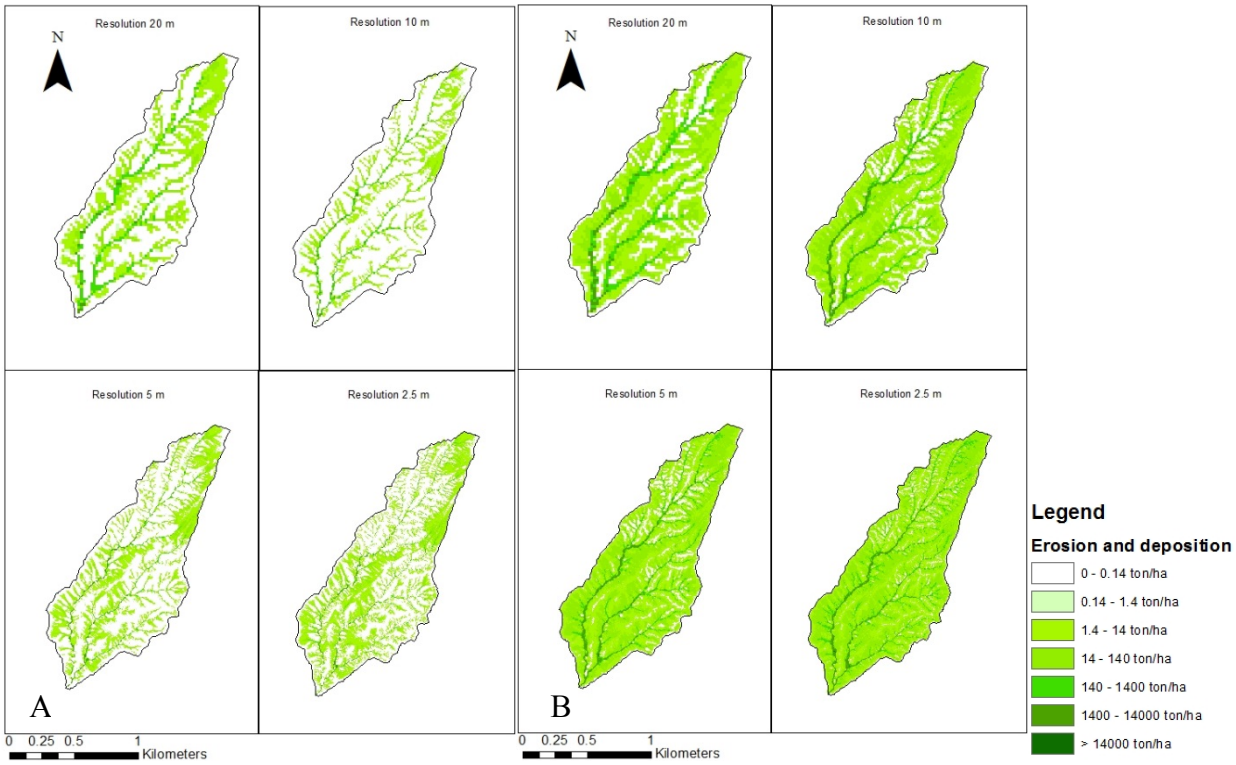

Figure A. 50 with A - Maps of the RMSE of erosion and deposition with 1st type of error for LCL scenario, B - Maps of the RMSE of erosion and deposition with 2nd type of error for LCL scenario

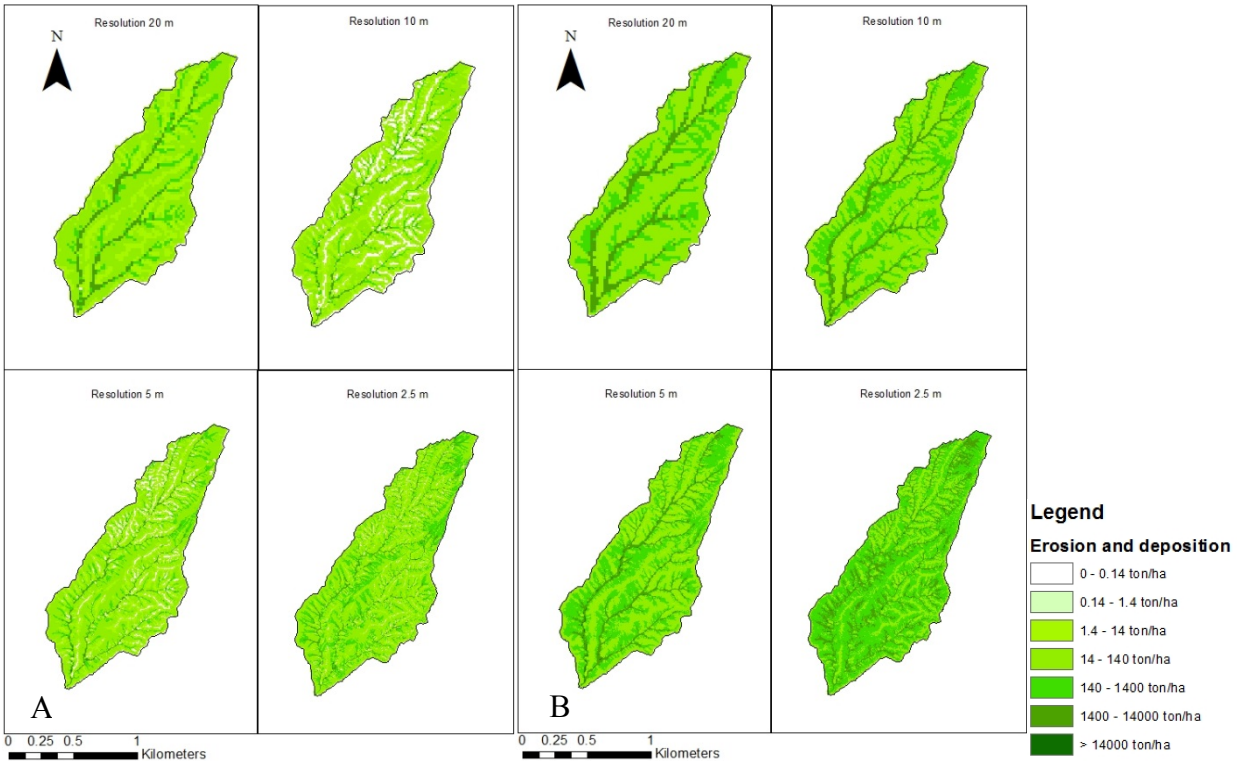

Figure A. 51 with A - Maps of the RMSE of erosion and deposition with 1st type of error for HCL scenario, B - Maps of the RMSE of erosion and deposition with 2nd type of error for HCL scenario